



## Pontificia Universidad Católica del Perú

Escuela de Posgrado

# Tesis

Investigations and simulations of magneto elastomer materials (MSE) influenced by static magnetic fields for soft robotics applications

Tesis para obtener el grado de  
Magíster en Ingeniería Mecánica

Presentado por: Alexander Richard López Ochoa

Tutor Responsable (TU Ilmenau): Prof. Dr.-Ing. habil. Valter Böhm  
M.Sc. Jhohan Chavez Vega

Professor Responsable (TU Ilmenau): Univ.-Prof. Dr.-Ing. habil. Klaus  
Zimmermann

Professor Responsable (PUCP): Prof. Dr. -Ing. Rolf Grieseler

Fecha y Lugar: 02/09/2019, Lima

# Kurzfassung

Magneto-sensitive Elastomere sind Verbundwerkstoffe, die hauptsächlich aus einer Elastomermatrix bestehen, in der magnetischen Partikeln dispergiert sind. Ein ins magneto-sensitive Elastomer eingreifende Magnetfeld bewirkt Änderungen der Eigenschaften dieses Materials. Diese Qualität macht die MSE zu einer Option mit hohem Potenzial für Soft Robotics-Anwendungen. Für die Realisierung dieser Masterarbeit wurden MSE-Proben aus einer Elastomermatrix, Silikonöl und Carbonschwarzpartikeln hergestellt.

Tests wurden durchgeführt, um Verbesserungen zu entwickeln, die sich auf Soft-Robot-Anwendungen konzentrieren, insbesondere bei Endeffektoren. In dieser Arbeit wurden die Eigenschaften von magneto-sensitive Elastomerproben in Abwesenheit und Gegenwart eines Magnetfeldes experimentell untersucht. Die Untersuchungen wurden mittels eines Magnetfeldes realisiert, das durch einen Permanentmagneten induziert wurde. Um die Intensität zu variieren, wurde der Permanentmagnet in unterschiedlichen Abständen zur Probe positioniert. Die experimentell erhaltenen Ergebnisse wurden verwendet, um den Einfluss der MF über der MSE zu verstehen und ein geeignetes Materialmodell unter Verwendung der Finite-Elemente-Methode zu entwickeln.

# Abstract

Magneto-sensitive elastomers are composite materials made mainly of an elastomer matrix, in which magnetic particles are dispersed. A magnetic field applied in the magneto-sensitive elastomers achieves changes in the properties of this material. This quality turns the magneto-sensitive elastomers in an option with high potential in soft robotics applications. In the present thesis, samples of magneto-sensitive elastomers containing an elastomeric matrix, silicone oil and carbonyl iron particles were produced.

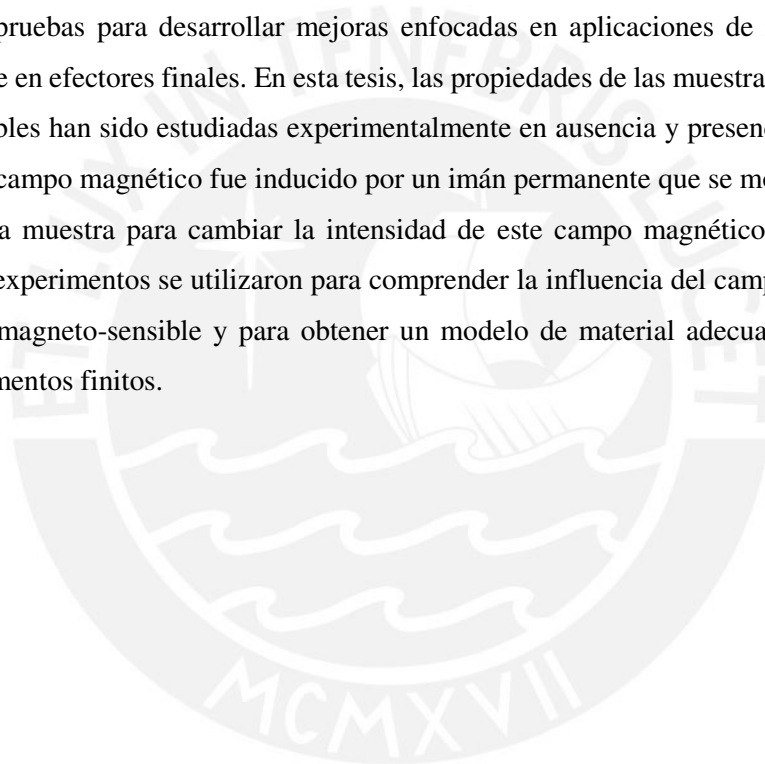
Tests were performed in order to develop improvements focused on soft robotic applications, particularly in end effectors. In this thesis, the properties of magneto-sensitive elastomers samples have been experimentally studied in the absence and presence of a magnetic field. The magnetic field was induced by a permanent magnet that was moved at different distances from the sample to change the intensity of the magnetic field. The results obtained by experiments were used to understand the influence of the magnetic field on the magneto-sensitive elastomer and to obtain a suitable material model using finite element method.



# Resumen

Los elastómeros magneto-sensibles son materiales compuestos hechos principalmente de una matriz de elastómero, en la que se dispersan las partículas magnéticas. Un campo magnético aplicado en los elastómeros magneto-sensibles logra cambios en las propiedades de este material. Esta cualidad convierte los elastómeros magneto-sensibles en una opción con alto potencial en aplicaciones de robótica blanda. En la presente tesis, se fabricaron muestras de elastómeros magneto-sensibles que contenían una matriz elastomérica, aceite de silicona y partículas de hierro carbonilo.

Se realizaron pruebas para desarrollar mejoras enfocadas en aplicaciones de robótica blanda, particularmente en efectores finales. En esta tesis, las propiedades de las muestras de elastómeros magneto-sensibles han sido estudiadas experimentalmente en ausencia y presencia de un campo magnético. El campo magnético fue inducido por un imán permanente que se movió a diferentes distancias de la muestra para cambiar la intensidad de este campo magnético. Los resultados obtenidos por experimentos se utilizaron para comprender la influencia del campo magnético en el elastómero magneto-sensible y para obtener un modelo de material adecuado utilizando el método de elementos finitos.



# Acknowledgements

I thank God for life and all the opportunities he gives me.

I would like to thank to my parents, Gladys and Vidal, for teaching me each day how to reach my goals and never give up, to support me unconditionally, and being the best parents that God could give me. To my brother Edwin, for being the best example to follow, and my sister Elizabeth for taking care of my parents and keeping together our family despite the distance.

This Master thesis could not have been accomplished without all the help and support of my advisors. I want to thank especially to Univ.-Prof. Dr.-Ing. habil. Klaus Zimmermann and Prof. Dr. -Ing. Rolf Grieseler for trusting me and letting me work on this topic; similarly, to my advisors Prof. Dr.-Ing. habil. Valter Böhm and M.Sc. Jhohan Chavez Vega for mentoring and accompanying me to achieve this master thesis.

Additionally, I would like to extend my gratitude to Univ.- Prof. Dr.-Ing. René Theska and Prof. Dr. Ing. Jorge Rodriguez, the responsible for the double degree program between Technische Universität Ilmenau and Pontificia Universidad Católica del Perú.

Finally, to all my family and friends: Estef, Michael, Tasha, Sheila, Jessica, Audrey, Cesar, David, Edu, Jorge, Erick, aunt Ida and all the people that I have met in this time.

# Content

1. Introduction .....	1
1.1. Motivation of work.....	1
1.2. Objectives of the thesis .....	1
2. State of the art .....	3
2.1. Magneto-sensitive elastomers .....	3
2.2. Microstructure of the MSE - isotropic and anisotropic .....	4
2.3. Additives - silicone oil .....	5
2.4. Permanent magnet .....	7
2.5. Soft robotic grippers.....	8
2.5.1. Related works .....	9
3. Experiments.....	13
3.1. Materials for fabrication of samples.....	13
3.1.1. Silicone matrix: Alpa-Sil Classic and Neukasil RTV 26 .....	13
3.1.2. Silicone oil.....	15
3.1.3. Iron powder .....	15
3.2. Attractive force on MSE samples due to a magnetic field .....	16
3.2.1. Sample for test: cylinders of different size.....	16
3.2.2. Testing configuration .....	18
3.2.3. Testing results .....	20

3.3.	Stiffness changes due to a magnetic field .....	27
3.4.	Deformation due to a magnetic field.....	36
3.4.1.	Testing configuration .....	36
4.	Material Modeling.....	45
4.1.	Theoretical fundamentals.....	45
4.2.	Hyperelastic models .....	45
5.	Conclusions and future work.....	50
5.1.	Conclusions .....	50
5.2.	Future work .....	51
6.	Bibliography.....	52
	Appendices.....	I
	Appendix A: Technical data of permanent magnet.....	I
	Appendix B: Technical data of Alpa-Sil Classic.....	IV
	Appendix C: Technical data of Neukasil RTV 26 .....	VII
	Appendix D: Technical data of Xiameter PMX-200 silicone fluid.....	IX
	Appendix E: Technical data of carbonyl iron powder.....	XII
	Appendix F: Technical data of force sensor.....	XIV
	Appendix G: Technical data of laser sensor.....	XIX

# Figures

Fig. 2.1: Scanning electron microscopy (SEM) images of magneto sensitive elastomer (MSE) material samples: Fig. a) isotropic material. Fig. b) anisotropic material with the direction of the particle alignment (green arrow) [10]. ..... 4

Fig. 2.2: Distribution of microstructures within the elastomeric matrix [12]..... 6

Fig. 2.3: Fig. a) MSE without any silicone oil, the particles disperse randomly in the matrix. Fig. b) MSE with 20% of silicone oil, the particles are attached to each other and form a partial microstructure [12]. ..... 6

Fig. 2.4: Diagram of magnet dimensions [20]..... 8

Fig. 2.5: Adhesion diagram of permanent magnet S-70-35-N [22]. ..... 8

Fig. 2.6: MSE gripper under an MF, saving the shape produced by the cube [23]..... 10

Fig. 2.7: Magnetorheological fluid-based gripper: Fig. a) with normal housing, Fig. b) with collar housing [24]. ..... 11

Fig. 2.8: Universal robot gripper using MR $\alpha$  fluid [25]..... 11

Fig. 2.9: Shape memory effect presented in composite elastomer [4]. ..... 12

Fig. 2.10 Versaball: jamming-based robotic gripper [26]. ..... 12

Fig. 3.1: Diagram of volume distribution for MSE..... 16

Fig. 3.2: MSE cylinders: Fig. a)  $\varnothing 16 \times H12$ , Fig. b)  $\varnothing 16 \times H6$ , Fig. c)  $\varnothing 16 \times H3$ . Units: diameter  $\varnothing$  [mm], height H [mm]. ..... 17

Fig. 3.3: Configuration of the setup for attractive forces measurement. .... 20

Fig. 3.4: Attractive forces evaluated at different distance: magnet upper surface - MSE cylinder bottom, for samples of MSE with 00%vol silicone oil and 10%, 20%, 30%, 40% vol. iron. .... 21

Fig. 3.5: Maximum attractive forces - %vol. iron concentration. .... 22



Fig. 3.6: Attractive forces evaluated at different distance magnet upper surface - MSE cylinder bottom, for samples MSE 00%vol. silicone oil and MSE 45%vol. silicone oil. ....	23
Fig. 3.7: Diagram of contiguous positions for MSE samples: Fig. a) Ø16xH12, Fig. b) Ø16xH6, and Fig. c) Ø16xH3. Units: [mm]. ....	25
Fig. 3.8: Accumulated attractive force for MSE: 00%vol. silicone oil and 10%, 20% vol. iron. ....	25
Fig. 3.9: Maximum accumulated attractive force vs mass error for MSE: 00%vol. silicone oil and 10%, 20% vol. iron. ....	26
Fig. 3.10: Diagram of volume distribution for MSE. ....	27
Fig. 3.11: Configuration of the setup for compressive forces measurement. ....	29
Fig. 3.12: Force vs deformation for the four samples of MSE cylinder Ø16xH12, composition matrix 45%vol. silicone oil and 30%vol. iron, under MF 141.2 mT. ....	31
Fig. 3.13: Force vs deformation for different intensities of MF, in the MSE cylinder Ø16xH12, composition: a) 10%, b) 20%, c) 30%, and d) 40% vol. iron. ....	32
Fig. 3.14: Maximum values obtained for different intensities of MF, in the MSE cylinder Ø16xH12, composition: a) 10%, b) 20%, c) 30%, d) 40% vol. iron. ....	33
Fig. 3.15: Stress vs strain for different intensities of MF, in the MSE cylinder Ø16xH12, composition: a) 10%, b) 20%, c) 30%, d) 40% vol. iron. ....	34
Fig. 3.16: Configuration of the setup for deformation measurement of discs due to MF. ....	37
Fig. 3.17: Main dimension of MSE disc. ....	37
Fig. 3.18: Fig. a) Disc in presence of a high MF and close to a permanent magnet, Fig. b) Disc in presence of low MF and far from the permanent magnet. ....	39
Fig. 3.19: Graphs deformations vs. diameter for discs Ø50xH3, MSE matrix 45%vol. silicone oil and: a) 10%vol. iron, b) 20%vol. iron, c) 30%vol. iron, d) 40%vol. iron. ....	39

Fig. 3.20: Maximum deformation vs. Magnetic field for discs Ø50xH3, MSE matrix 45%vol. silicone oil and: a) 10%vol. iron, b) 20%vol. iron, c) 30%vol. iron, and d) 40%vol. iron.....	40
Fig. 3.21: Discs of MSE matrix 45%vol. silicone oil and 30%vol. iron: Fig. a) Ø64xH3, Fig. b) Ø48xH6, Fig. c) Ø32xH3, and Fig. d) Ø16xH3.....	42
Fig. 3.22: Testing dispositions for discs: Fig. a) Up, Fig. b) Down.....	42
Fig. 3.23: Graphs deformations vs. diameter for discs made of MSE matrix 45%vol. silicone oil and 30%vol. iron, with diameter: a) 16 mm, b) 32 mm, c) 48 mm, and d) 64 mm.....	44
Fig. 4.1: Modeling parameters vs. magnetic field for MSE matrix 45%vol. silicone oil and 10%, 20%, 30%, and 40%vol. iron. For NH: a) $\mu$ . For MR3: b) $C_{10}$ , c) $C_{01}$ , and d) $C_{11}$ .....	47
Fig. 4.2: Compressive forces vs deformation in MSE of matrix 45% vol. sil. oil and 30% vol. iron under different magnitudes of MF.....	49

## Tables

Tab. 3.1: Properties of silicone matrix, silicone oil and magnetic particles.....	15
Tab. 3.2: Mass, volume and volumetric percentage for the concentrations of MSE cylinders Ø16xH12 without silicone oil and 10%, 20%, 30%, 40% vol. iron. Units: mass [g], vol. [ $\text{cm}^3$ ], %vol. [%].....	17
Tab. 3.3: Mass, volume and volumetric percentage for the concentration of MSE cylinders Ø16xH12 with 45%vol. silicone oil and 10%vol., 20%vol., 30%vol. iron. Units: mass [g], vol. [ $\text{cm}^3$ ], %vol. [%]. .....	18
Tab. 3.4: Mass composition for cylinders Ø16xH6 and Ø16xH3, MSE without silicone oil and 10%, 20% vol. iron.....	18
Tab. 3.5: Average magnetic field for the samples for different distances between the magnet upper surface and MSE cylinder bottom.....	19
Tab. 3.6: Attractive force ratio between cylinders Ø16xH12 of MSE: 00%vol. silicone oil and 20%, 30%, 40% vol. iron with respect to 10% vol. iron. ....	22

Tab. 3.7: Attractive force ratio between cylinders of MSE: 45%vol. silicone oil and 20%, 30%vol. iron with respect to 10%vol. iron. ....	24
Tab. 3.8: Force increase for MSE with 45%vol. silicone oil respect to MSE with 00%vol. silicone oil. ....	24
Tab. 3.9: Comparison of theoretical and real mass for MSE samples. ....	26
Tab. 3.10: Mass and volumetric percentage for cylinder Ø16xH12 of MSE matrix 45%vol. silicone oil and 10%, 20%, 30%, 40%vol. iron. Units: mass [g], %vol. [%].....	28
Tab. 3.11: Average magnetic field for the samples at different distances between the magnet upper surface and MSE cylinder bottom. ....	30
Tab. 3.12: Maximum values obtained for different intensities of MF, in the MSE cylinder Ø16xH12, composition: a) 10%, b) 20%, c) 30%, d) 40% vol. iron. ....	32
Tab. 3.13: Average force increase for 141.2 mT in comparison to 0 mT for MSE cylinder Ø16xH12, composition: a) 10%, b) 20%, c) 30%, d) 40% vol. iron. ....	33
Tab. 3.14: Results when considering the MSE as an elastic material for the minimum and maximum MF. ....	35
Tab. 3.15: Mass composition for disc Ø50xH3, MSE matrix 45%vol. silicone oil and 10%, 20%, 30%, 40% vol. iron. ....	38
Tab. 3.16: Distance magnet - MSE disc Ø50 mm for each MF. ....	38
Tab. 3.17: Distance magnet - MSE disc: Ø16, Ø32, Ø48, and Ø64 mm for each MF. ....	43
Tab. 4.1: Neo Hookean model for MSE matrix 45%vol. silicone oil and 10%, 20%, 30%, and 40%vol. iron. ....	47
Tab. 4.2: Mooney Rivlin 3 parameters model for MSE matrix 45%vol. silicone oil and 10%, 20%, and 30%vol. iron. ....	48

# 1. Introduction

## 1.1. Motivation of work

Gripping objects with complex shapes without damaging them has been a challenge in the development of grippers [1]. Soft robotic grippers are those that have a high potential to solve this problem. There is a wide variety of materials that are being implemented in soft robotic applications, but above all, the use of intelligent materials has been intensified [2]. Despite the great variety of soft robotic grippers that are being developed with the use of smart materials, few studies have exploited the potential of magneto-sensitive elastomers. Therefore, the possibility to exploit that potential is open and it is a great opportunity to discover new behaviors or effects in this novel material.

For being a new material in the field of soft robotics, different tests can be performed to improve or obtain new applications. In addition to carrying out different tests, the concentration can be varied and thus the influence of the components can be investigated.

The magnetorheological properties are characterized by the capacity to be varied by applying a magnetic field. The MSE (magneto-sensitive elastomers) also presents that kind of property: the change in stiffness, shape-memory effect or magnetostriction. Thus, those are some of the main properties that should be taken into account when a soft gripper is designed with MSE.

In this thesis are studied the following properties of the MSE: the attractive force due to a MF, the stiffness changes due to a MF, and the deformation due to a MF. These tests were carried out with samples of different concentration.

## 1.2. Objectives of the thesis

The principal aim of this thesis is to study the changes in MSE properties and shape-adaptation quality when different magnitudes of static MFs are presented. In addition to that, a comparison between experimental results and FEM simulations can be obtained. Thereby, new insides of MSE are achieved that will help the approach of future designs and the manufacture of an optimized end-effector for gripper applications. In order to achieve the principal aim, the following specific objectives will be accomplished in the work:

- Designing and manufacturing MSE-based samples with different concentrations of silicone oil and iron.

- Implementation of an experimental test stand and measurement of MSE properties (magnetic attractive force, stiffness change, shape adaptation) due to different MFs.
- Material modeling based on experimental results, FEM simulation for samples and comparison with experimental results



## 2. State of the art

In this chapter, the basic knowledge is presented in order to understand the magneto-sensitive material. Then, researches of soft robotics grippers and MSE related to this thesis are introduced.

### 2.1. Magneto-sensitive elastomers

Magneto-sensitive elastomers are composite materials made of an elastomer base, additives as silicone oil, and magnetic particles. The main characteristic of the MSE is that it reaches changes in its properties by applying a magnetic field.

There are several magnetic-dependent properties that MSE presents. Among the main features related to this thesis are: reversible or tunable stiffness, shape-memory effect and magnetostrictive effect. Properties which provide to the MSE with multiple applications in the field of sensors, actuators, soft robotic grippers, among others.

Reversible stiffness is a phenomenon that MSE exhibits when the magnetic particles are polarized due to a MF. Consequently, forces are generated between these particles thus transforming the stiffness of the MSE. When removing the MF, the MSE returns to its original state, as well as its stiffness [3].

Shape-memory effect in the MSE is the capability to assume a temporary shape produced by a deformation and then recover the original shape. The temporary shape remains present throughout the time that the MSE is under the influence of the magnetic field. [4]

Magnetostrictive effect exhibited in the MSE can be described mainly as a phenomenon of induced change in shape and dimensions due to the application of a magnetic field. [5]

It should be noted that these properties can be controlled according to the requirements of use. However, the responses of this material to different conditions must be studied. To understand in a general way the behavior of the MSE, it can be treated as the superposition of internal magnetic and elastic forces held by the matrix [6] or the addition of viscoelastic properties with zero MF and elastic/plastic properties due to interparticle magnetic force [7].

But to get an idea of the behavior on a smaller scale, the following can be considered. The behavior depends strongly on their magnetic particle's interaction. Given the magnetically permeable particles suspended in the matrix, the creation of a three-dimensional crosslink network is allowed. This network is integrated by three adjacent magnetic particles. This network keeps a form that seeks to keep stable

when presenting external loads. The stability of this network will be able to support higher loads in the presence of an MF [8].

## 2.2. Microstructure of the MSE - isotropic and anisotropic

Another interesting feature of the MSE is that its microstructure can be altered and controlled. This is achieved by applying an MF during chemical crosslinking. This procedure is very common to obtain specific behaviors of the MSE because when changing the microstructure, it also changes its properties. The result of this manipulation during crosslinking is an anisotropic material [3,7].

Under this premise, the MSE can be classified into two class of microstructure: isotropic and anisotropic. It is understood that the isotropic MSE is the material cured in the absence of MF. It shows randomly dispersed iron particles, and for this reason it is also known as unstructured MSE. On the other hand, the anisotropic MSE presents the iron particles linked into chain structures, and it is known as pre-structured MSE [8,9].

Fig. 2.1 clearly shows the microstructural difference in the isotropic and anisotropic MSE. In Fig. 2.1a no specific order is observed, but a more uniform distribution of iron particles. While in Fig. 2.1b the alignment of the iron particles in one direction is observed.

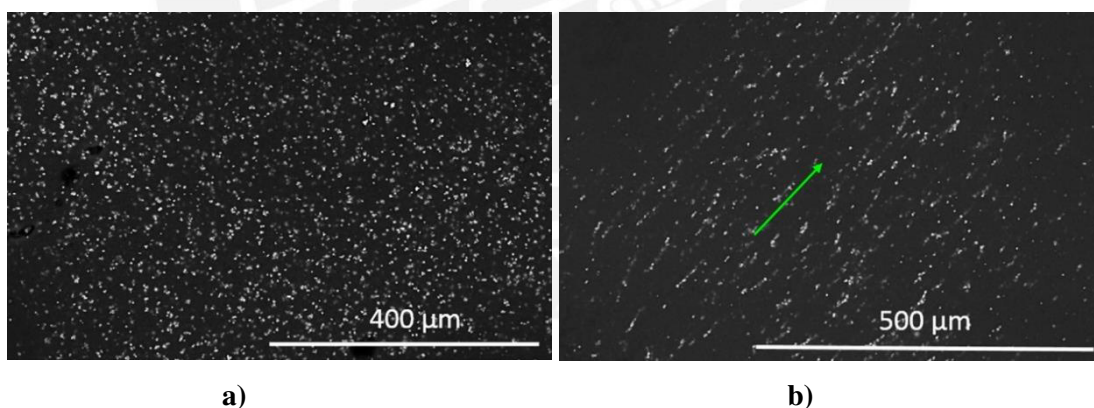


Fig. 2.1: Scanning electron microscopy (SEM) images of magneto sensitive elastomer (MSE) material samples: Fig. a) isotropic material. Fig. b) anisotropic material with the direction of the particle alignment (green arrow) [10].

The differences between the two materials are not only reflected in the structure [11]. In the following, the differences between isotropic and anisotropic MSE will be discussed to justify the used microstructure in this thesis. In terms of production, the isotropic MSE does not need a source that provides a magnetic field during the curing. Meanwhile, the anisotropic MSE needs that source, resulting in a more complex process and equipment of production [12].

In terms of achieving an entire microstructure, getting an isotropic MSE needs a proper stirring and removing of the gas trapped of the mixture [8]. And in the other hand, getting an anisotropic MSE needs also both conditions beside a uniform magnetic flux density through the sample. Nonetheless, the last condition is complex to fulfill because the density decreases considerably when the thickness increases [12] and it would be necessary a strong MF, generally above 800 mT [8].

Finally, the isotropic MSE does not have a microstructure that increases the magneto-sensitive effects depending on the relative direction to the magnetic field applied. In contrast to the first microstructure, the anisotropic MSE has a certain chain direction [10]. And in order to optimize the magneto-sensitive effects, this direction should be considered during the application of the magnetic field [12].

The comparison between the two microstructures shows the advantages of the isotropic MSE and the shortcomings of the anisotropic that evidence the limitations of its applications in the industry [12]. And taking into consideration the previous comparison, the isotropic MSE is the chosen material for this thesis.

### **2.3. Additives - silicone oil**

An MSE can be composed by an elastomeric matrix and magnetic particles, but in order to include or modify properties, extra components are added. The type of elastomer selected in this thesis is the silicone rubber as they are generally soft and/or deformable at room temperature [11]. The magnetic particle selected is iron powder. And the extra component is silicone oil that is the usual component added in the manufacture of MSE [8,13] in order to provide the following properties. It promotes a reduction of conglutination of the molecules [8]. It also allows an increasing of the plasticity in the matrix [14]. And it achieves a better internal distribution of stresses that are reflected under mechanical loads [15].

These qualities that the silicone oil provides to the MSE are directly related to the microstructure. For that reason, is important to understand the interaction of the silicone oil with the other components of the MSE: elastomer base and iron particles described in Sec. 3.1.

A mixture composed by an elastomer and carbonyl iron particles produces an MSE with dispersed particles within the elastomeric matrix. Nevertheless, the inclusion of the silicone oil generates a different reaction. During the stirring of the mixture, the interaction between the silicone oil and the iron particles allows the attachment among them [12]. Consequently, it is produced the formation of scattered microstructures within the elastomeric matrix [12]. Fig. 2.2 shows a representation of how are the microstructures distributed within the elastomeric matrix using as reference the source [12].



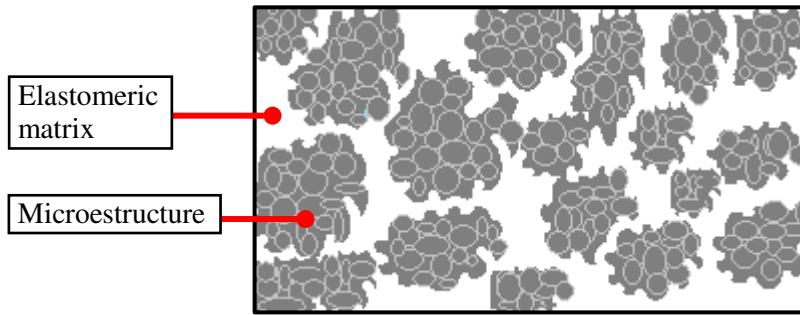


Fig. 2.2: Distribution of microstructures within the elastomeric matrix [12].

The iron particles are lubricated due to the presence of the silicone oil. Thus, the particles are able to slip inside the microstructure. When applying an MF penetrating the MSE with silicone oil, the iron particles are magnetized and moved. Subsequently, the microstructures experience a reordering, turning into more regular constructions that increase the magneto-rheological (MR) effects [12]. Fig. 2.3 presents two images in which the difference is shown between an MSE without silicone oil (Fig. 2.3 a) and an MSE with silicone oil (Fig. 2.3 b).

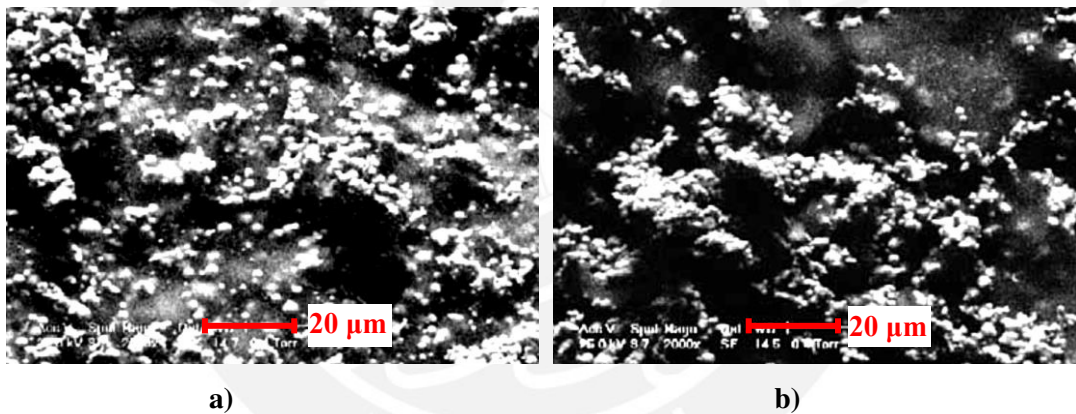


Fig. 2.3: Fig. a) MSE without any silicone oil, the particles disperse randomly in the matrix. Fig. b) MSE with 20% of silicone oil, the particles are attached to each other and form a partial microstructure [12].

### Silicone oil viscosity

Studies and experiments revealed that in the MSE behavior a clear dependence exists between the quantity and viscosity of the used silicone oil. To determine the type of silicone oil used for MSE samples, previous works related to this thesis were taken as a reference [16,17,18]. First of all, these works consisted of a comparison of the shape adaptation using field-induced plasticity in MSE samples with silicone oils of different viscosities. The usual viscosity given by the providers is the cinematic viscosity, so the values were: 5, 200, 500 and 1000 cSt. The results of these tests showed that samples with oils of higher viscosity achieve a significantly higher shape saving capability. The second part of that work was concerned in the comparison of the stiffness changes due to a static magnetic field in the same MSE samples from the first test. The results showed a greater change of the elastic modulus for

the MSE sample with the 500 cSt silicone oil. Hence, according to both tests, the silicone oil with 500 cSt was selected for future studies, including this thesis.

## 2.4. Permanent magnet

For this thesis and the studying of the MSE, different tests were carried out that to a large extent depended on the use of a magnetic field. Due to the necessity to reach high MF values, a permanent magnet was used for the experiments.

The permanent magnet used, S-70-35-N, was provided by Supermagnete. This magnet with disc shape (Fig. 2.4) has a 70 mm diameter and a 35 mm height. Its main features indicated by the provider are the remanence field or residual magnetism ( $B_r$ ): between 1.32-1.37 T. The coercive field strengths  $bH_c$  and  $iH_c$ : between 860-995 kA/m and above 955 kA/m respectively. To review more the properties of the permanent magnet, examine Appendix A.

Furthermore, with this magnet it an axially symmetric MF can be obtained, but not uniform in the thickness direction [19]. In order to obtain the value of the MF at different distances from the magnet, equation (1) can be used [20]. Based on this equation, the magnetic field reached at the surface of the magnet ( $z=0$ ) is 466 mT or 4.66 kG. This value decreases with the increasing of the distance  $z$ .

$$B = \frac{B_r}{2} \left( \frac{D+z}{\sqrt{R^2 + (D+z)^2}} - \frac{z}{\sqrt{R^2 + z^2}} \right) \quad (1)$$

where:

B: Magnetic Field

$B_r$ : Remanence field, independent of the magnet's geometry

$z$ : Distance from a pole face on the symmetrical axis

D: Thickness (or height) of the cylinder

R: Semi-diameter (radius) of the cylinder

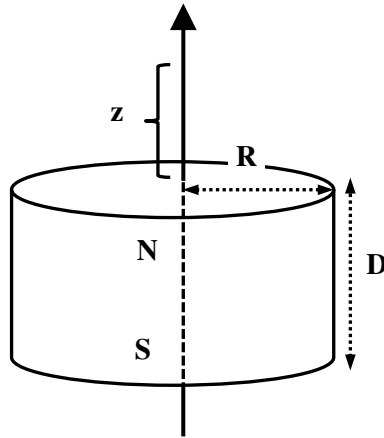


Fig. 2.4: Diagram of magnet dimensions [20].

Additionally, the magnet capacity can be described by the following property given by the provider, adhesive force [21]. It quantifies approximately the maximum capacity of attractive force between the magnet and an iron plate. For the case of an iron plate 10 mm thickness, the adhesion diagram is shown on Fig. 2.5.

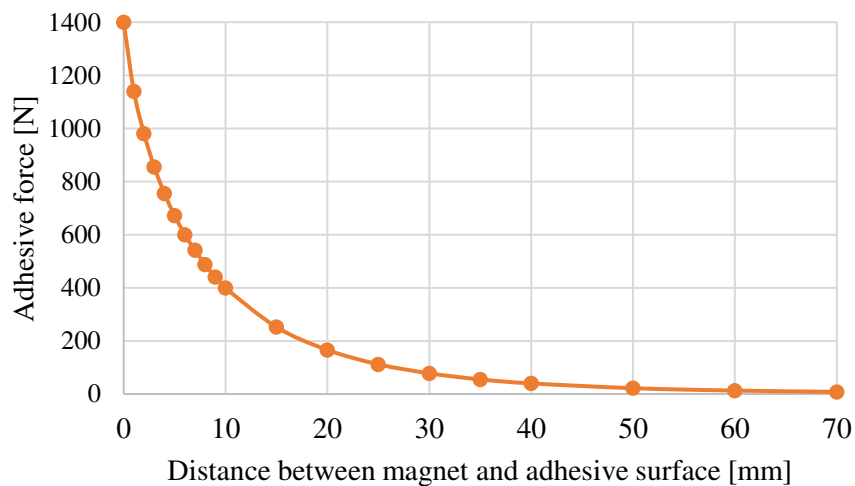


Fig. 2.5: Adhesion diagram of permanent magnet S-70-35-N [22].

## 2.5. Soft robotic grippers

The use of new technologies and materials in the field of gripping and manipulation has resulted in the development of soft robotics grippers.

One of the most common problems or challenges in the design of a gripper is the ability to manipulate an object with a non-regular shape without damaging it. This type of grippers (with soft robotics technology) have many advantages, such as: they are capable to adapt their shape to the surface of the object. This property can be used in different shapes and also it is a reliable gripping. For these reasons

this type of gripper is valuable in the industry to accomplish the requirement to grab uncommon or unknown objects especially deformed ones. [1]

To manufacture these grippers the components that are used must be flexible and soft. Nowadays there are advanced materials that meets the previous requirements and are studied for their properties; for example, silicone elastomers, shape memory materials, active polymers and gels [2].

This property of soft gripping can be accomplished by three different technologies: actuation, controlled stiffness or controlled adhesion [2].

The method of gripping by controlled stiffness consists first in setting the gripper in its “soft” configuration, then approaching the object to be grabbed and it must be enveloped by the gripper molding its geometry, and by last the configuration of the gripper must be changed by stiffening it and in that way the object is held through caging [2]. When the inside object must be released, the “soft” material returns to a more fluid state to allow it released [1].

This technology uses materials that can change their viscosity. The configuration of the gripper typically is with an outer skin with these materials inside, which can be electrorheological (ER) fluid, magnetorheological (MR) fluid, or pellets. [1]

### **2.5.1. Related works**

#### **Hemispherical end effector made of MSE layer**

The most recently study related to this thesis, is the work realized by Y. Jin [23]. An MSE end-effector was developed for that work. The gripper with hemispherical shape had a layer of MSE and elastomer, filled by air and oil. In order to develop this end effector, properties of the MSE as the stiffness and the field-induced plasticity were studied. This gripper provides some advantages: recording a shape under an MF, gripping objects with different shapes and changing its properties by the application of an MF. The gripper is shown in Fig. 2.6.

This MSE gripper operates in the following way: it is deformed by an external load (object with specific shape). Without removing the load, a MF is induced by a permanent magnet for the deformed gripper. Then, maintaining the MF, the load is removed, obtaining a gripper with the object shape recorded. After removing the MF, the gripper recovers its initial hemispherical shape.

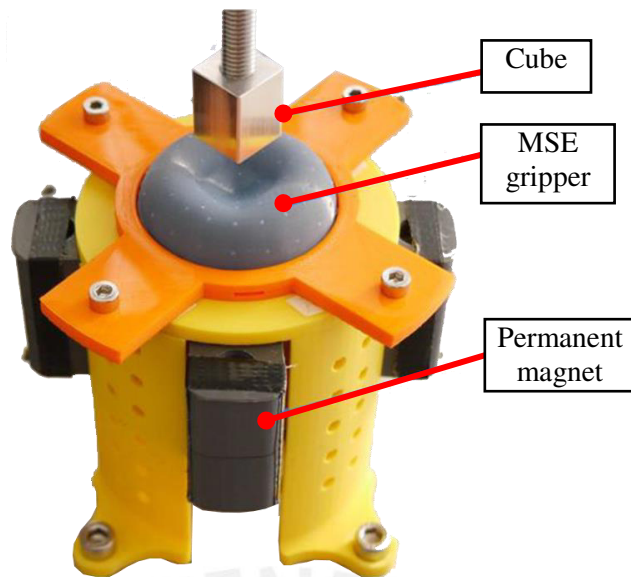


Fig. 2.6: MSE gripper under an MF, saving the shape produced by the cube [23].

### Magnetorheological fluid-based robotic gripper

C. M. Hartzell [24] as well as Y. Okatani and T. Nishida [25] developed and fabricated universal grippers that work by applying a magnetic field. These grippers had a similar structure: an MSE membrane and inside a magnetorheological fluid composed of iron and oil. The MF was produced by an adjustable electromagnet. These grippers can reach holding forces of high values due to the application of a magnetorheological fluid under a MF. Their capability to hold also depend on the housing, geometry, and composition.

In the Fig.2.7 the result of the deformed gripper designed by C. M. Hartzell [24] is shown. In this image, the influence of the housing is exhibited. Fig. 2.7a shows a housing that does not present an extra restriction, while Fig. 2.7b presents a collar housing that limits the radial deformations.

In Fig.2.8 the structure of the gripper developed by Y. Okatani and T. Nishida [25] is shown. Among the main characteristics of this gripper, is the using of a novel magnetorheological fluid called MR $\alpha$  fluid.

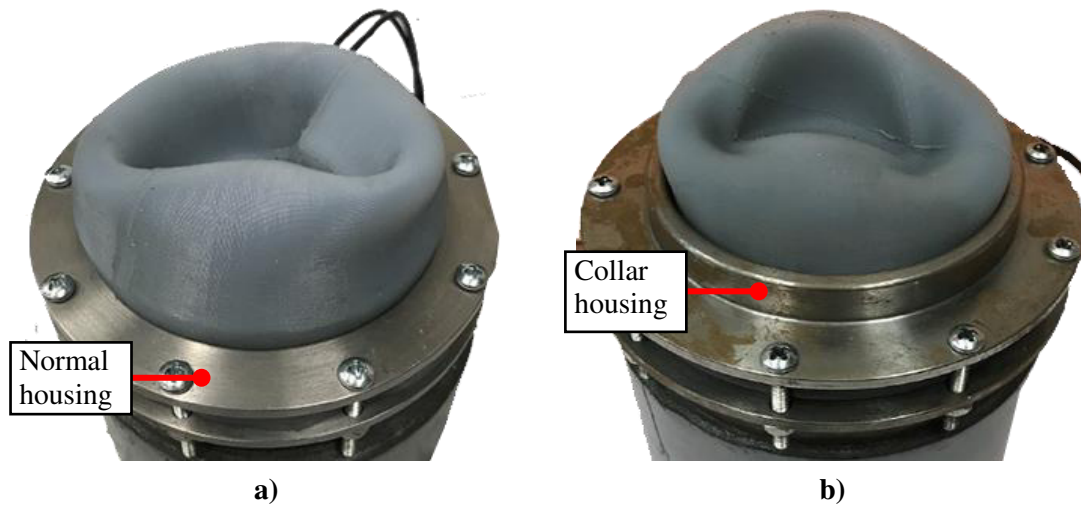


Fig. 2.7: Magnetorheological fluid-based gripper: Fig. a) with normal housing, Fig. b) with collar housing [24].

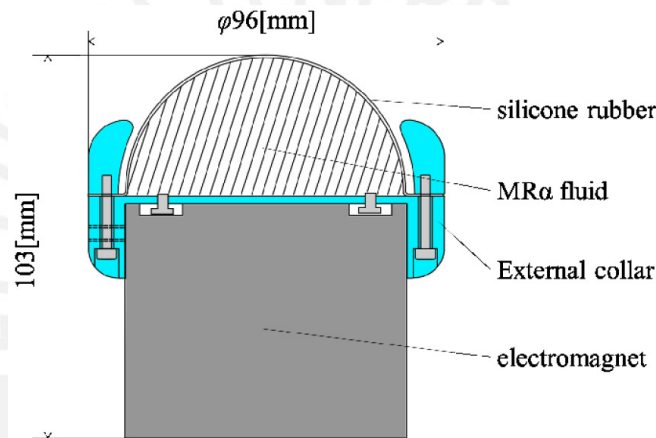


Fig. 2.8: Universal robot gripper using MR $\alpha$  fluid [25].

### Composite elastomer with magnetically shape-memory

In this work the shape-memory effect in magnetic composite elastomer was studied [4]. Although a gripper with this material was not fabricated, the results obtained by this author are useful to understand more about the behavior of magnetic composites under MFs.

The test performed to evaluate this effect followed these steps: a disk of the composite material was embossed with a certain profile. Then, a MF was applied and for several days the disk was under the same MF. The shape was retained for that time, but when the MF was removed, the disk recovered its initial form (Fig. 2.9). It can be concluded that shape-memory is presented as long as the MF is also present.

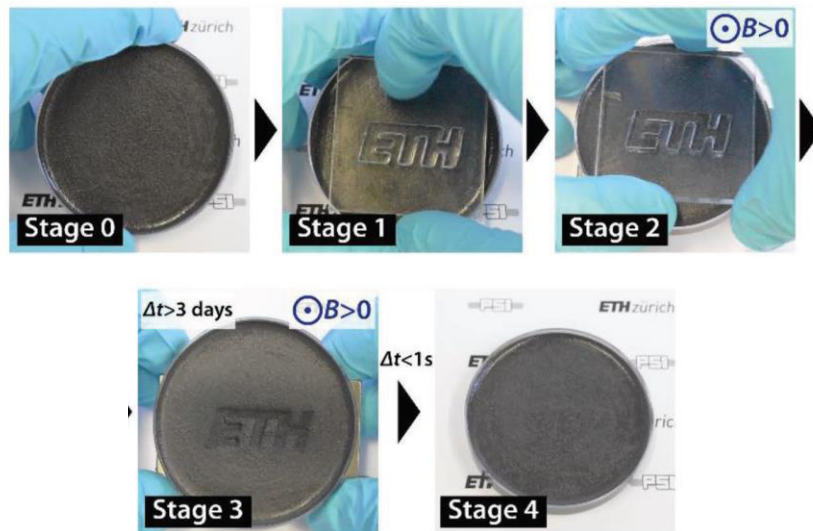


Fig. 2.9: Shape memory effect presented in composite elastomer [4].

### Versaball

Versaball is a jamming-based robotic gripper and is commercialized by EmpireRobotics. This gripper has a flexible membrane filled by granular material. This gripper provides some advantages: the capacity of grip a wide variety of randomly shapes objects and adapt the shape of the objects. Furthermore, it can change its stiffness by controlling the pressure of the air inside the gripper. The gripper is shown in Fig. 2.10.

This gripper operates in the following way: by modulating the air pressure the stiffness is reduced and the gripper is able to cover the object. After the shape of the object is copied, the stiffness increases and the object get hold by the gripper. To release the object, the pressure is reduced again.



Fig. 2.10 Versaball: jamming-based robotic gripper [26].

## 3. Experiments

For this thesis, several MSE samples were fabricated and tested in order to study the changing of properties related to soft robotics applications. In this chapter, for each test the fabrication of used samples is explained followed by the set up and finally, the analyzing of results.

First, the materials are described that were used for the elaboration of the MSE samples. Then, the whole procedure for the three required tests is explained: (i) attractive force due to a magnetic field, (ii) stiffness change due to a magnetic field, and (iii) deformation due to a magnetic field.

### 3.1. Materials for fabrication of samples

The magneto-sensitive elastomer is composed by a silicone matrix, magnetic particles and additives that give specific properties to the final material. Determining properly the components and their concentrations is a fundamental part of obtaining better mechanical properties and greater magneto-sensitive effects [3,27].

#### 3.1.1. Silicone matrix: Alpa-Sil Classic and Neukasil RTV 26

The silicone matrix is the elastomeric base for the MSE. Base in which are dispersed randomly the additives and magnetic particles. This base consisted of two components: a liquid silicone rubber base and a curing agent or catalyst.

In the first stage Alpa-Sil Classic was used. For a second stage a change of the materials provider was necessary, thus Neukasil RTV 26 was used that showed similar behavior regarding the properties and the processing.

#### Alpa-Sil Classic

At the beginning of the experiments and in previous works related to this thesis [17], the silicone matrix used was Alpa-Sil Classic provided by Alpina Technische Produkte GmbH. For this silicone, the base was component A and the curing agent was component B.

Relevant features pointed by the provider in terms of processing this material are the density:  $1.05\text{g/cm}^3$  and  $1.10\text{g/cm}^3$  for components A and B respectively. The hardness of the silicone produced: arranged to be from 6 to 8 in the Shore A scale. And the vulcanization time is a matter of minutes. Thus, the



processing time must be controlled and the carrying out should take around 5 to 10 minutes. Concluded that time, the vulcanization is started and it is not advisable to handle the mixture.

According to the provider, those components have a curing process by addition that provides advantages as far as production is concerned. E.g. the curing can be heat accelerated or can exhibit virtually no shrinkage when cured at room temperature.

For recommendation of the provider, the mass proportion followed between components A and B should be 10:1 respectively. And for a proper mixture stirring, the order of component addition into the beaker is as follows: component A is the first constituent of the mixture. Then, the additive that gives specific properties are added. Finally, component B is added.

In order to obtain a bubble-free vulcanized material, it is suggested to place the beaker with the mixture inside a chamber vacuum at the end of the stirring. Consequently, the gas trapped in the mixture is removed. It is essential to realize this process for the preservation of the magnetic permeability and the uniformity of the MSE [8].

In the appendix B are shown all the properties given by the provider for component A, component B and the silicone produced.

### **Neukasil RTV 26**

The new silicone selected and used to continue the thesis was Neukasil RTV 26 provided by Altropol. For this silicone, the base was Neukasil RTV 26 and the curing agent was Neukasil crosslinker A7.

Important features given for the silicone provider in terms of processing these materials are the density:  $1.2 \text{ g/cm}^3$  and  $0.96 \text{ g/cm}^3$  for the base and the crosslinker respectively. The hardness of the silicone produced: approximately 7 in the Shore A scale, reaching a similar value to Alpa-Sil Classic. The mixture viscosity before vulcanization: approximately value of 6250 cSt at  $25^\circ\text{C}$ . And vulcanization time: above 24 hours at  $20\text{-}25^\circ\text{C}$ . Despite the long time to complete the vulcanization, its speed is also temperature dependent, hence it can be accelerated by increasing the temperature.

According to the provider those components have a curing process by addition-crosslinking without separation of reaction products. And the mass mixing ratio between the base and the crosslinker should be 5:2 respectively. With this mass ratio is obtained a mixture with  $1.12 \text{ g/cm}^3$  density. Furthermore, appendix C shows the properties given by the provider for both components and the vulcanized mixture.

As well as for Alpa-Sil Classic, in order to obtain a bubble-free vulcanized mixture, it is suggested to use a chamber vacuum at the end of the blending. And it is important to realize that process to accomplish the preservation of the same properties already mentioned [8].

### 3.1.2. Silicone oil

Additive used for both silicone bases previously mentioned. The silicone oil used was Xiameter PMX-200 silicone fluid 500 cSt with 0.97 g/cm<sup>3</sup> density and it was provided by Xiameter. This additive is also described in Sec. 2.3 but for more information and properties given by the provider, review appendix D.

### 3.1.3. Iron powder

The carbonyl iron powder (CIP) works as the magnetic particles that the MSE requires. This is the component that gives the magnetic properties to the mixture. The concentration, particle size and permeability are the main properties that should be considered when a magnetic particle is selected. The CIP was provided by BASF Chemical Company. And it was presented in different grades depending on several characteristics. The used grade was CEP CC with a 99.5% minimum percentage of iron, and the 90% of the particles has size of 6.5-10 µm. For more property details of the CIP, review appendix E.

A summary of the main properties of the MSE components is presented in Tab. 3.1.

Tab. 3.1: Properties of silicone matrix, silicone oil and magnetic particles.

Silicone matrix	Alpa-Sil classic	Neukasil RTV 26
cinematic viscosity [cSt]	-	6250
density [g/cm <sup>3</sup> ]	1.05	1.12
hardness [Shore A]	6-8	7
vulcanization temperature [°C]	23	20-25
vulcanization time	30 min	24 hours
Silicone oil	Xiameter PMX-200	
cinematic viscosity [cSt]	500	
density [g/cm <sup>3</sup> ]	0.97	
appearance	Crystal clear	
Magnetic particles	Carbonyl iron powder	
grade	CEP CC	
Fe min [%]	99.5	
d90 [µm]	6.5-10.0	

### 3.2. Attractive force on MSE samples due to a magnetic field

The aim of this test is to determine and characterize the attractive forces produced by a magnetic field on MSE cylinders. This MF was generated by the permanent magnet: disc shape 70 mm diameter and a 35 mm height;  $B_r$  of 1.32-1.37 T;  $bH_c$  of 860-995 kA/m and  $iH_c$  above 955 kA/m. The MSE cylinders were coaxially located with the cylindrical magnet and above it. In order to reach different intensities of magnetic fields the sample was being approached to the magnet and located at different distance. Finally, the obtaining of the attractive forces consisted of measuring the force exerted on the sample located at different distances respect to the magnet.

For this test several samples were fabricated varying its concentrations and dimensions. This was realized with the purpose of analyzing in regards to the attractive forces: (i) the influence of the iron concentration, (ii) the influence of the silicone oil's presence, and (iii) the accumulative effect.

#### 3.2.1. Sample for test: cylinders of different size

The MSE samples for this test were made of Alpa-Sil Classic, silicone oil 500 cSt and CIP. As it was mentioned, samples of various compositions and sizes were produced for certain purposes related to the attractive forces.

The materials concentrations used for the fabrication of the below MSE samples were based on previous works from the same research area to which this thesis belongs [17,18,28].

The concentrations in volume (vol.) used from this test were calculated as follows: the iron vol. is 10%, 20%, 30%, 40% of total vol. Then, silicone oil (sil. oil) vol. is 0%, 45% of total vol. The remaining vol. corresponds to the elastomer vol. and it is calculated from the difference of total vol. and iron plus sil. oil vol. This elastomer vol. is distributed between the components A and B. In the recommended mass ratio A:B (10:1), the silicone oil mass replaced an amount of component A, changing the mass ratio to sil. oil+A:B (10:1). The diagram shown in Fig. 3.1 helps to understand the calculations.

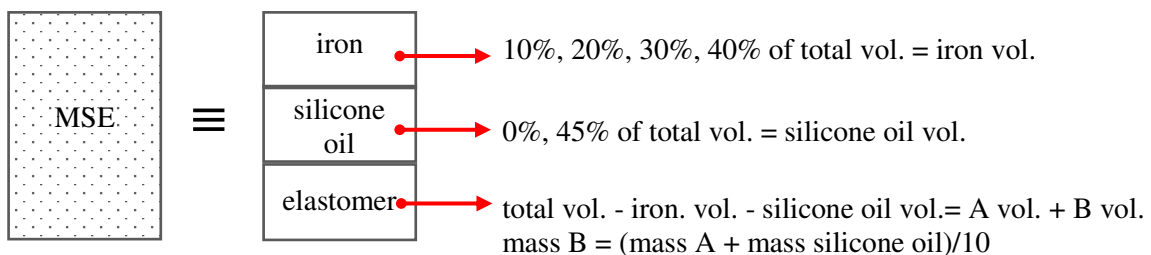


Fig. 3.1: Diagram of volume distribution for MSE.

First, for analyzing the influence of the iron concentration on the attractive forces, were fabricated the following samples. MSE cylinders with dimensions: 16 mm diameter ( $\emptyset$ ) and 12 mm height (H) as is shown in Fig. 3.2a. There were four compositions mainly characterized for the absence of silicone oil and for the four volumetric percentages of iron: 10%, 20%, 30%, 40%. Four samples of each concentration type were fabricated, giving a total of 16 samples. The mass compositions, volume compositions and volumetric percentage of each concentration are shown in Tab. 3.2.

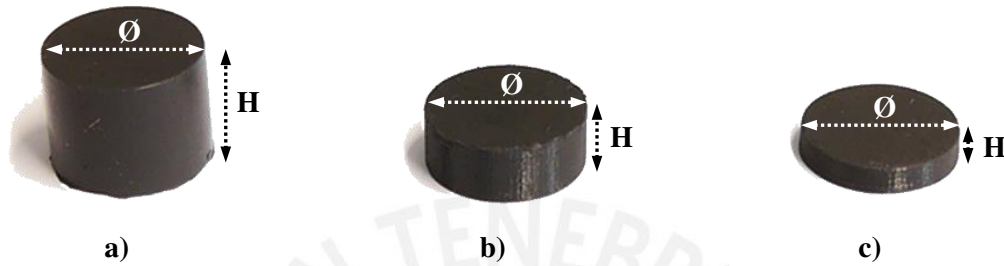


Fig. 3.2: MSE cylinders: Fig. a)  $\emptyset 16 \times H12$ , Fig. b)  $\emptyset 16 \times H6$ , Fig. c)  $\emptyset 16 \times H3$ . Units: diameter  $\emptyset$  [mm], height H [mm].

Tab. 3.2: Mass, volume and volumetric percentage for the concentrations of MSE cylinders  $\emptyset 16 \times H12$  without silicone oil and 10%, 20%, 30%, 40% vol. iron. Units: mass [g], vol. [ $\text{cm}^3$ ], %vol. [%].

Cylinder $\emptyset 16 \times H12$	10%vol. iron			20%vol. iron			30%vol. iron			40%vol. iron		
	mass	vol.	%vol.	mass	vol.	%vol.	mass	vol.	%vol.	mass	vol.	%vol.
Comp. A	2.081	1.98	82.16	1.850	1.76	73.03	1.619	1.54	63.90	1.388	1.32	54.77
Iron	1.899	0.24	10.00	3.798	0.48	20.00	5.696	0.72	30.00	7.595	0.97	40.00
Comp. B	0.208	0.19	7.84	0.185	0.17	6.97	0.162	0.15	6.10	0.139	0.13	5.23
Total	4.188	2.41	100.0	5.833	2.41	100.0	7.477	2.41	100.0	9.122	2.41	100.0

Then, for analyzing the influence of the silicone oil's presence on the attractive forces, the samples described below were fabricated. MSE cylinders with dimensions: 16 mm diameter ( $\emptyset$ ) and 12 mm height (H) as is also shown in Fig. 3.2a. As the main focus was put on the influence of the silicone oil, the fabrication of samples with several iron concentrations was not required. For this reason, there were only three compositions mainly characterized for the 45% vol. silicone oil and three volumetric percentages of iron: 10%, 20%, and 30%. Furthermore, four samples of each concentration type were fabricated, giving a total of 12 samples. The mass compositions, volume compositions and volumetric percentage of each concentration are shown in Tab. 3.3.

Tab. 3.3: Mass, volume and volumetric percentage for the concentration of MSE cylinders Ø16xH12 with 45%vol. silicone oil and 10%vol., 20%vol., 30%vol. iron. Units: mass [g], vol. [cm<sup>3</sup>], %vol. [%].

Cylinder Ø16xH12	45%vol. sil. oil 10%vol. iron			45%vol. sil. oil 20%vol. iron			45%vol. sil. oil 30%vol. iron		
	mass	vol.	%vol.	mass	vol.	%vol.	mass	vol.	%vol.
Comp. A	0.949	0.90	37.46	0.718	0.68	28.33	0.486	0.46	19.20
Sil. oil 500cSt	1.053	1.09	45.00	1.053	1.09	45.00	1.053	1.09	45.00
Iron	1.899	0.24	10.00	3.798	0.48	20.00	5.696	0.72	30.00
Comp. B	0.200	0.18	7.54	0.177	0.16	6.67	0.154	0.14	5.80
Total	4.101	2.41	100.00	5.746	2.41	100.00	7.390	2.41	100.00

To complete the third analysis, the accumulative effect on the attractive forces, additional samples were produced. MSE cylinders with two different sizes: 16 mm diameter (Ø) with 6 mm height (H) and 16 mm diameter (Ø) with 3 mm height (H) as are also shown in Fig. 3.2b and Fig. 3.2c respectively. Because the influence of the iron concentration and the silicone oil's presence on the attractive forces were already analyzed, was not required the fabrication of samples with several iron concentrations neither the using of silicone oil. Considering this, there were only two compositions principally characterized absence of silicone oil and two volumetric percentages of iron: 10%, 20%. Four samples of each concentration type and each size were fabricated, giving a total of 16 samples. And the mass composition for each concentration is shown in Tab. 3.4.

Tab. 3.4: Mass composition for cylinders Ø16xH6 and Ø16xH3, MSE without silicone oil and 10%, 20% vol. iron.

Mass composition [g]	Cylinder Ø16xH6		Cylinder Ø16xH3	
	10%vol. iron	20%vol. iron	10%vol. iron	20%vol. iron
Comp. A	1.041	0.925	0.520	0.463
Iron	0.949	1.899	0.475	0.949
Comp. B	0.104	0.093	0.052	0.046
Total	2.094	2.916	1.047	1.458

### 3.2.2. Testing configuration

To accomplish the measuring the attractive forces on the MSE samples due different intensities of MF, an experimental setup was configured as is illustrated in Fig. 3.3. The principal components of the setup were: (i) permanent magnet described on Sec. 2.4, (ii) MSE cylinder contained in a housing (used to handle the sample in a controlled volume), and (iii) force sensor.

The MF induced by the permanent magnet generates forces directed towards the magnet core. For this reason and in order to obtain a higher and more uniform magnetic flux through the sample, the MSE cylinder was placed above the magnet by matching its symmetric axes.

Tab. 3.5: Average magnetic field for the samples for different distances between the magnet upper surface and MSE cylinder bottom.

Distance magnet upper surface - MSE cylinder bottom [mm]	Average MF for the sample [mT]
5	328.6
10	271.6
15	222.1
20	180.8
25	147.1
30	120.1
35	98.6
40	81.4
45	67.8
50	56.8
55	48.0
60	40.8

The MF values were calculated with the equation 1 mentioned in Sec. 2.4. Additionally, it was considered a relative permeability ( $\mu_r$ ) equal to 1 for every MSE cylinders, due to measuring of the MF in each point of the samples would be complex during the experiments. In Tab. 3.5 the values are shown for the average magnetic field within the samples at different vertical distances from the magnet upper surface to the MSE cylinder bottom. The average of MF was obtained with values calculated each 0.5 mm, from the bottom to the top of the MSE cylinder, located at each step shown in the first column of Tab. 3.5. It should be noted that the shortest distance is 5 mm due to the thickness of the housing bottom (see Fig.3.3).

To reach the different intensities of MF above the MSE, the sample was moved to different heights using the linear axis while the magnet stayed fixed to the setup base. Starting from a certain distance, the sample was approaching to the magnet upper surface and stopping for instants at each step. Thereby, the measuring of the attractive forces was realized using the force sensor (see Fig.3.3) during the instants in which the sample was stopped at the different distance from the permanent magnet. The force sensor had a range of work from -20N to +20N. And to review more information about it, refer to appendix F.

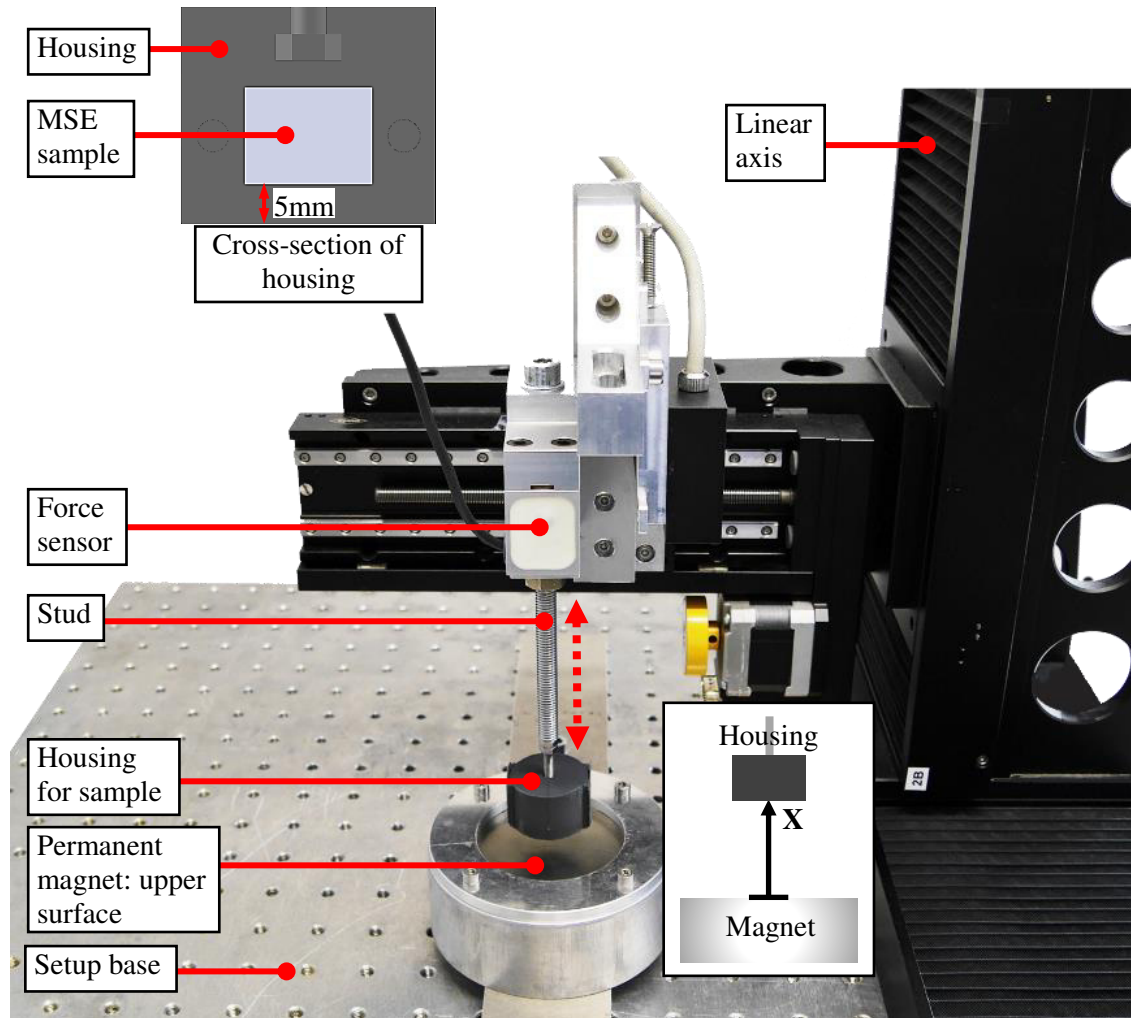


Fig. 3.3: Configuration of the setup for attractive forces measurement.

Additionally, it was taken into account that the housing and stud used to handle the samples had influence in the force sensor measurements. The weight or a possible attraction by the magnetic field would represent extra forces. Hence, those forces were also measured in order to get separately the attractive forces on the MSE samples.

### 3.2.3. Testing results

#### Influence of the iron concentration on attractive forces

In order to understand the effect of the iron concentration on the attractive forces exerted above the MSE. It was carried out the testing and forces measuring using the samples of dimensions:  $\text{Ø}16 \times \text{H}12$  and concentrations: 00%vol. silicone oil and 10%, 20%, 30%, 40% vol. iron (see Tab. 3.2). The 16 samples were tested once, obtaining one batch of results per sample. An average of the results obtained (attractive forces) was calculated with the samples of each concentration. Additionally, the error of each average was calculated by the division of the standard deviation of the results obtained (attractive forces)

by the average. The errors are: 2.76%, 0.60%, 0.54%, and 0.67% for concentrations 10%, 20%, 30%, and 40% vol. iron respectively. With these values was plotted the graph shown in Fig. 3.4.

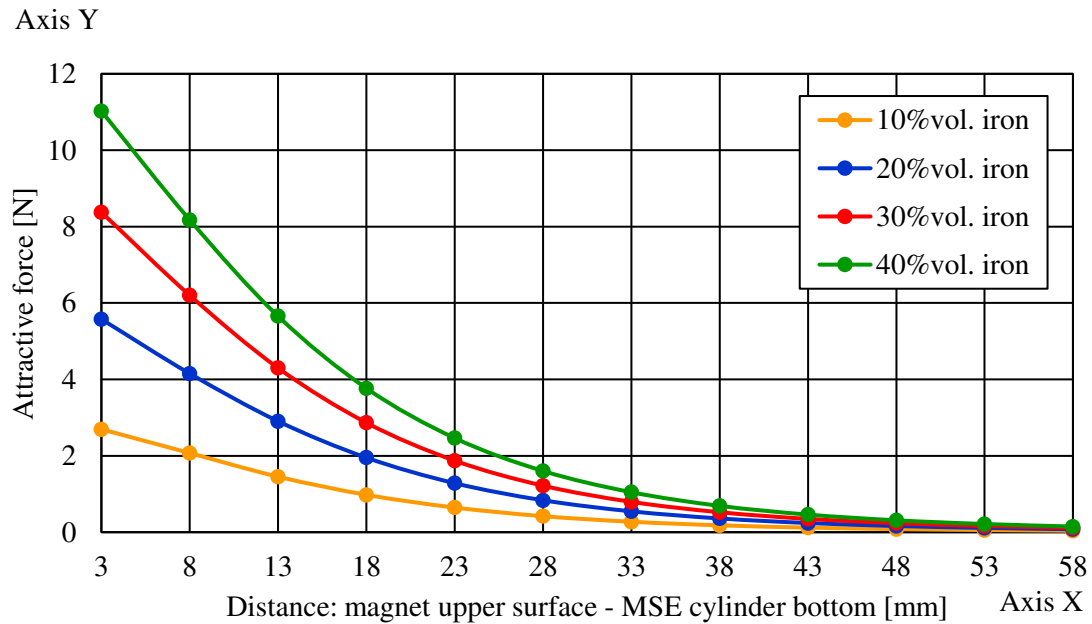


Fig. 3.4: Attractive forces evaluated at different distance: magnet upper surface - MSE cylinder bottom, for samples of MSE with 00%vol silicone oil and 10%, 20%, 30%, 40% vol. iron.

The plotted curves of attractive forces for MSE of each concentration in Fig. 3.4 got a behavior and tendency of results as the expected, taking into account the source reviewed on Sec. 2.4. Moreover, making a comparison between the curves shown in Fig. 3.4 and Fig. 2.5, it can be clearly noticed the similarity between them. And the clear difference of forces is due to the iron amount used in each case: iron powder dispersed in an elastomeric matrix and a solid iron plate for Fig. 3.4 and Fig. 2.5 respectively. Therefore, the iron effectively provides the MSE sample with ferromagnetic properties.

It can be observed also that the results of attractive forces (Fig. 3.4) adopt similar tendencies between them. Reducing rapidly its attractive force values while increasing the distance values. Additionally, the forces approach values near 0 N for the largest distances (43-58 mm).

Another observation is that the attractive force curves for each concentration were plotted one above the other (see Fig.3.4). The ascending order is as follows: MSE with 10%, 20%, 30%, and 40%vol. iron. Thereby, the attractive forces for MSE with higher iron concentrations are placed above the ones with lower concentrations. E.g. the maximum attractive forces obtained at distance (axis X in Fig. 3.4) 3 mm for each concentration: 2.69 N, 5.57 N, 8.37 N, and 11.02 N for 10%, 20%, 30%, and 40% vol. iron respectively. Therefore, the iron concentration on the MSE favorably influences the increase in attractive forces. This is also demonstrated with the graph of maximum attractive force vs iron concentration that



shown in Fig. 3.5. From this graph, it is possible to see a linear relation between the maximum attractive force and the iron concentration.

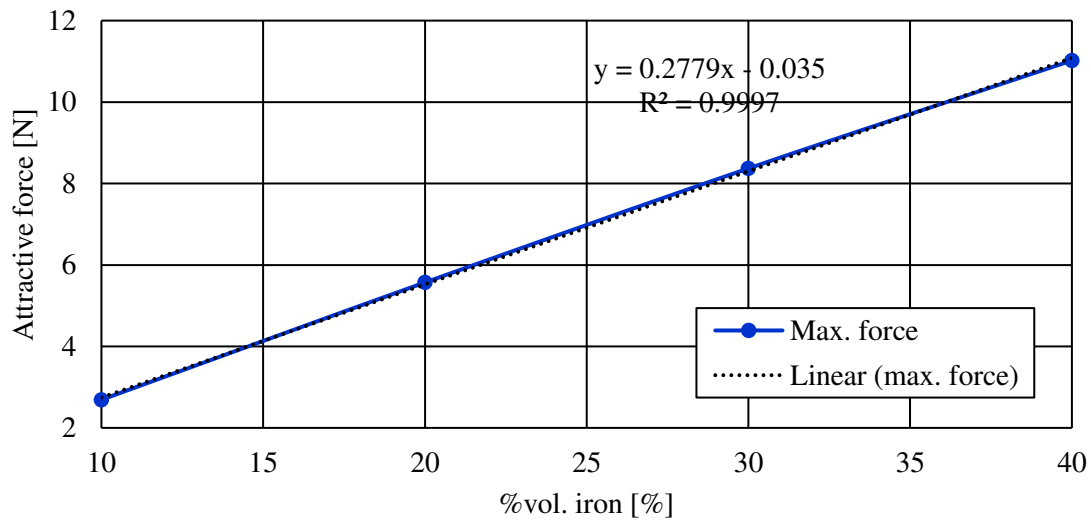


Fig. 3.5: Maximum attractive forces - %vol. iron concentration.

Additionally, a comparison was made between the values of attractive forces by concentration of iron and it was obtained that these were increasing proportionally. In order to present that proportionality, the average ratio of attractive forces between the three highest iron concentrations (20%, 30% and 40%vol.) and the lowest concentration (10%vol.) is shown in Tab. 3.6.

Thus, with respect to the samples with 10%vol. iron, those with 20%, 30%, and 40%vol. iron obtained an attractive force to the magnet approximately equal to 2, 3 and 4 times respectively. These ratios are the same in terms of the concentrations of iron. Accordingly, can be considered as directly proportional to the relation between attractive forces to the magnet and the iron concentration on the MSE samples.

Tab. 3.6: Attractive force ratio between cylinders Ø16xH12 of MSE: 00%vol. silicone oil and 20%, 30%, 40% vol. iron with respect to 10% vol. iron.

Cylinder Ø16xH12		
Ratio of forces with respect to forces of MSE 10 vol% iron		
20%vol. iron	30%vol. iron	40%vol. iron
2.002	2.925	3.853

As is shown in Fig. 3.4 the attractive force reaches higher values while the distance: magnet upper surface - MSE cylinder bottom decrease. This behavior is expected because the attractive forces on the MSE are caused by a magnetic field which its intensity increases when the distances to the magnet get shorter, as Sec. 2.4 explained. According to this, it could be suggested that the magnetic effects of the MSE increase when working close to the magnet.

### Influence of the silicone oil's presence on attractive forces

It is sought to understand the effect of the silicone oil by means of the attractive forces analysis since this research is oriented to soft robotics applications (grippers) made of an MSE with a considerable oil concentration. According to this, additional samples were tested. These samples had the following dimensions:  $\varnothing 16 \times H 12$  and concentration: 45%vol. silicone oil and 10%, 20%, 30% vol. iron (see Tab. 3.3). The 12 samples were tested once, obtaining one batch of results per sample. An average of the results obtained (attractive forces) with the samples of each concentration was calculated. Additionally, the error of each average was calculated by the division of the standard deviation of the results obtained (attractive forces) by the average. The errors are: 0.96%, 0.79%, and 0.83% for concentrations 10%, 20%, and 30% vol. iron respectively. Based on these results, the graph shown in Fig. 3.6 was plotted. In this graph (Fig. 3.6) are also plotted the results for MSE without silicone oil shown in Fig. 3.4 but only of the concentrations 10%, 20% and 30% vol. iron.

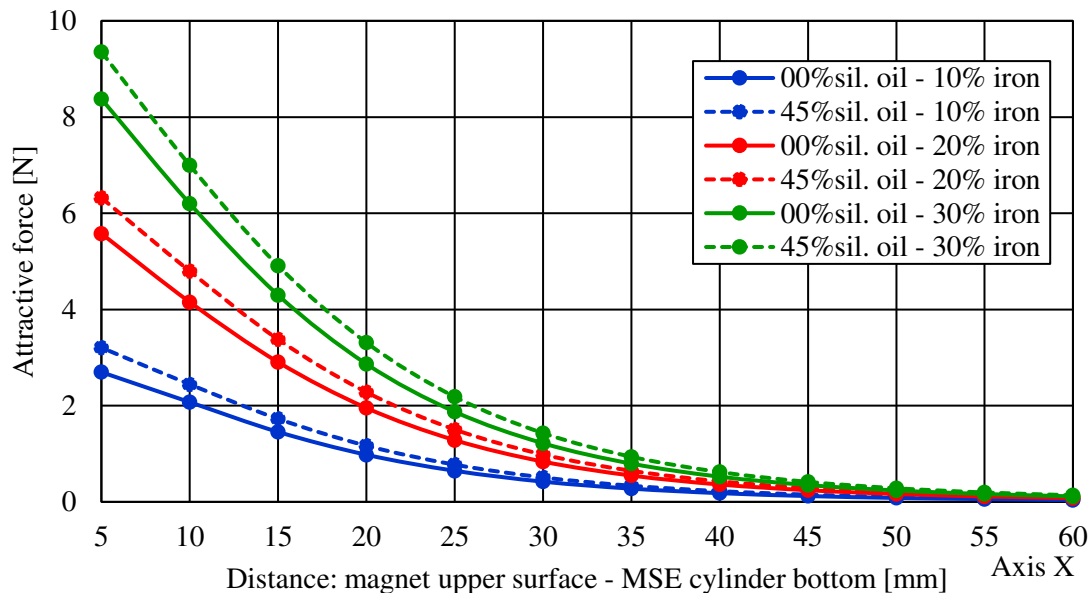


Fig. 3.6: Attractive forces evaluated at different distance magnet upper surface - MSE cylinder bottom, for samples MSE 00%vol. silicone oil and MSE 45%vol. silicone oil.

The curves of attractive forces for MSE samples with the 45%vol. silicone oil samples also followed the two expected results. First it is seen that the forces decrease as the distance to the magnet increases [29]. It can also be seen that the forces increased proportionally to the concentrations. Making a comparison again with respect to the results obtained for 10%vol. iron, Tab. 3.7 is obtained. In which it is seen that the results were double and triple for 20%vol. and 30%vol. respectively.

Tab. 3.7: Attractive force ratio between cylinders of MSE: 45%vol. silicone oil and 20%, 30%vol. iron with respect to 10%vol. iron.

Cylinder Ø16xH12		
Ratio of measured forces with respect to forces of MSE 10 vol% iron		
45%vol. sil. oil 10%vol. iron	45%vol. sil. Oil 20%vol. Iron	45%vol. sil. Oil 30%vol. iron
1.000	1.933	2.807

In Fig. 3.6 it is also observed that the results of attractive forces for samples with 45%vol. silicone oil are above the results of samples without silicone oil. This indicates that the MSE sample with silicone oil is experiences a greater attractive force. It should be noted that the iron mass and iron volume concentration for both samples, with and without silicone oil, is the same as shown in Tab. 3.2 and Tab. 3.3.

The influence of the presence of the silicone oil in the samples is best explained by a percentage comparison of the increase in forces as shown in Tab. 3.8. The increase in forces might be attributed to the characteristics that oil would give iron particles [12], as is explained in Sec. 2.3. This characteristic refers to the possibility of partially allowing the rearrangement or alignment regarding the flow lines of the magnetic field. Thus, it is raised the hypothesis that the alignment of the particles would contribute to greater magnetorheological effects. Effects that also includes a higher attractive force in comparison to disordered particles and with greater difficulty of alignment to the magnetic field.

Tab. 3.8: Force increase for MSE with 45%vol. silicone oil respect to MSE with 00%vol. silicone oil.

Cylinder Ø16xH12		
Force increases 45%vol. sil. oil respect to 00%vol. sil. oil		
10% vol. iron	20% vol. iron	30% vol. iron
17.87%	14.94%	14.43%

### Accumulative effect on attractive forces

The accumulative effect describes the capacity to sum the properties measures of small bodies to obtain the properties measure of a larger body. In order to understand the accumulative effect of the attractive forces realized on the MSE. It was carried out also the forces measuring of samples with two smaller dimensions (see Fig. 3.2b and Fig. 3.2c) with concentrations: 10%, 20% vol. iron (see Tab. 3.4).

The 16 samples were tested once, obtaining one batch of results per sample. An average of the results obtained (attractive forces) with the samples of each concentration and size was calculated. The error of the averages was calculated in the same way as the previous ones. These errors are: 4.05%, 1.79%, for dimension Ø16xH6 and Ø16xH3 of concentration 10%vol. iron respectively; and 1.16%, 1.76% for

dimension  $\text{Ø}16 \times \text{H}6$  and  $\text{Ø}16 \times \text{H}3$  of concentration 20%vol. iron respectively. Sums were performed with the forces of two 6 mm height samples, located every 6 mm at the measurement points (see Fig. 3.7). Other sums were also performed with forces of 4 contiguous test pieces of 3 mm height (see Fig. 3.7). With the results of these sums and the forces of the 12 mm height samples, a graph of accumulated attractive force - distance to the magnet is plotted and shown in Fig. 3.8.

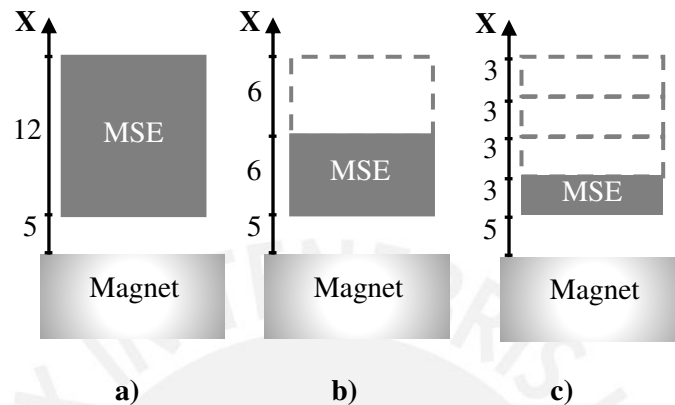


Fig. 3.7: Diagram of contiguous positions for MSE samples: Fig. a)  $\text{Ø}16 \times \text{H}12$ , Fig. b)  $\text{Ø}16 \times \text{H}6$ , and Fig. c)  $\text{Ø}16 \times \text{H}3$ . Units: [mm].

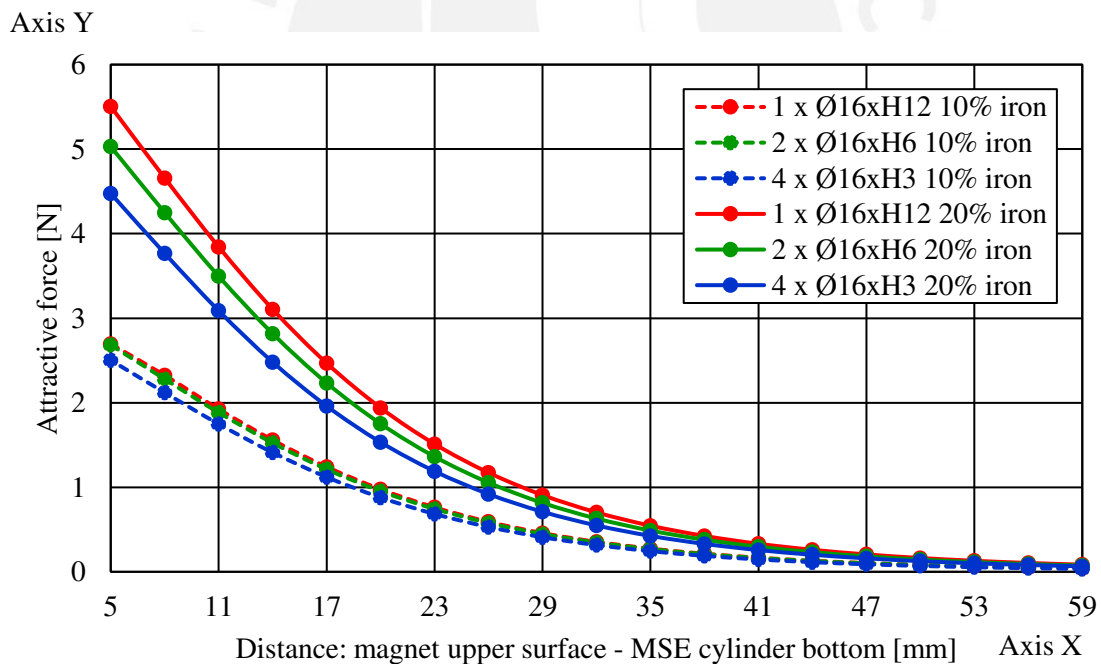


Fig. 3.8: Accumulated attractive force for MSE: 00%vol. silicone oil and 10%, 20% vol. iron.

The graph (Fig. 3.8) shows the results of the sums of forces, but these results were not exactly as expected. It was expected that the sums of forces would reach approximately the same values, for both the concentration of 10% iron and 20% iron.

The differences observed between the results of the sums forces may be due to sources of error during the sample fabrication (mass error) or the forces measuring. In the Tab. 3.9 is shown the theoretic and

average real masses besides the mass error. From the values shown (Tab. 3.9), it is observed that the greatest errors are given for the test pieces of Ø16xH3. This is also reflected in Fig. 3.8 that shows a greater difference between the sum forces curves for 1 x Ø16xH12 and 4 x Ø16xH3 in both concentrations. As well as a smaller difference between the sum forces curves for 1 x Ø16xH12 and 2 x Ø16xH6 in both concentrations, since the error between of theoretical and real mass for these is smaller. In order to demonstrate a relation between attractive forces and the mass error, a graph of maximum force – mass error is plotted and shown in Fig. 3.9. From this graph is possible to see a linear curve that confirms a simple relation between the accumulated force and the mass error. Following the linear regressions with high coefficient of determination (Fig. 3.9), possible values can be obtained for accumulated forces with mass error 0%. The values are: 6.012 N and 2.762 N for concentration 10% and 20% vol. iron respectively.

Tab. 3.9: Comparison of theoretical and real mass for MSE samples.

	Theoretical mass [g]	Average real mass [g]	Mass error [%]
00%vol. sil. oil - 10%vol. iron			
Ø16xH12	4.19	4.12	1.59%
Ø16xH6	2.09	1.98	5.37%
Ø16xH3	1.05	0.95	9.61%
00%vol. sil. oil - 20%vol. iron			
Ø16xH12	5.83	5.67	2.73%
Ø16xH6	2.92	2.73	6.53%
Ø16xH3	1.46	1.33	8.59%

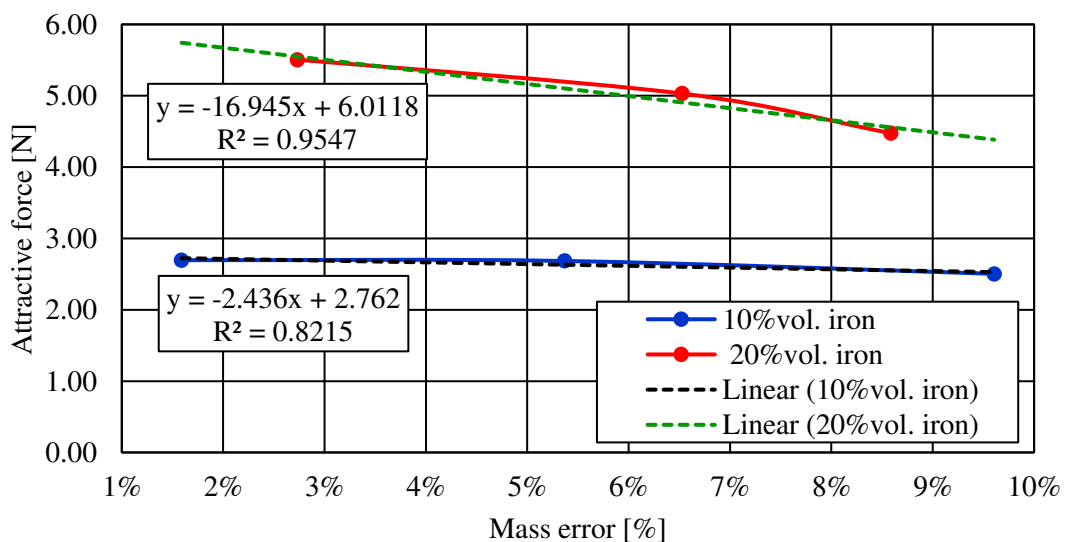


Fig. 3.9: Maximum accumulated attractive force vs mass error for MSE: 00%vol. silicone oil and 10%, 20% vol. iron.

Given the results on Tab. 3.9 and Fig. 3.9, it can be considered the existence of the source of error on the masses of the samples. Furthermore, despite the differences between the curves of attractive forces

sums (Fig. 3.8) a certain approaching between the curves is reached. Therefore, it would be hypothesized that the attractive forces on the MSE exhibit an accumulative effect and it may be increased by reducing the sources of error.

Considering the accumulative effect presented by the MSE, it can be understood that an MSE sample can be discretized in small parts and distribute its effect (attractive force) proportionally to the size of those parts. It is observed that the forces of two 6 mm height samples located one above the other (Fig.3.7) would add an approximate force to the 12 mm sample. In the same way, the force of four 3 mm samples (Fig.3.7) add up to a force of approximately 12 mm sample. By having the same behavior for the 10% and 20% iron samples, it can be indicated that the discretization of the attractive forces will be independent of the iron concentration of the MSE sample.

### 3.3. Stiffness changes due to a magnetic field

The aim of this test is to determine the influence of the MFs on the MSE properties, mainly the stiffness. Compression tests under different MFs were carried out for MSE cylinders of several concentrations. The variation of the MF magnitudes was reached by moving the permanent magnet away and close to the MSE samples. The results obtained with this test were analyzed and used to determine the MSE concentration able to offer better properties for soft robotics applications (grippers).

As it was mentioned on Sec.3.1.1, the silicone matrix was changed and obtaining as components for the MSE: Neukasil RTV 26, silicone oil 500cSt, and CIP. Consequently, the concentrations were also changed looking for improvements. The concentrations in volume (vol.) used from this test onwards were calculated as follows: the iron vol. is 10%, 20%, 30%, 40% of total vol. Then, the remaining vol. is calculated from the difference of total and iron volumes. This remaining vol. is distributed between the silicone oil and the elastomer RTV 26. The silicone oil vol. is calculated from the 45% of the remaining vol. while the other 55% of volume correspond to the elastomer vol. The diagram shown in Fig. 3.10 helps to understand the calculations.

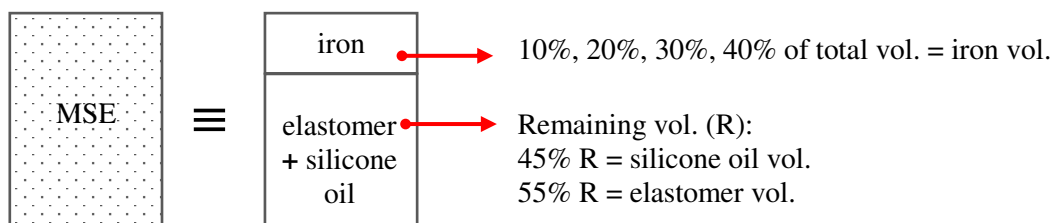


Fig. 3.10: Diagram of volume distribution for MSE.

When the elements are mixed, the elastomer and the silicone oil form an elastomeric matrix that serves to contain the iron particles. Taking this into account in addition to the new proportion between the matrix components, it can be concluded that the matrix will have a volumetric concentration of 45% silicone oil, independently of the iron concentration in the MSE.

Therefore, for all the tests the same elastomeric matrix was used. This provides mainly two characteristics: greater uniformity over the fabrication of the MSE and more order in the property comparison depending on the composition.

The samples used for the compression test were MSE cylinders with dimensions: 16 mm diameter ( $\emptyset$ ) and 12 mm height (H) as is shown in Fig. 3.2a. There were four compositions mainly characterized for the matrix 45%vol. silicone oil and the four volumetric percentages of iron: 10%, 20%, 30%, and 40%. Four samples of each concentration type were fabricated. The mass compositions and volumetric percentage of each concentration are shown in Tab. 3.10.

Tab. 3.10: Mass and volumetric percentage for cylinder  $\emptyset$ 16xH12 of MSE matrix 45%vol. silicone oil and 10%, 20%, 30%, 40%vol. iron. Units: mass [g], %vol. [%].

Cylinder $\emptyset$ 16xH12	Matrix 45%vol. sil. oil - 10%vol. iron		Matrix 45%vol. sil. oil - 20%vol. iron		Matrix 45%vol. sil. oil - 30%vol. iron		Matrix 45%vol. sil. oil - 40%vol. iron	
	mass	%vol.	mass	%vol.	mass	%vol.	mass	%vol.
RTV 26	0.955	33.00	0.849	29.33	0.743	25.67	0.637	22.00
Sil. oil 500cSt	0.948	40.50	0.843	36.00	0.737	31.50	0.632	27.00
Iron	1.899	10.00	3.798	20.00	5.696	30.00	7.595	40.00
A7	0.382	16.50	0.340	14.67	0.297	12.83	0.255	11.00
Total	4.184	100.00	5.829	100.00	7.474	100.00	9.119	100.00

This test was based mainly on the compression of the test samples made of MSE under the influence of a magnetic field. For this, the standard ISO 7743: Rubber, vulcanized or thermoplastic – Determination of compression stress-strain properties, was used adding the required conditions for this thesis. These conditions are: the use of a different type of material (MSE) to the one commonly tested with the ISO 7743 and the application of an MF during the test which is not considered by the ISO 7743.

For the performance of the test, the use of the setup shown in Fig. 3.11 was required. The MSE sample is placed between the upper and lower compression plates. The upper compression plate is connected to the force sensor by a stub. While the lower compression plate is fixed to the cylindrical support. The cylindrical support is also used to move the permanent magnet away and close to the MSE samples. In addition, a thin layer of oil was placed in both compression plates in order to reduce friction with the samples, as recommended in ISO 7743. To prevent that the sample could escape from the compression area, the lower compression plate was designed with a hole of higher diameter than the sample and 2 mm depth.

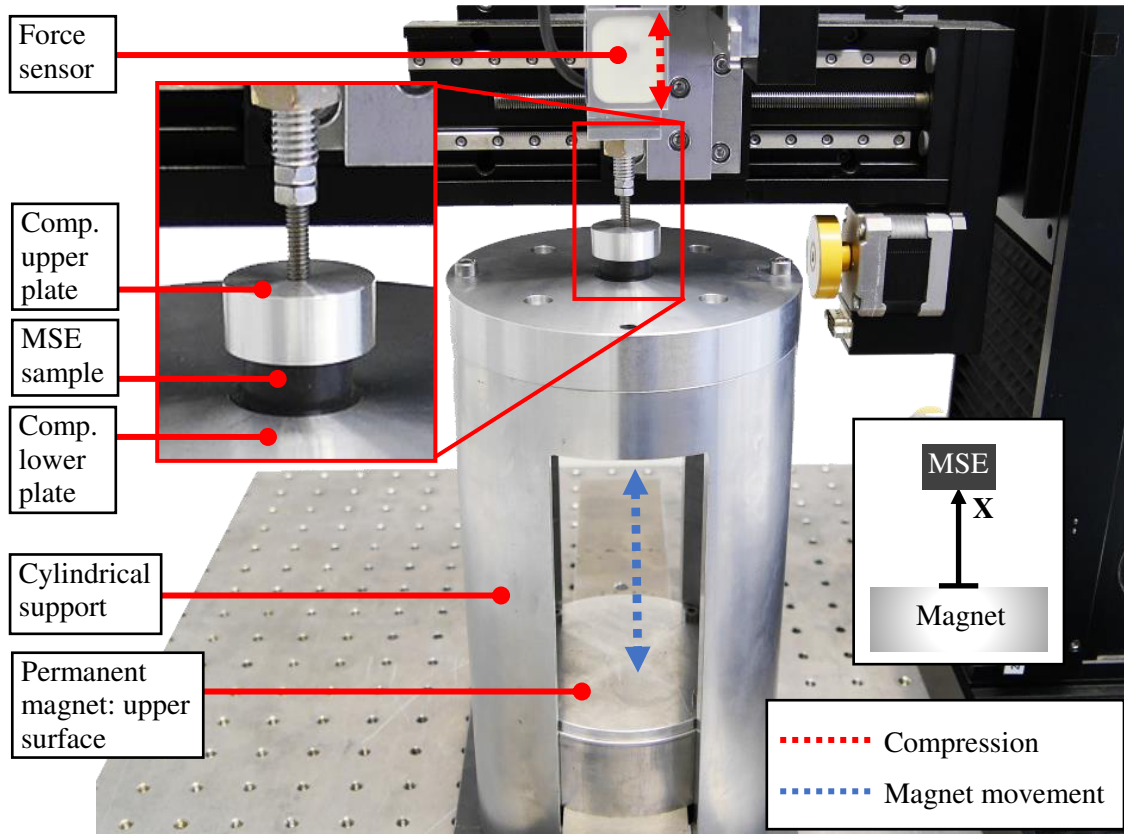


Fig. 3.11: Configuration of the setup for compressive forces measurement.

This test was divided into three parts, the first was the compression for initialization of the samples in the absence of a MF. The second part consisted on the compression and force measurement performed in the absence of a MF. And the third part consisted on the compression and force measurement carried out in the presence of MFs with different magnitudes.

To obtain a MF of magnitude 0 mT, the permanent magnet shown in the setup (Fig. 3.11) was retrieved. And in order to obtain different magnitudes of MF above the MSE sample, the permanent magnet moved to different heights. In the setup, it can be observed that the cylindrical support was designed to allow the displacement of the magnet in the vertical direction. The magnet was placed in five different positions so the samples could be under different intensities of the MF generated by the permanent magnet. The location was measured by the distance from the magnet upper surface to the MSE cylinder bottom. Tab. 3.11 shows the locations and the magnitudes of the average MF within the sample, including the case without MF. The values shown in Tab. 3.11 were calculated in the same way as in Sec. 3.2.2, using the equation 1, considering a relative permeability ( $\mu_r$ ) equal to 1 for every MSE cylinders, and with an average of the magnitudes for MF each 0.5 mm from the bottom to the top of the MSE samples.



Tab. 3.11: Average magnetic field for the samples at different distances between the magnet upper surface and MSE cylinder bottom.

	Average MF for the sample [mT]	Distance magnet upper surface - MSE cylinder bottom [mm]
MF_0	0	inf.
MF_1	8.0	126
MF_2	78.5	41
MF_3	94.8	36
MF_4	115.4	31
MF_5	141.2	26

The compression test of the MSE samples was carried out by placing the samples above the hole of the compression lower plate. Then, the compression upper plate was descending with a constant speed of 0.2 mm/s until a setup point and then moving away from the sample with the same speed. The setup point was established in order to reach a 3 mm deformation, value obtained by the 25% of the sample height (12 mm) as recommended on ISO7743.

The compression of initialization for the sample was performed giving a deformation of 5 mm four times in a row, in absence of MF. This step is needed for the MSE samples, in order to set them a stable state in terms of stresses. This state will be present as long as the next compressions, reach lower deformations than those given in the initialization [30,31].

After the initialization, the compression test for the MSE samples and force measurement were performed with MFs of different magnitudes, including magnitude 0 mT (without MF). The four sample of each concentration (Tab.3.10) were tested 4 times with MF equal to 0 mT. And for the other MF magnitudes, the samples were tested once, in order to obtain the forces for the sample without remaining deformations.

The forces measurements gave graphs of force versus deformation as is shown in Fig. 3.12. This graph shows the values while the compression upper plate was compressing the sample and when it was releasing the sample. The behavior of the forces curve, reveals the hysteresis of the material. The hysteresis on the MSE exhibits an expected difference of force values during the load and unload cycles [31,32]. But this property was not studied because the results of this thesis will be oriented to the grabbing of objects by grippers however the releasing of them has a lack of importance. For this reason, only the loading or compressing section was taken into account for the following analysis.

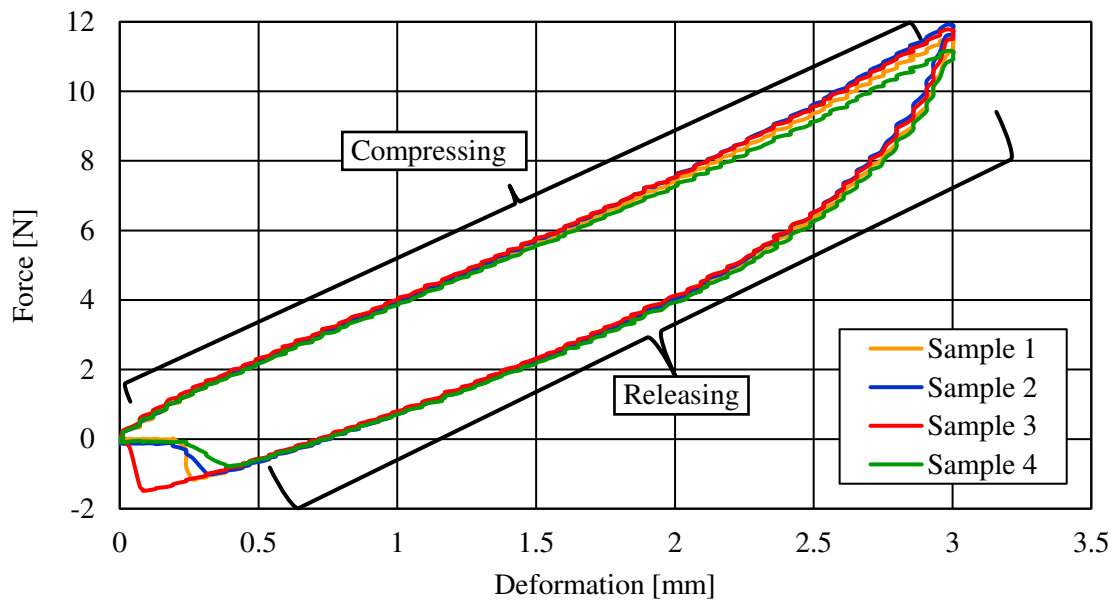


Fig. 3.12: Force vs deformation for the four samples of MSE cylinder  $\text{\O}16 \times H12$ , composition matrix 45%vol. silicone oil and 30%vol. iron, under MF 141.2 mT.

For the following analysis, the results obtained were averaged according to the iron concentration and magnitude of the magnetic field applied, thus giving the compressive force – deformation graphs shown in Fig. 3.13.

From the four graphs, similar behavior can be observed in all the curves. The curves show the increase of forces as the intensity of the magnetic field increases. It is observed that the forces curves of MF\_0 (0 mT), are below the others. This means that MSE sample without the influence of MF have lower stiffness and because of that it is required lower forces for the same deformation. The curves of MF\_5 (141.2 mT) are the ones that show the greatest force due to the compression, which means that it presents a higher stiffness. According to this, it may be concluded that stiffness of MSE samples increases when getting higher MF intensity.

In Fig. 3.13 is shown that the forces reach higher values in the presence of a higher iron concentration in the MSE. Tab. 3.12 shows the maximum values measured for each iron concentration, under different MF intensities and Fig. 3.13 shows the same values in order to recognize the presence of a saturation. But this graph does not show the behavior of a possible saturation.

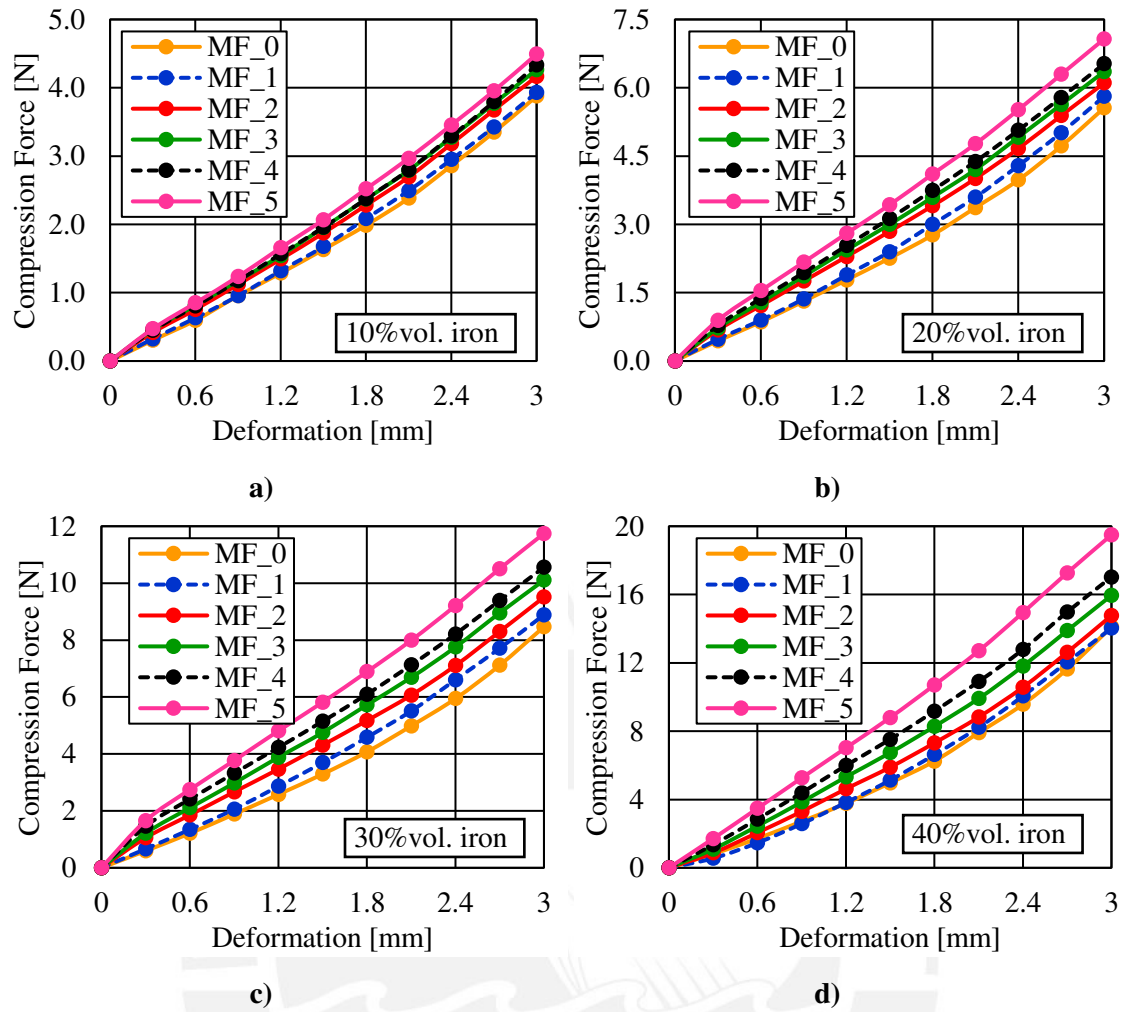


Fig. 3.13: Force vs deformation for different intensities of MF, in the MSE cylinder  $\text{\O}16 \times \text{H}12$ , composition: a) 10%, b) 20%, c) 30%, and d) 40% vol. iron.

Tab. 3.12: Maximum values obtained for different intensities of MF, in the MSE cylinder  $\text{\O}16 \times \text{H}12$ , composition: a) 10%, b) 20%, c) 30%, d) 40% vol. iron.

Cylinder $\text{\O}16 \times \text{H}12$	Maximum values obtained [N]					
	MF_0	MF_1	MF_2	MF_3	MF_4	MF_5
Matrix 45%vol. sil. oil - 10%vol. iron	3.877	3.931	4.165	4.265	4.336	4.492
Matrix 45%vol. sil. oil - 20%vol. iron	5.557	5.813	6.104	6.355	6.526	7.070
Matrix 45%vol. sil. oil - 30%vol. iron	8.467	8.887	9.508	10.104	10.557	11.745
Matrix 45%vol. sil. oil - 40%vol. iron	14.104	14.030	14.771	15.950	17.021	19.495

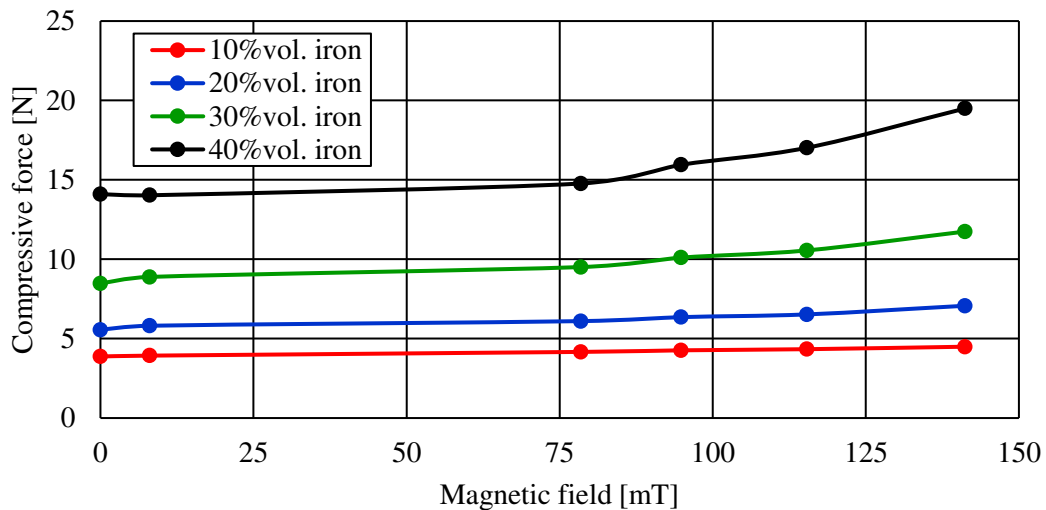


Fig. 3.14: Maximum values obtained for different intensities of MF, in the MSE cylinder Ø16xH12, composition: a) 10%, b) 20%, c) 30%, d) 40% vol. iron.

From Tab.3.12, it is observed that the maximum forces obtained for a lower iron concentration do not even reach the maximum forces for the next iron concentration. E.g. the maximum value for concentration 10%vol. iron is 4.492 N, while the minimum value for 20%vol. iron is 5.557 N. But in the case of 40%vol. iron this tendency was not fulfilled for MF\_0 and MF\_1. This exception might be due to an error on the measuring or of the mass concentration of the samples. Assuming that exception as an isolated error, the tendency of the values shows that stiffness increases considerably when the iron concentration gets higher percentages. Furthermore, the increase of stiffness due to the iron concentration may be exceeds the increase due to MF.

It was observed on Fig. 3.13 that measured forces increased as the magnitude of MF increased. However, the percentage of increase is not the same for all concentrations. Tab. 3.13 shows the increase of values that has the forces measured for compression with MF equal to 141.2 mT in comparison to the forces measured when there is no magnetic field presence.

Tab. 3.13: Average force increase for 141.2 mT in comparison to 0 mT for MSE cylinder Ø16xH12, composition: a) 10%, b) 20%, c) 30%, d) 40% vol. iron.

Cylinder Ø16xH12			
Increase of force for 141.2 mT in comparison to 0 mT, at 3mm of deformation			
Matrix 45%vol. sil. oil - 10%vol. iron	Matrix 45%vol. sil. oil - 20%vol. iron	Matrix 45%vol. sil. oil - 30%vol. iron	Matrix 45%vol. sil. oil - 40%vol. iron
15.9%	27.2%	38.7%	38.2%

The table shows that the increase in forces is considerable for the four concentrations. The MSE with 30% and 40% vol. iron show an increase in force equal to 38.7% and 38.2% respectively, being the highest average increments in the four concentrations. It was expected that the greatest increase would be seen in the MSE with greater iron concentration (40% vol. iron). However, it can be considered that

may be the samples with 30% vol. iron have a composition that benefits that increase. A saturation with this concentration (30% vol. iron) is discarded as is shown in Fig. 3.14. Should be remembered that each component adds properties to the MSE, hence, the concentration of the other components may be is allowing that behavior of the MSE.

Stress and strain values were obtained using the dimensions of the test samples. These values can be observed in Fig. 3.15.

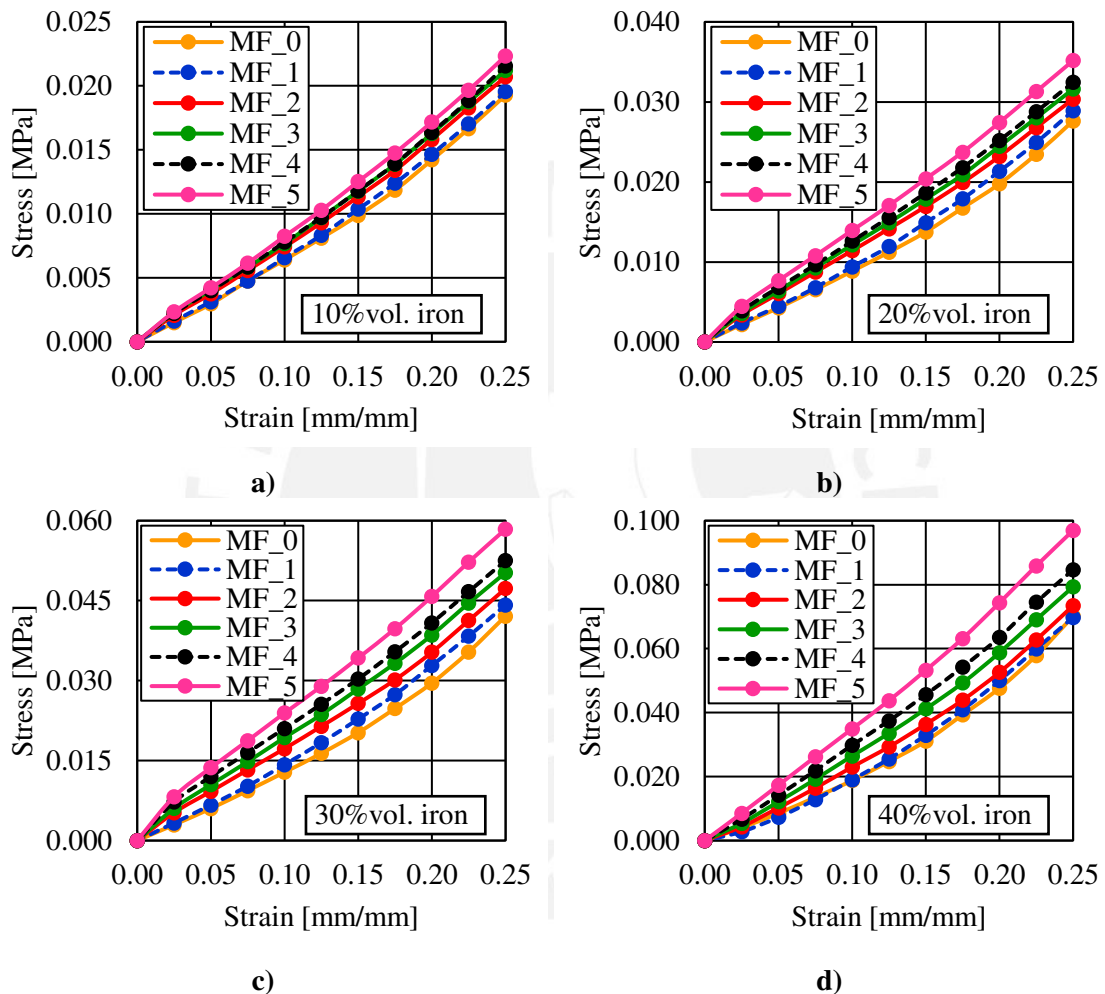


Fig. 3.15: Stress vs strain for different intensities of MF, in the MSE cylinder  $\varnothing 16 \times H 12$ , composition: a) 10%, b) 20%, c) 30%, d) 40% vol. iron.

Since the stress were obtained from the division of the forces on the transverse area of the test samples, they have the same trend as the forces.

The stresses follow as expected by forming a non-linear curve [19]. This verifies the type of material that describes the MSE since it is a hyperelastic material. And within the characteristics of this type of material, is the change of the elasticity modulus (E) and therefore, the variation of stiffness [33].

In an elastic material, the graph of stress-strain is linear belonging to the elastic zone of the material and from which a constant value of modulus of elasticity (E) could be obtained. Materials with different properties including E-modulus will have different stiffness in the same way. For this reason, the MSE of each concentration at different intensities of MF were evaluated as if they were different materials, but with elastic behavior. In this way, it was possible to verify if they present a different E-modulus as a consequence of the MF [32].

From the stress-strain graphs (Fig. 3.15) linear regressions of each complete curve were made, in order to be able to describe the MSE as elastic materials. Tab. 3.14 shows the values obtained for the minimum and maximum magnetic field.

Tab. 3.14: Results when considering the MSE as an elastic material for the minimum and maximum MF.

	MF	Lineal regression	Coefficient of determination	E-modulus [MPa]	$\Delta$ E-modulus [MPa]
Matrix 45%vol. sil. oil - 10%vol. iron	0 mT	$y = 0.0758x - 0.0008$	$R^2 = 0.9910$	0.0758	0.012
	141.2 mT	$y = 0.0878x - 0.0003$	$R^2 = 0.9976$	0.0878	
Matrix 45%vol. sil. oil - 20%vol. iron	0 mT	$y = 0.1073x - 0.0012$	$R^2 = 0.9874$	0.1073	0.029
	141.2 mT	$y = 0.1363x + 0.0004$	$R^2 = 0.9984$	0.1363	
Matrix 45%vol. sil. oil - 30%vol. iron	0 mT	$y = 0.1633x - 0.0023$	$R^2 = 0.9829$	0.1633	0.061
	141.2 mT	$y = 0.2243x + 0.0014$	$R^2 = 0.9977$	0.2243	
Matrix 45%vol. sil. oil - 40%vol. iron	0 mT	$y = 0.2718x - 0.0053$	$R^2 = 0.9708$	0.2718	0.113
	141.2 mT	$y = 0.3846x - 0.0022$	$R^2 = 0.9968$	0.3846	

Tab. 3.14 shows values of E from 0.0758 MPa to 0.3846 MPa. These values cannot be compared directly with results from other studies because the composition and conditions are specific for this thesis. However, the source [32] will be used to compare the values due to the similarities presented. This source carried out compression tests on MSE cylinders made of an elastomeric matrix without silicone oil and 33%vol. iron. And with the same procedure shown in Tab. 3.14, values of E were obtained. These values of E were approximately: 2.45 MPa and 2.75 MPa for 0 mT and 130 mT respectively. The E values of the source [32] are higher than the values of this thesis, but it can be expected since the MSE for this thesis uses silicone oil, component that can reduce considerably the stiffness [34].

From Tab. 3.14 it can be seen that for each concentration of MSE there is a change in the values of E due to the increase of applied magnetic field. In all cases when comparing the results between 0 mT and 141.2 mT, there is an increase of E-modulus. In addition, as the concentration of iron increases, the values and ranges of the E-modulus also increase.

With this, it can be confirmed that the properties of the MSEs e.g. the stiffness, vary along with the intensity of the applied magnetic field and the concentration of its components.

### **3.4. Deformation due to a magnetic field**

The aim of this test is to characterize the deformation of the MSE not by a mechanical load, but by a magnetic field. The deformation of the MSE disc was measured under different MF magnitudes. In order to reach different intensities of MF the permanent magnet was being approached to the sample and located at different distance. Finally, the obtaining of the deformations consisted in measuring the location of different points of the sample surface with a laser sensor. The results obtained with this test were analyzed and used to determine the MSE concentration able to offer better properties for soft robotics applications (grippers).

This experiment was divided into two parts: (i) evaluation of deformation for MSE discs with four concentrations and determining one concentration to perform the second part, (ii) evaluation of deformation for MSE disc with four sizes with the selected concentration. For the both parts the MSE composite discs were manufactured using Neukasil RTV26, silicone oil and CIP.

#### **3.4.1. Testing configuration**

This test is based on the measurement of the deformation of a disc, made of MSE, with different intensities of an MF. This evaluation used the same structure shown in Sec. 3.3. In addition, housings were designed to hold the discs of each diameter and the deformation of the discs in the vertical axis (see Fig. 3.16) is measured through the use of a triangulation laser sensor. And as in Sec. 3.3, tests were carried out with and without magnet, so at first, the magnet is not placed, and then is included in the experimental setup in order to apply a MF to the samples. Fig. 3.16 shows the experimental setup including the magnet.

As seen in Fig. 3.16, the laser sensor points the MSE disc. This was placed at a specific distance so that the deformations are within the measuring range of the sensor. The sensor was displaced above the disc the disc, making the measurement with steps equal to 1 mm. In this way, the location of the upper surface of the disc was measured from the edge to the midpoint of the disc. However, due to the operation of the sensor, the measurements at the ends of the disc were not useful for the description of the deformation. For this reason, the results show the deformations of all possible points within the following range:  $[-r + 1; r-1]$ , where  $r$  is the radius of the discs (Fig. 3.17).

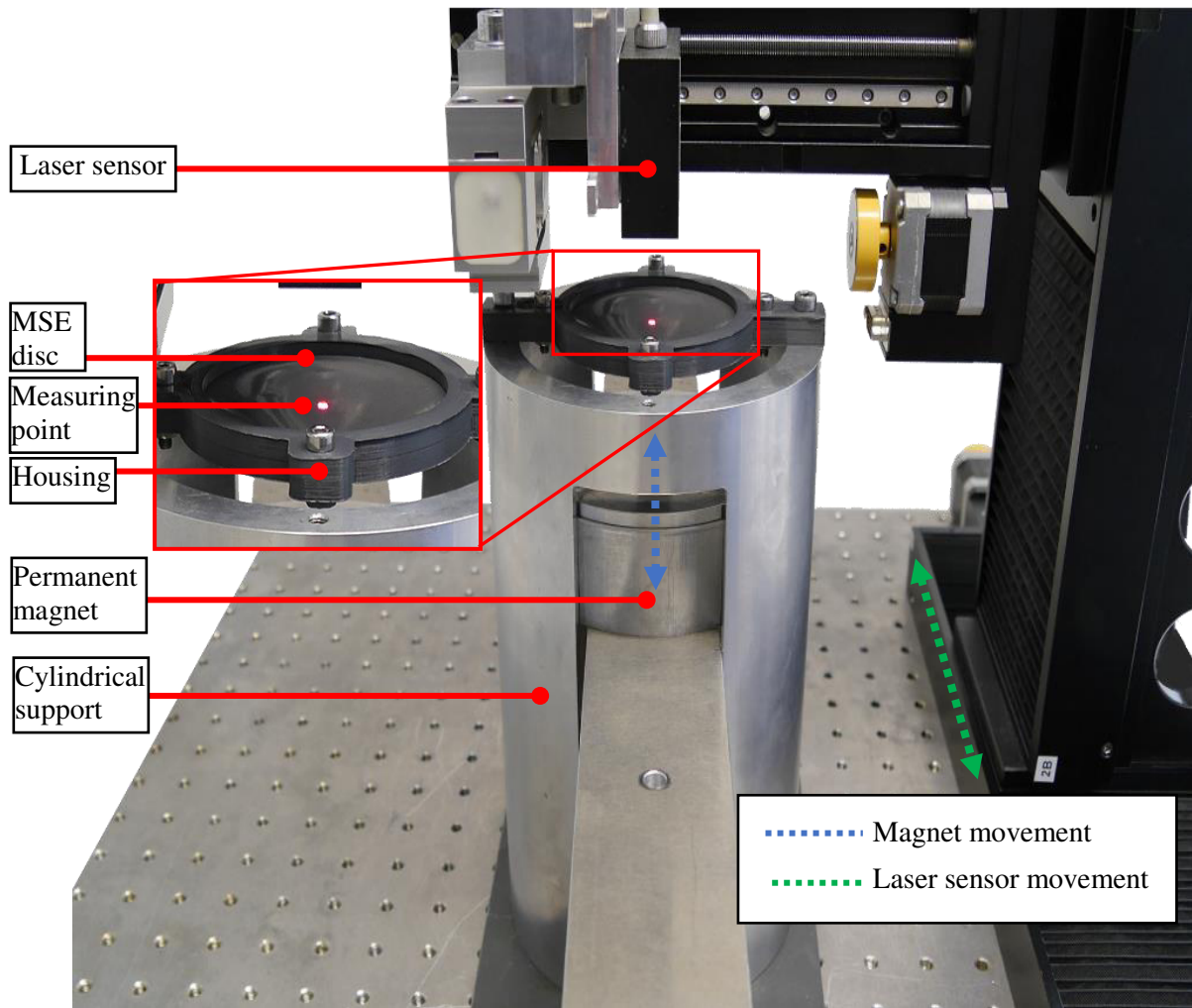


Fig. 3.16: Configuration of the setup for deformation measurement of discs due to MF.

### First part: deformation of disc Ø50

The concentrations used were the same as for tests in Sec. 3.3. Hence, these discs were made of MSE matrix 45% vol. silicone oil and 10%, 20%, 30%, 40% vol. iron. One test piece of each concentration was manufactured and the main dimensions of these discs were: diameter of 50 mm ( $\varnothing$ ), thickness of 3 mm (H) (Fig. 3.17). The 4 compositions used in the manufacturing are shown in Tab. 3.15.

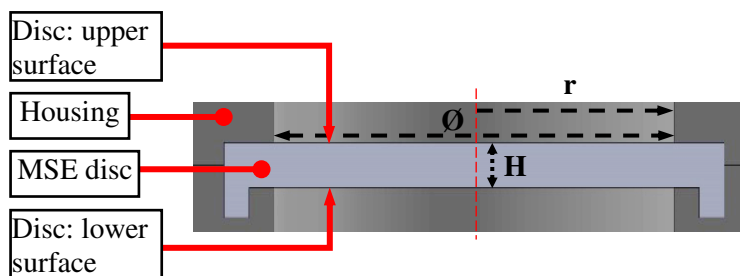


Fig. 3.17: Main dimension of MSE disc.



Tab. 3.15: Mass composition for disc Ø50xH3, MSE matrix 45%vol. silicone oil and 10%, 20%, 30%, 40% vol. iron.

Disc Ø50xH3	Mass composition (mixture) [g]			
	Matrix 45%vol. sil. oil - 10%vol. iron	Matrix 45%vol. sil. oil - 20%vol. iron	Matrix 45%vol. sil. oil - 30%vol. iron	Matrix 45%vol. sil. oil - 40%vol. iron
RTV 26	3.68	3.27	2.86	2.45
Sil. oil 500cSt	3.65	3.24	2.84	2.43
Iron	7.31	14.61	21.92	29.22
A7	1.47	1.31	1.14	0.98
Total	5.06	13.16	24.99	40.56

The test consisted of making the measurements with 50 mm diameter MSE discs (see Fig. 3.17). The disc was held in the housing and was fixed to the cylindrical structure, as shown in Fig. 3.16. Then the measurements were started with a zero MF, so there was the only deformation by its weight. Then the magnet was incorporated into the structure and the deformations were measured under different intensities of MF. For this, it began by placing the magnet at 112 mm from the disc, then it was moved closer to increase the intensity of the MF, until a distance of 32 mm between the magnet and the disc. Those distance represent the distance between the upper surface of the magnet and the lower surface of the disc without deformations. Tab. 3.16 shows all the testing distances.

The MF shown in Tab. 3.16 was obtained by averaging the MF calculated at different points on the disc, considering a relative permeability ( $\mu_r$ ) equal to 1 for every MSE discs, and using the equation 1 mentioned in Sec. 2.4. The points were located on the axis of symmetry of the disc and with steps of 0.5 mm, from the lower surface to the upper surface, and taking the distances from the disc to the magnet shown in Tab. 3.16.

Tab. 3.16: Distance magnet - MSE disc Ø50 mm for each MF.

	Magnetic field [mT]	Distance magnet - disc [mm]
MF_0	0.0	Inf.
MF_1	11.7	112
MF_2	18.7	92
MF_3	32.2	72
MF_4	61.4	52
MF_5	88.6	42
MF_6	107.5	37
MF_7	131.4	32

To understand the physical influence of the distance between the magnet and the MSE disc previous to the analysis the results, Fig. 3.18 is shown. In the Fig. 3.18a) the distance from the magnet to the samples is short, so the disc obtained a high deformation. In the other hand, Fig. 3.18b) the distance was larger and the sample does not exhibit a considerable.

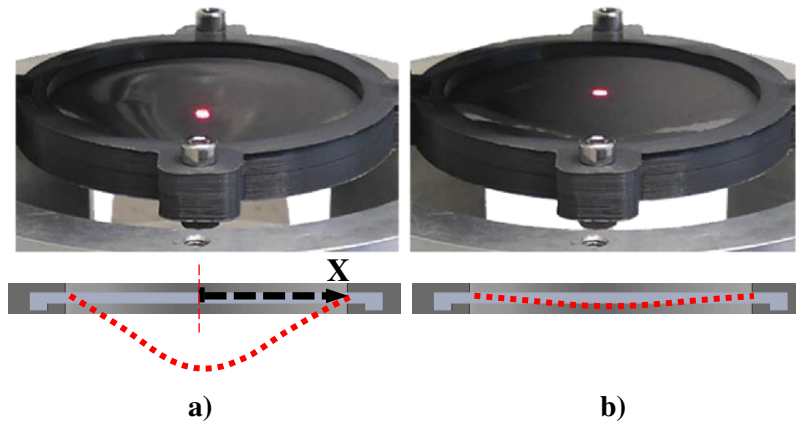


Fig. 3.18: Fig. a) Disc in presence of a high MF and close to a permanent magnet, Fig. b) Disc in presence of low MF and far from the permanent magnet.

Fig. 3.19 shows the deformations of 50 mm diameter discs and as it was mentioned, the data that is shown does not cover the full diameter.

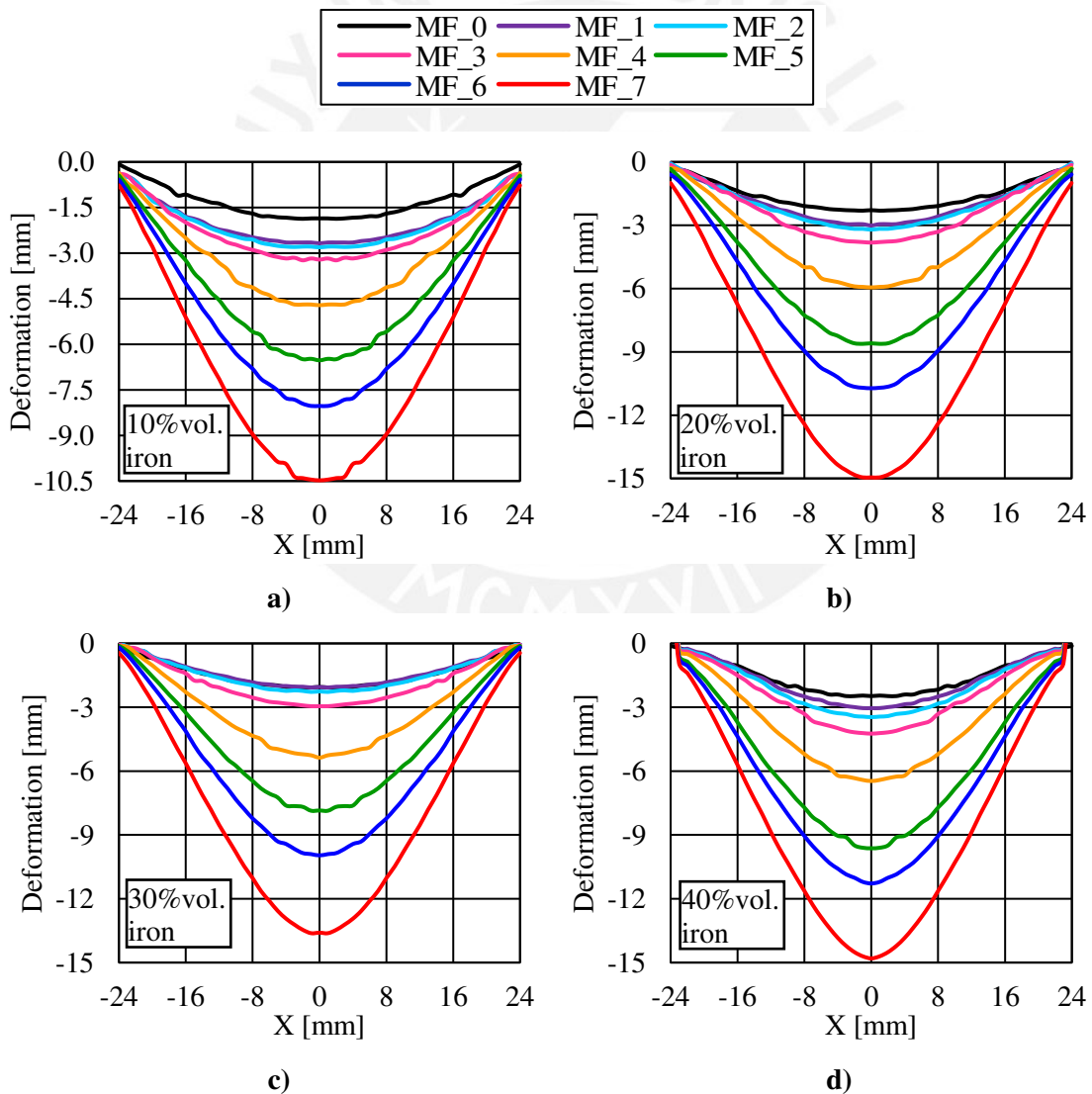


Fig. 3.19: Graphs deformations vs. diameter for discs  $\text{\O}50 \times H3$ , MSE matrix 45%vol. silicone oil and: a) 10%vol. iron, b) 20%vol. iron, c) 30%vol. iron, d) 40%vol. iron.

This figure shows the deformations for each concentration used. These deformations are due to the weight of each disc, in addition to the attractive force that the MF exerts over them. It is observed that the discs concentrate the greatest deformation in the central part. While at the extremes the values become closer to zero because it is the part that is fixed to the housing.

It is observed that the four curves with less deformation, of each graph, are close to each other. Showing a minimal influence of the concentration of iron on the deformation at low values of MF. While the four curves with greater deformation, the opposite is shown. These curves are clearly separated and show greater deformations for a higher MF.

With a concentration of 10%vol. iron, the smallest deformations are presented, reaching a maximum point of -10.47 mm. This low deformation is expected because, as it was possible to see in the results of Sec. 3.2, the test pieces with 10% iron obtained lower attractive forces. Based on Sec. 3.2, it is might also expect that, as the iron concentration increases, the deformations will increase. However, in Fig. 3.20 it can be observed that the behavior is different from the expected one. This graph shows the maximum values of each curve for each concentration.

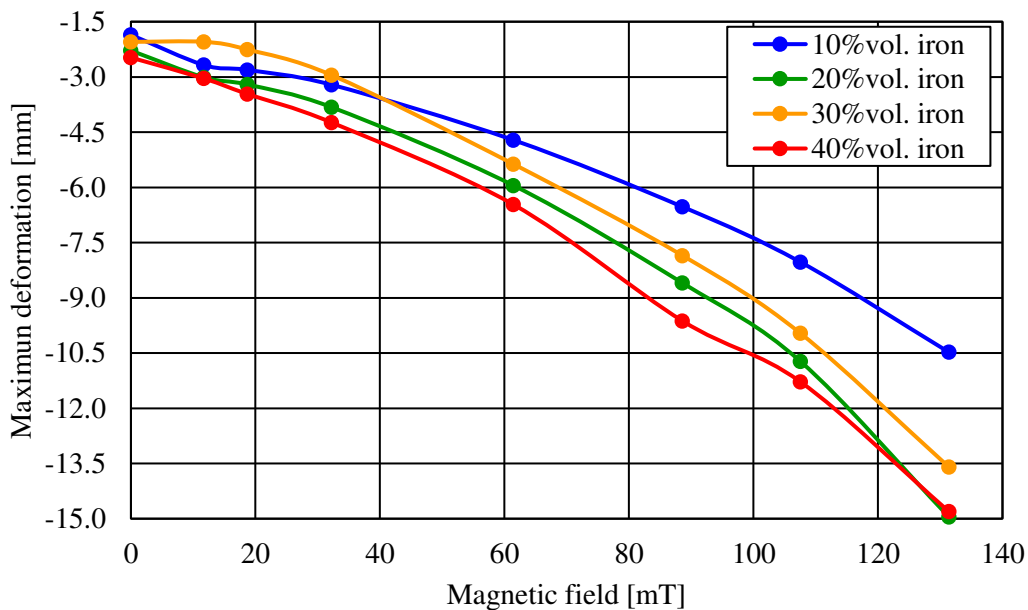


Fig. 3.20: Maximum deformation vs. Magnetic field for discs Ø50xH3, MSE matrix 45%vol. silicone oil and: a) 10%vol. iron, b) 20%vol. iron, c) 30%vol. iron, and d) 40%vol. iron.

The graph shows that the lowest values predominate to the 10%vol. iron curve, however, with low intensities of MF, the 30% iron curve shows lower values. After the 10%vol. iron curve, an intermediate curve is shown, but this is the 30%vol. iron curve. Finally, the curves of 20%vol. and 40%vol. iron, are those that show the highest values and very close to each other.

In the graph, can be seen that the disc with 20%vol. iron, having a lower amount of iron, deforms more than the disc with 30%vol. iron. On one hand, it shows the lower stiffness that present the MSE with 20%vol. iron as the results of Sec. 3.3 shown. But on the other hand, from results of Sec. 3.2, a higher deformation due to a higher concentration of iron was expected. However, analyzing the mass composition shown in Tab. 3.15, the oil mass concentration is approximately 50% higher. This difference in the amount of oil is what may be explain that the deformation increases as it intervenes directly in the properties of the material. [12].

When comparing values of 20% and 40% vol. iron, it can be seen that points of 40%vol. iron curve are higher, but the difference is minimal. From Sec.3.3, a higher stiffness was expected for an MSE with higher iron concentration, but in this test the MSE disc with high difference in concentration exhibit apparently a similar stiffness. Additionally, from Sec. 3.2 a higher difference in deformations for the MSE disc with 40%vol. iron and 20%vol. iron was expected because of the high difference of attractive force that should generate each concentration of iron under a MF. However, analyzing the mass composition shown in Tab. 3.15, the oil mass concentration is higher for the MSE disc of 20%vol. iron. This difference in the amount of oil may be explain also this behavior.

As shown in Sec. 3.2, it is clear that the attractive forces on MSE samples increase with iron concentration and consequently, the attractive force above the MSE disc increase its deformations. From Sec. 3.3 the stiffness decreases with a lower iron concentration and consequently, the attractive forces above the MSE disc are allow to generate larger deformations.

From this behavior shown by the discs, it can be understood that the deformation of an MSE layer obtained under an MF will not depend only on the iron concentration and the attractive force on them. But it will also depend on the resulting properties of the concentrations of each MSE. Considering this, the disc of MSE with 30%vol. iron is the sample that exhibit in its deformation an equilibrium between the attractive forces and the stiffness.

With the results obtained from this test, it could be considered that the MSE of 20% and 30% vol. iron would be convenient to carry out more studies for the good performance that both concentration present. In addition, with results from Sec. 3.3 it was determined that the MSE of 30% and 40% vol. iron obtained greater changes in rigidity, but using a smaller amount of iron to better see the MSE of 30%. For these two reasons, it was decided to use the 30% vol. iron MSE to carry out the following studies.

### **Second part: deformation of MSE discs with 30% vol. iron**

The samples for this test were also made by MSE matrix 45%vol. silicone oil and 30%vol. iron. This concentration was chosen due to the results of Sec. 3.3 and the first part of this section. Discs of four

different diameters were produced and for each type there are 4 samples. The main dimensions of those samples were the 3 mm thickness and diameters: 16 mm, 32 mm, 48 mm and 64 mm. The four discs are shown in Fig. 3.21.

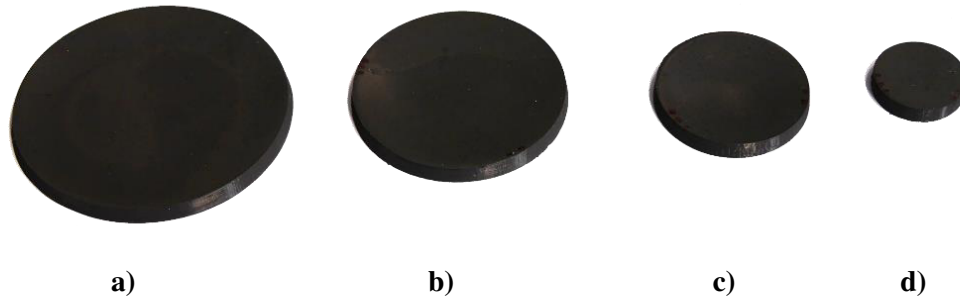


Fig. 3.21: Discs of MSE matrix 45%vol. silicone oil and 30%vol. iron: Fig. a)  $\text{Ø}64 \times \text{H}3$ , Fig. b)  $\text{Ø}48 \times \text{H}6$ , Fig. c)  $\text{Ø}32 \times \text{H}3$ , and Fig. d)  $\text{Ø}16 \times \text{H}3$ .

This test consisted in performing the same type of measurement, with discs of diameters: 16 mm, 32 mm, 48 mm, and 64 mm. In addition to only having a concentration of 30% iron. It should be noted that in this test, the discs were analyzed in two different ways. In future work for the design of a gripper, the housing of fixing will be taken into account. For this reason, this test is carried out in two different ways to observe if there is an influence of the fixing on the deformation. And the circular shape of the housing is because the grippers in which is focused this work are hemispherical and consequently the housing are circular too. The Fig. 3.22 shows the two dispositions in which the discs were evaluated.

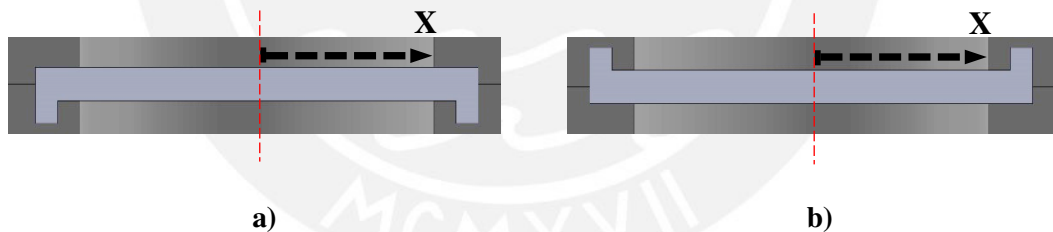


Fig. 3.22: Testing dispositions for discs: Fig. a) Up, Fig. b) Down.

The measurement was started without MF and then the sample deformation was measured with different intensities of MF. Different intensities of MF were achieved by varying the height of the magnet (see Fig. 3.16). The distances that were used are shown in Tab. 3.17. It should be noted that the distances of the magnet to the surface of the discs did not change when changing from the Up to Down arrangement. This is because the housing was developed so that the surface closest to the magnet is at the same height in both arrangements of the disc.

The MF values shown in Tab. 3.17 were obtained in the same way as the first part of this experiment. Hence, by averaging the MF calculated at different points on the disc, considering a relative permeability ( $\mu_r$ ) equal to 1 for every MSE discs, and using the equation 1 mentioned in Sec. 2.4. The points were

located on the axis of symmetry of the disc and with steps of 0.5 mm, from the lower surface to the upper surface, and taking the distances from the magnet to the disc shown in Tab. 3.17.

Tab. 3.17: Distance magnet - MSE disc: Ø16, Ø32, Ø48, and Ø64 mm for each MF.

	Magnetic field [mT]	Distance magnet - disc [mm]	Disc diameter			
			Ø16	Ø32	Ø48	Ø64
MF_0	0.0	Inf.	x	x	x	x
MF_1	38.1	66.5		x	x	x
MF_2	52.6	56.5		x	x	x
MF_3	62.5	51.5		x	x	x
MF_4	74.9	46.5		x	x	x
MF_5	90.3	41.5		x	x	x
MF_6	109.7	36.5	x			
MF_7	134.1	31.5	x			
MF_8	164.7	26.5	x			
MF_9	202.6	21.5	x			
MF_10	248.9	16.5	x			

In the case of the 16 mm discs, shorter distances were used in order to produce considerable variations of deformations. While for larger discs the use of short distances was limited because the attractive forces were higher than the forces of fixing above the discs.

The results obtained for the 4 discs of each diameter were averaged. And as for the first part of the test, the data taken does not cover correctly the boundary between the disc and the housing. The results for the deformations of the four sizes of disc and the two positions in which they were evaluated are shown in Fig. 3.23.

From these graphs (Fig. 3.23), a behavior similar to the graphs of discs diameter 50 mm can be noticed. As expected, the discs get more deformed as the intensity of MF increases. In addition to concentrating the major deformations in the center of the disc because the edges are subject to the housing.

In the graph, the variation that exists between the deformation curves when the discs are in both positions can be seen. The curves of the UP position show a greater deformation than the DOWN position for the larger diameters: 32 mm, 48 mm, and 64 mm. However, the differences are not so great as to notice an appreciable influence by the clamping mode when there are high magnitudes of MF.

On the other hand, for the disc of diameter 16 mm, the DOWN position curves reach greater deformations. In addition, the differences between UP and DOWN deformations can also be considered low.

It is important to remember that the MF used to analyze the disc of diameter 16 mm were of greater intensity since, with lower intensities, the deformations were not noticeable. Because of this, the maximum deformations obtained are similar to those of the 32 mm diameter disc.

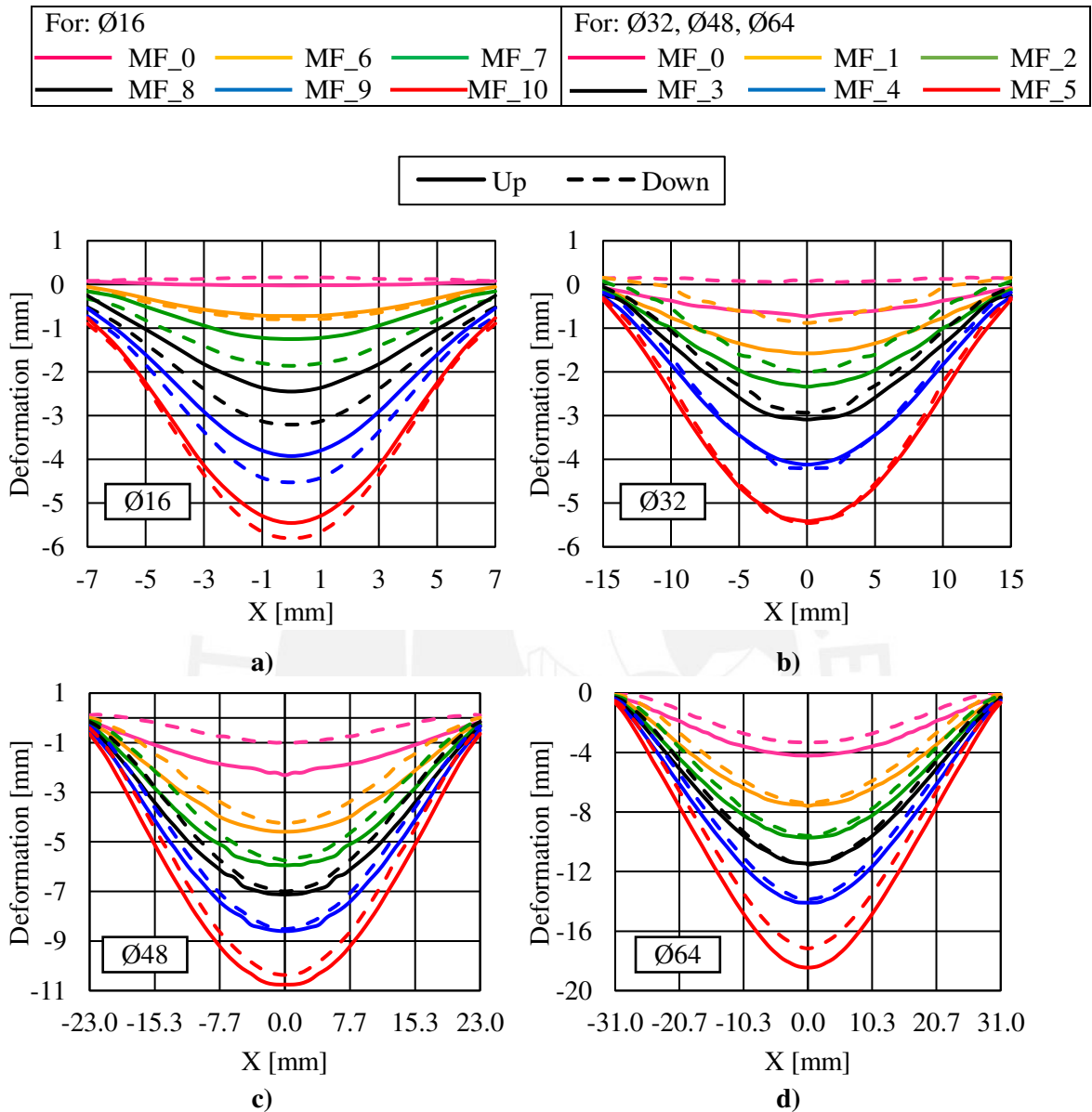


Fig. 3.23: Graphs deformations vs. diameter for discs made of MSE matrix 45%vol. silicone oil and 30%vol. iron, with diameter: a) 16 mm, b) 32 mm, c) 48 mm, and d) 64 mm.

It is noticed that having a diameter of 16 mm, the magnetic field on the disc is more uniform than in discs with larger diameters. This condition could be one more reason to obtain a different behavior compared to the larger discs, in which the magnetic field varies more within its area. It can also be observed that the deformations with MF\_0 do not follow the general behavior of the disc, the Down curve gets above the Up curve. In addition, both curves show positive values indicating in this way that the deformation by the weight itself was not significant. And it can be added that the subsection also contributed to the surface being above zero.

## 4. Material Modeling

### 4.1. Theoretical fundamentals

Considering that elastomers belong to the great variety of hyperelastic materials, the MSEs of this thesis work will be considered in the same way. The hyperelastic materials are characterized by presenting large deformations under low loads, as well as non-linear mechanical properties. Due to this, the non-linear theory of elasticity is used. Which, with a strain-energy function ( $W$ ) describes the mechanical behavior in energetic terms [35].

### 4.2. Hyperelastic models

Although the non-linear theory has reached to know and understand the operation of hyperelastic materials. Finding a unique hyperelastic model that reproduces the complete behavior of elastomers is complicated [33], and this becomes more complicated when the aim is the studying of the MSE behavior. Due to this, modeling in Ansys Workbench® with different materials and subsequent comparison was carried out in order to achieve an appropriate modeling. These were the following material modeling: Neo Hookean (NH), Arruda Boyce (AB), Gent, Blatz Ko (BK), Mooney Rivlin 2 parameters (MR2), and Mooney Rivlin 3 parameters (MR3).

There is a wide variety of models that describe the behavior of hyperelastic materials, however, these can be complicated to model due to the number of parameters that may be required [33]. Parameters that can be obtained from experimental data. These values were achieved using the Ansys curve-fitting tool. This tool fits the model parameters to a set of experimental data, given by the user, using a least-squares minimization [36].

The modeling of a hyperelastic material can be formulated in different ways and within that is the use of experimental data [33]. To model the MSE, the data obtained from the Sec. 3.3 experiments were required. In this way, was modeled the cylindrical samples of MSE matrix 45%vol. silicone oil and 10%, 20%, 30%, 40% vol. iron for the different intensities of MF. In this modeling, the magnetic field was not modeled since it was sought to know only the behavior of the MSE with the properties already established due to the MF.

In order to obtain the models that best replicate the results of the MSE samples of the four concentrations and the six MF intensities, the results under a compressive force of each hyperelastic model were compared with the experimental data. This comparison was divided by the four MSE concentrations, hence the best models were obtained per each concentration. It sought: to obtain a tendency between its



parameters and the MF intensity; to have low errors with respect to the experimental results; to have results at tensile stress that can be considered correct since the experimental data was only for compressive forces; and to comply with restrictions in the case of models MR2 and MR3. The restriction based on the material constants of MR2 and MR3 are:  $C_{10} + C_{01} \geq 0$  with  $C_{01} \geq 0$ , and  $C_{10} + C_{01} \geq 0$  with  $C_{11} \geq 0$ , respectively [37]. And those constants represent: the elastic behavior ( $C_{10}$ ) and the deviation from the elasticity and increasing of non-linearity ( $C_{01}$ ,  $C_{11}$ ) [37].

For the MSE matrix 45%vol. silicone oil and 10%, 20% and 30%vol. iron, the NH and MR3 models obtained the best results. The initial shear modulus  $\mu$  for NH models got a clear tendency of increasing with the magnitude of MF (Fig.4.1a). The material constants ( $C_{10}$ ,  $C_{01}$  and,  $C_{11}$ ) also got a tendency with the increase of MF (Fig.4.1b, Fig.4.1c, Fig.4.1d), but there were two exceptions: the values of 30%vol. iron under MF\_1, and the values of 10%vol. iron under MF\_4 and MF\_5.

The average errors were obtained from the single errors of each force value and for each MF, obtaining six average errors per each MSE concentration and material model. The errors with NH models for the MSE matrix 45%vol. silicone oil and 10%, 20% and 30%vol. iron were: 1.47% to 6.43%, 1.63% to 10.38%, and 0.59% to 12.28% respectively. And for MR3 were: 0.86% to 2.24%, 0.52% to 2.57%, and 0.46% to 3.39, following the same order of MSE concentrations. It can be noticed that the errors for NH models are higher than MR3 models, and it may have a base on the using of more parameters.

For the three MSE concentrations mentioned, NH and MR3 models gave reasonable results for tensile stress, even without experimental data from that kind of stress. It means that the values of stress increased with the MF and with the iron concentration for the same strain.

For the MSE matrix 45%vol. silicone oil and 40%vol. iron, the NH models obtained the best results. The initial shear modulus  $\mu$  also got a clear tendency with the increase of MF (Fig.4.1a). But there was an exception for the magnitude of MF\_1, and it may be due to the isolated error for the same MSE concentration under MF\_1 noticed for Tab. 3.12. The errors with respect to the experimental data got high values: from 1.69% to 15.63%. But the results for tensile stress were reasonable and can be considered useful.

The other hyperelastic models were discarded due to incomplete or without tendency in its parameters, higher errors, or results at tensile stress that cannot be considered useful. In the case of the MR2 model, it was discarded due to several values of  $C_{01}$  were negatives. The MR3 model for the MSE concentration of 40%vol. iron was discarded for the  $C_{11}$  negative values and the useless results for tensile stress.

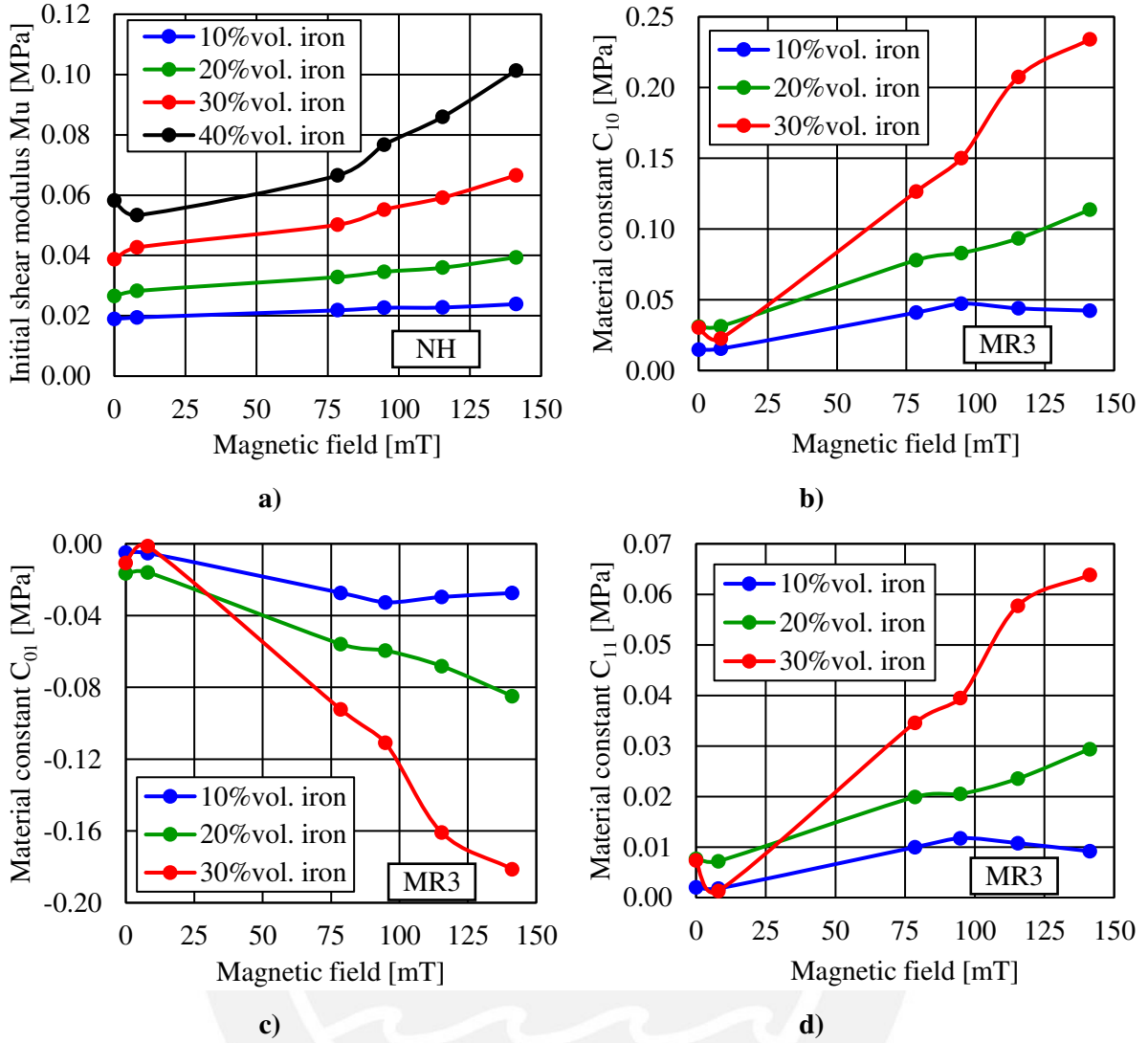


Fig. 4.1: Modeling parameters vs. magnetic field for MSE matrix 45%vol. silicone oil and 10%, 20%, 30%, and 40%vol. iron. For NH: a)  $\mu$ . For MR3: b)  $C_{10}$ , c)  $C_{01}$ , and d)  $C_{11}$ .

The values of the parameters for the two hyperelastic models (NH and MR3) are shown in the following tables.

Tab. 4.1: Neo Hookean model for MSE matrix 45%vol. silicone oil and 10%, 20%, 30%, and 40%vol. iron.

%vol. iron		MF_0 (0 mT)	MF_1 (8 mT)	MF_2 (78.5 mT)	MF_3 (94.8 mT)	MF_4 (115.4 mT)	MF_5 (141.2 mT)
10%	Initial shear modulus $\mu$ [MPa]	0.0189	0.0195	0.0218	0.0226	0.0227	0.0239
20%	Initial shear modulus $\mu$ [MPa]	0.0266	0.0282	0.0328	0.0346	0.0359	0.0394
30%	Initial shear modulus $\mu$ [MPa]	0.0387	0.0427	0.0502	0.0552	0.0592	0.0666
40%	Initial shear modulus $\mu$ [MPa]	0.0582	0.0534	0.0666	0.0767	0.0860	0.1014
10%, 20%, 30%, 40%	Incompressibility parameter D1 [MPa <sup>-1</sup> ]	0	0	0	0	0	0

Tab. 4.2: Mooney Rivlin 3 parameters model for MSE matrix 45%vol. silicone oil and 10%, 20%, and 30%vol. iron.

Iron %vol.		MF_0 (0 mT)	MF_1 (8 mT)	MF_2 (78.5 mT)	MF_3 (94.8 mT)	MF_4 (115.4 mT)	MF_5 (141.2 mT)
10%	Material constant C <sub>10</sub> [MPa]	0.0148	0.0154	0.0409	0.0472	0.0439	0.0423
20%	Material constant C <sub>10</sub> [MPa]	0.0310	0.0312	0.0780	0.0830	0.0934	0.1136
30%	Material constant C <sub>10</sub> [MPa]	0.0304	0.0226	0.1264	0.1500	0.2074	0.2340
10%	Material constant C <sub>01</sub> [MPa]	-0.0049	-0.0051	-0.0273	-0.0326	-0.0296	-0.0274
20%	Material constant C <sub>01</sub> [MPa]	-0.0165	-0.0159	-0.0559	-0.0594	-0.0681	-0.0848
30%	Material constant C <sub>01</sub> [MPa]	-0.0107	-0.0013	-0.0923	-0.1109	-0.1609	-0.1813
10%	Material constant C <sub>11</sub> [MPa]	0.0020	0.0018	0.0100	0.0118	0.0108	0.0092
20%	Material constant C <sub>11</sub> [MPa]	0.0077	0.0072	0.0199	0.0205	0.0235	0.0294
30%	Material constant C <sub>11</sub> [MPa]	0.0074	0.0013	0.0346	0.0395	0.0577	0.0638
10%, 20%, 30%	Incompressibility parameter D <sub>1</sub> [MPa <sup>-1</sup> ]	0	0	0	0	0	0

In this thesis work was observed interesting results and behaviors for the MSE of matrix 45% vol. sil. oil and 30% vol. iron (see Sec. 3.3 and Sec. 3.4). Hence the results of the two material models and the experimental data for this MSE concentration are shown in Fig.4.2. With those graphs, the behavior of the results can be analyzed. For MF\_0 and MF\_1 the curves do not show inflections and the difference between them are minimal. From MF\_2 to MF\_5 the experimental curves show a light inflection that increases with the MF. The NH curves exhibit an increase of difference with the experimental curves, while the MR3 curves exhibit a slight difference with the experimental curves as well as inflections. The MR3 curves can fit better with the experimental values and even with the inflections, due to the parameters that allow this material model to vary the non-linearity of the curves. In spite of the great potential that MR3 shows, it is complicated in some cases to get the correct parameters to fit a curve and comply with the restrictions.

According to the analysis made for the material models and experimental data, it was concluded that for the single concentrations of MSE matrix 45%vol. silicone oil and 10%, 20% and 30%vol. iron the model of Mooney Rivlin 3 parameters was the suitable material model in order to replicate the experimental results and get values for tensile stress, for different MF intensities. It was also concluded that for the whole group of concentrations, MSE matrix 45%vol. silicone oil and 10%, 20% and 30%vol. iron, the Neo Hookean model was the most adequate option, even with higher differences with the experimental results than MR3 models got. This conclusion is based upon the clear tendency that the parameters

adopted with the increase of MF, the reasonable results for tensile stress, and the low complexity that this material model presents to fit the experimental results in comparison with MR3 model.

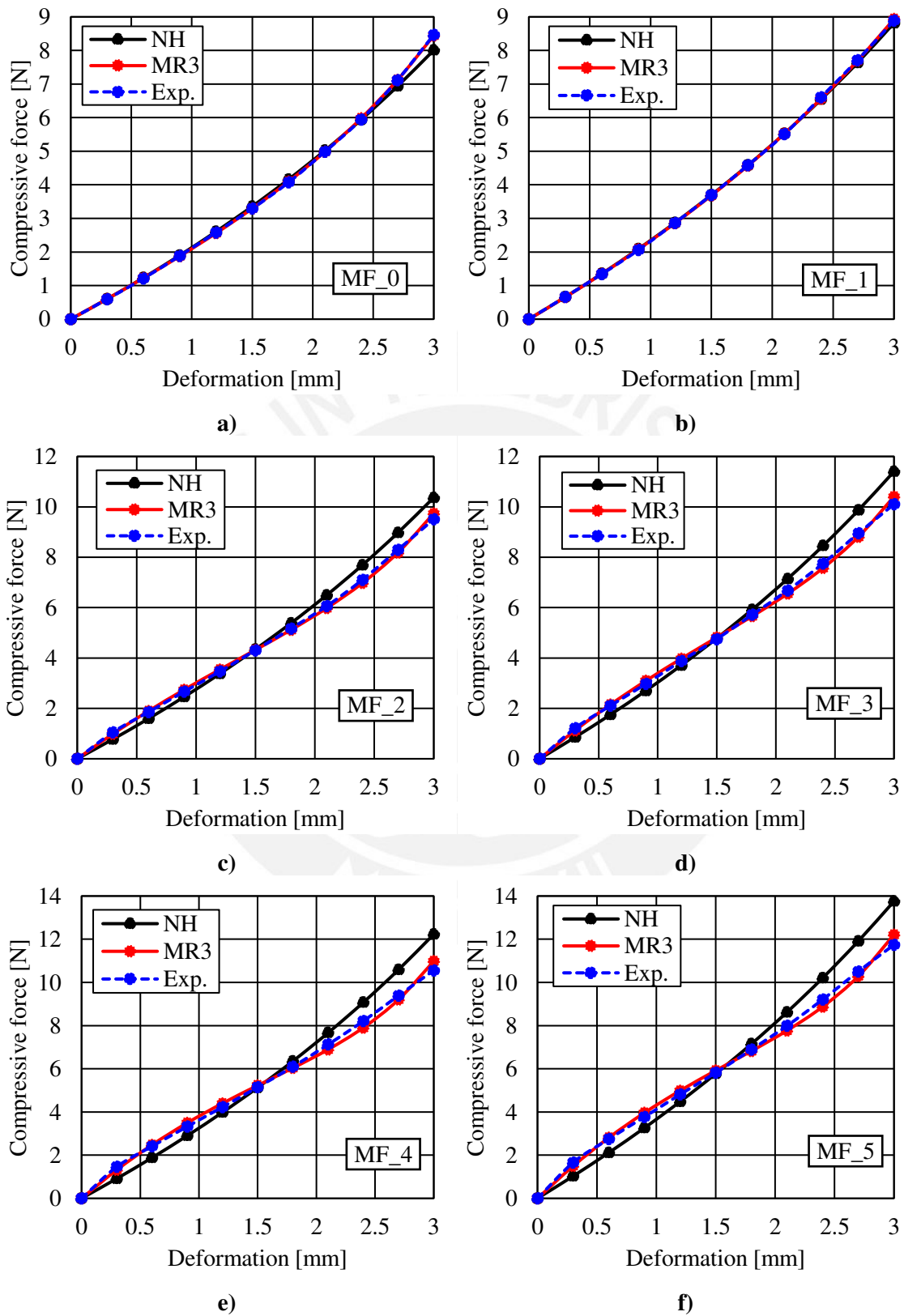


Fig. 4.2: Compressive forces vs deformation in MSE of matrix 45% vol. sil. oil and 30% vol. iron under different magnitudes of MF.

## 5. Conclusions and future work

In this work a study of the dependence of MSE properties based on MF induced by a permanent magnet, beside an MSE composition favorable for soft robotic applications is presented.

In this chapter the most remarkable conclusions, possible future works of the work are presented.

### 5.1. Conclusions

As concluded on the Sec.3.2, the attractive forces due to a MF on the MSE samples, exhibit a considerable degree of accumulative effect, and this effect may be increased by reducing the sources of error. Furthermore, a discretization of mass can be linked to the magnetic forces above an MSE sample. This characteristic of the MSE can be considered a property useful to analyze higher dimensions samples from the analysis of smaller and simpler pieces of MSE.

It is concluded from Sec. 3.3 that stiffness on MSE samples depends considerably on the MF applied and on the volumetric percentage of iron. Nevertheless, the influence of the iron exceeds the influence of MF. Furthermore and besides the increase of stiffness due to the iron concentration, the MSE with matrix 45%vol. silicone oil and 30%vol. iron obtained a 38.7% of increase in compressive force, similar to the MSE with 40%vol. iron. Concluding that this increase does not depend on the iron concentration of the MSE.

As concluded on the Sec.3.4, discs of MSE with matrix 45%vol. silicone oil and 30%vol. iron exhibit an equilibrium between the deformation that attractive forces (due to a MF) generate and the deformation that the stiffness can allow. This can be applied on the development of MSE gripper in order to control the induced deformations by MF during the gripping.

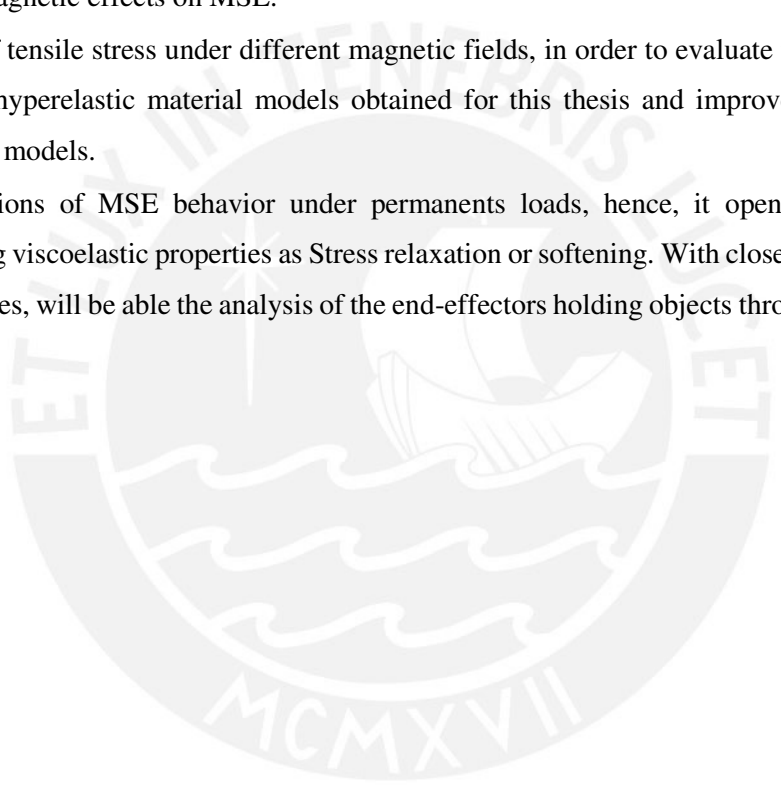
It is concluded considering the experiments carried out, that a balance in the concentrations of MSE components can give great results with magneto-sensitive effects. Thus, that composition could present great changes in properties, mainly the stiffness. Therefore, the concentration that was defined as the one that provides the best results for soft robotic application is MSE matrix 45%vol. silicone oil and 30% vol. iron. Furthermore, in Sec. 3.3 the E-modulus were obtained for this MSE under different MF. These values are in a range: 0.1643-0.2243 MPa for a range of MF: 0-141.2 mT.

As concluded on Sec. 4.2, with the MSE as a hyperelastic material, the Neo Hookean model was established as the most suitable model to replicate and predict results of the four concentrations of MSE

under the different MF intensities. This is supported by the clear tendency of the initial shear modulus  $\mu$  with the increase of the MF intensity, and the low complexity to fit experimental results.

## 5.2. Future work

- Tests with higher intensities of magnetic field and grippers made of the MSE compositions obtained in this thesis could provide a more complete view of the performance and the features of this material.
- The developed property of discretization on MSE, was proved for magnetic forces. A more detailed research focused on this property could extend the application of the discretization to other magnetic effects on MSE.
- Tests of tensile stress under different magnetic fields, in order to evaluate the results predicted by the hyperelastic material models obtained for this thesis and improve them to get more suitable models.
- Simulations of MSE behavior under permanent loads, hence, it opens the possibility of studying viscoelastic properties as Stress relaxation or softening. With close knowledge of those properties, will be able the analysis of the end-effectors holding objects through periods of time.



## 6. Bibliography

- [1] K. Tai, A.-R. El-Sayed, M. Shahriari, M. Biglarbegian and S. Mahmud, "State of the Art Robotic Grippers and Applications," *Robotics*, vol. 5, no. 1, pp. 1-20, 2016.
- [2] J. Shintake, V. Cacucciolo, D. Floreano and H. Shea, "Soft Robotic Grippers," *WILEY-VCH Verlag GmbH & Co. KGaA, Weinheim*, pp. 1-33, 2018.
- [3] Fraunhofer Institute for Silicate Research ISC, *Magnetorheological Elastomers with Continual Adjustable Hardness*, Wurzberg: Fraunhofer Institute for Silicate Research ISC, 2013.
- [4] P. Testa, R. W. Style, J. Cui, C. Donnelly, E. Borisova, P. M. Derlet, E. R. Dufresne and L. J. Heyderman, "Magnetically Addressable Shape-Memory and Stiffening," *Advanced materials*, 2019.
- [5] X. Guana, X. Donga and J. Oua, "Magnetostrictive effect of magnetorheological elastomer," *ScienceDirect*, vol. 320, pp. 158-163, 2007.
- [6] Boese and Holger, "Viscoelastic Properties of Silicone-based Magnetorheological Elastomers," *International Journal of Modern Physics N*, vol. 21, no. 28 & \29, pp. 4790-4979, 2007.
- [7] M. R. Jolly, J. D. Carlson and B. C. Munoz, "A model of the behaviour of magnetorheological materials," *Smart Materials and Structures*, vol. 5, no. 5, pp. 607-614, 19 July 1996.
- [8] L. Yancheng, L. Jianchun, L. Weihua and D. Haiping, "A state-of-the-art review on magnetorheological elastomer devices," *IOP Science*, vol. 23, no. 12, pp. 1-24, 2014.
- [9] W. H. Li, X. Zhang and H. Du, "Magnetorheological Elastomers and Their Applications," in *Advances in Elastomers I*, Australia, Springer, 2013, pp. 357-374.
- [10] J. G. Puente-Cordova, M. E. Reyes-Melo, L. M. Palacios-Pineda, I. A. Martinez-Perales, O. Martinez-Romero and A. Elias-Zuniga, "Fabrication and Characterization of Isotropic and Anisotropic Magnetorheological Elastomers, Based on Silicone Rubber and Carbonyl Iron Microparticles," *MDPI: Polymers*, vol. 10, no. 1343, pp. 1-13, 2018.
- [11] C. Ruddy, E. Ahearne and G. Byrne, "A review of magnetorheological elastomers: properties and applications," Advanced Manufacturing Science Research Centre, 2014.
- [12] X. Gong, X. Zhang and P. Zhang, "Material Behaviour, Fabrication and characterization of isotropic magnetorheological elastomers," *Polymer Testing*, vol. 24, no. 5, pp. 669-676, 2005.
- [13] A. Nedjar, S. Aguib, T. Djedid, A. Nour, A. Settet and M. Tourab, "Analysis of the Dynamic Behavior of Magnetorheological Elastomer Composite: Elaboration and Identification of Rheological Properties," *Silicon*, pp. 1-7, 2018.

- [14] S. S. Abramchuk, D. A. Grishin, E. Y. Kramarenko, G. V. Stepanov and A. R. Khokhlov, "Effect of a Homogeneous Magnetic Field on the Mechanical Behavior of Soft Magnetic Elastomers," *Polymer Science, Ser. A*, vol. 48, no. 2, pp. 138-145, 2006.
- [15] J. L. Leblanc, "Rubber-Filler Interactions and rheological properties in filled compounds," *Progress in Polymer Science*, vol. 27, pp. 627-687, 2001.
- [16] J. Chavez Vega, T. Kaufhold, V. Böhm, T. Becker, K. Zimmermann, M. Martens, M. Schilling, T. Gundermann and S. Odenbach, "Field-induced plasticity of magneto-sensitive elastomers in context with soft robotic gripper applications," *PAMM*, vol. 17, no. 1, pp. 23-26, 2018.
- [17] K. Zimmermann, V. Bohm, T. Kaufhold, J. Chavez Vega, T. Becker, S. Odenbach, T. Gundermann, M. Schilling and M. Martens, "Investigations and Simulations on the Mechanical Behaviour of Magneto-Sensitive Elastomers in Context with Soft Robotic Gripper Application," *International Scientific Journal of IFToMM*, vol. 65, no. 4, pp. 13-25, 2016.
- [18] S. Hermann, "Entwurf und Steuerung von Formschluss- und Kraftschlussgreifern," Masterarbeit, Technische Universität Ilmenau, Fakultät: Maschinenbau, Fachgebiet: Technische, 2016.
- [19] T. Kikuchi, Y. Kobayashi, M. Kawai and T. Mitsumata, "Elastic Properties of Magnetorheological Elastomers in a Heterogeneous Uniaxial Magnetic Field," *International Journal of Molecular Sciences*, vol. 19, no. 3045, pp. 1-9, 2018.
- [20] Supermagnete, "Supermagnete," [Online]. Available: <https://www.supermagnete.de/eng/faq/How-do-you-calculate-the-magnetic-flux-density>. [Accessed February 2019].
- [21] Supermagnete, "Supermagnete," [Online]. Available: <https://www.supermagnete.de/eng/faq/How-strong-is-this-magnet>. [Accessed March 2019].
- [22] Supermagnete, "Supermagnete," [Online]. Available: <https://www.supermagnete.de/eng/adhesive-force-calculation?paramset=i/70/d/45/70/35/Pure%20Iron/10/250>. [Accessed Marzo 2019].
- [23] Y. Jin, "Theoretische und experimentelle Untersuchungen zur Nutzung des Effektes der magnetfeldinduzierten Platizität bei MSE für eine Anwendung in der Greifertechnik," Masterarbeit, Technische Universität Ilmenau, Fakultät: Maschinenbau, Fachgebiet: Technische, 2018.
- [24] C. M. Hartzell, Y. T. Choi, N. M. Wereley and a. T. J. Leps, "Performance of a Magnetorheological Fluid-Based Robotic End Effector for Spacecraft Applications," *AIAA SPACE Forum*, 2018.
- [25] Y. Okatani, T. Nishida and K. Tadakuma, "Development of Universal Robot Gripper Using MR $\alpha$  Fluid," in *SCIS&ISIS 2014*, Kitakyushu Japan, November 2014.



- [26] J. Amend, N. Cheng, S. Fakhouri and B. Culley, "Soft Robotics Commercialization: Jamming Grippers from Research to Product," *SOFT ROBOTICS*, vol. 0, 2016.
- [27] S. Kashima, F. Miyasaka and K. Hirata, "Novel Soft Actuator Using Magnetorheological Elastomer," *IEEE Transactions on Magnetics*, vol. 48, no. 4, pp. 1649-1652, 2012.
- [28] T. I. Becker, V. Bohm, J. Chavez Vega, S. Odenbach, Y. L. Raikher and K. Zimmerman, "Magnetic-field-controlled Mechanical Behavior of Magneto-sensitive Elastomers in Applications for Actuator and Sensor Systems," *Springer*, vol. 89, no. 1, pp. 133-152, 2018.
- [29] J. Camacho and V. Sosa, "Alternative method to calculate the magnetic field of permanent magnets with azimuthal symmetry," *Revista Mexicana de Fisica*, vol. 59, pp. 8-17, 2013.
- [30] L. Mullins, "Softening of Rubber by Deformation," Natural Rubber Producers' Research Association, Hertfordshire, 1969.
- [31] K. Miller, *Testing Elastomers for Finite Element Analysis*, Axel Products, Inc., 2002.
- [32] M. Kukla, J. Gorecki, I. Malujda, K. Talaska and P. Tarkowski, "The determination of mechanical properties of magnetorheological elastomers," *Procedia Engineering*, vol. 177, pp. 324-330, 2017.
- [33] G. Marckmann and E. Verron, "Comparison of hyperelastic models for rubber-like materials," *Rubber Chemistry and Technology*, vol. 79, no. 5, pp. 835-858, 2006.
- [34] P. P. Luis Manuel, P. M. Imperio Anel, L. S. Luis M., M. R. Oscar, P. C. Jesús, Emmanuel, S. Cárdenas and E. Alex, "Experimental Investigation of the Magnetorheological Behavior of PDMS Elastomer Reinforced with Iron Micro/Nanoparticles," *Polymers*, vol. 9, no. 12, 2017.
- [35] P. Martins, R. N. Jorge and A. Ferreira, "A Comparative Study of Several Material Models for Prediction of Hyperelastic Properties: Application to Silicone-Rubber and Soft Tissues," *Strain*, vol. 42, pp. 135-147, 2006.
- [36] ANSYS, "Technology Demonstration Guide," 2019. [Online]. Available: [https://ansyshelp.ansys.com/account/secured?returnurl=/Views/Secured/corp/v194/ans\\_mat/ans\\_mat.html](https://ansyshelp.ansys.com/account/secured?returnurl=/Views/Secured/corp/v194/ans_mat/ans_mat.html). [Accessed 20 May 2019].
- [37] N. Kumar and V. V. Rao, "Hyperelastic Mooney-Rivlin Model: Determination and Physical Interpretation of Material Constants," *MIT International Journal of Mechanical Engineering*, vol. 6, no. 1, pp. 43-46, 2016.

# Appendices

## Appendix A: Technical data of permanent magnet



### Data sheet article S-70-35-N

Technical data and application safety

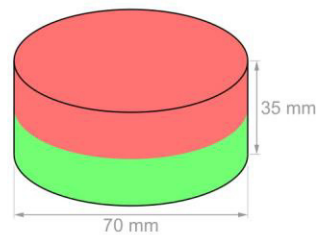
Webcraft GmbH  
Industriepark 206  
78244 Gottmadingen, Germany

Phone: +49 7731 939 839 2  
Fax: +49 7731 939 839 9

www.supermagnete.de  
support@supermagnete.de

#### 1. Technical information


Article ID	S-70-35-N
EAN	7640155438308
Material	NdFeB
Shape	Disc
Diameter	70 mm
Height	35 mm
Tolerance	+/- 0,1 mm
Direction of magnetisation	axial (parallel to height)
Coating	Nickel-plated (Ni-Cu-Ni)
Manufacturing method	sintered
Magnetisation	N45
Strength	approx. 140 kg (approx. 1370 N)
Max. working temperature	80°C
Weight	1,0236871 kg
Curie temperature	310 °C
Residual magnetism Br	13200-13700 G, 1.32-1.37 T
Coercive field strength bHc	10.8-12.5 kOe, 860-995 kA/m
Coercive field strength iHc	≥12 kOe, ≥955 kA/m
Energy product (BxH)max	43-45 MGOe, 342-358 kJ/m <sup>3</sup>




Pollutant-free according to RoHS Directive 2011/65/EU.


#### 2. Safety tips


<p><b>Warning</b></p>	<p><b>Contusions</b></p> <p>Big magnets have a very strong attractive force.</p> <ul style="list-style-type: none"> <li>• Unsafe handling could cause jamming of fingers or skin in between magnets. This may lead to contusions and bruises.</li> <li>• Powerful, very large magnets could cause bone fractures.</li> </ul> <p>Wear heavy protective gloves when handling larger magnets.</p>
<p><b>Warning</b></p>	<p><b>Pacemaker</b></p> <p>Magnets could affect the functioning of pacemakers and implanted heart defibrillators.</p> <ul style="list-style-type: none"> <li>• A pacemaker could switch into test mode and cause illness.</li> <li>• A heart defibrillator may stop working.</li> </ul> <ul style="list-style-type: none"> <li>• If you wear these devices keep sufficient distance to magnets: <a href="http://www.supermagnete.de/eng/faq/distance">www.supermagnete.de/eng/faq/distance</a></li> <li>• Warn others who wear these devices from getting too close to magnets.</li> </ul>


<b>Warning</b> 	<p><b>Heavy objects</b></p> <p>Too heavy loads, symptoms of fatigue as well as material defect could cause a magnet or magnetic hook to loosen from the surface that is attached to. Falling objects could lead to serious injuries.</p> <ul style="list-style-type: none"> <li>• The indicated adhesive force applies only to ideal conditions. Allow for a high safety cushion.</li> <li>• Don't use magnets in places where people could sustain injuries in case of material failure.</li> </ul>
---	--


<b>Warning</b> 	<p><b>Metal splinters</b></p> <p>Neodymium magnets are brittle. Colliding magnets could crack. Sharp splinters could be catapulted away for several meters and injure your eyes.</p> <ul style="list-style-type: none"> <li>• Avoid the collision of magnets.</li> <li>• Wear safety glasses when handling larger magnets.</li> <li>• Make sure that nearby people are also protected or keep their distance.</li> </ul>
---	--


### 3. Handling and storing


<b>Caution</b> 	<p><b>Magnetic field</b></p> <p>Magnets produce a far-reaching, strong magnetic field. They could damage TVs and laptops, computer hard drives, credit and ATM cards, data storage media, mechanical watches, hearing aids and speakers.</p> <ul style="list-style-type: none"> <li>• Keep magnets away from devices and objects that could be damaged by strong magnetic fields.</li> <li>• Please refer to our table of recommended distances: <a href="http://www.supermagnete.de/eng/faq/distance">www.supermagnete.de/eng/faq/distance</a></li> </ul>
---	--


<b>Caution</b> 	<p><b>Combustibility</b></p> <p>When machining magnets, the drilling dust could easily ignite.</p> <p>Stay away from machining magnets or use appropriate tools and sufficient cooling water.</p>
---	---


<b>Caution</b> 	<p><b>Nickel allergy</b></p> <p>Many of our magnets contain nickel, also those without nickel coating.</p> <ul style="list-style-type: none"> <li>• Some people have an allergic reaction when they come into contact with nickel.</li> <li>• Nickel allergies could develop from perpetual contact with nickel-plated objects.</li> </ul> <ul style="list-style-type: none"> <li>• Avoid perpetual skin contact with magnets.</li> <li>• Avoid contact with magnets if you already have a nickel allergy.</li> </ul>
---	---

<b>Notice</b> 	<p><b>Influence on people</b></p> <p>According to the current level of knowledge, magnetic fields of permanent magnets do not have a measurable positive or negative influence on people. It is unlikely that permanent magnets constitute a health risk, but it cannot be ruled out entirely.</p> <ul style="list-style-type: none"> <li>• For your own safety, avoid constant contact with magnets.</li> <li>• Store large magnets at least one metre away from your body.</li> </ul>
--	---


<b>Notice</b> 	<p><b>Splintering of coating</b></p> <p>Most of our neodymium magnets have a thin nickel-copper-nickel coating to protect them from erosion. This coating could splinter or crack due to collision or large pressure. This makes them vulnerable to environmental influences like moisture and they could oxidise.</p> <ul style="list-style-type: none"> <li>• Separate big magnets, especially spheres, with a piece of cardboard.</li> <li>• Avoid collisions of magnets as well as repeated mechanical exposure (e.g. blows, bashes).</li> </ul>
--	--


<b>Notice</b> 	<b>Oxidation, corrosion, rust</b>
	<p>Untreated neodymium magnets oxidise quickly and disintegrate. Most of our magnets have a nickel-copper-nickel coating to protect them from corrosion. This coating provides some protection against corrosion, but it is not robust enough for continuous outdoor use.</p> <ul style="list-style-type: none"> <li>• Use magnets only in the dry indoors or protect them against environmental influences.</li> <li>• Avoid damages to the coating.</li> </ul>

<b>Notice</b> 	<b>Temperature resistance</b>
	<p>Neodymium magnets have a maximum working temperature of 80 to 200°C. Most neodymium magnets lose part of their adhesive force permanently at a temperature of 80°C.</p> <ul style="list-style-type: none"> <li>• Don't use magnets in places where they are exposed to extreme heat.</li> <li>• If you use an adhesive, don't harden it with hot air.</li> </ul>

<b>Notice</b> 	<b>Mechanical treatment</b>
	<p>Neodymium magnets are brittle, heat-sensitive and oxidise easily.</p> <ul style="list-style-type: none"> <li>• When drilling or sawing a magnet with improper tools, the magnet may break.</li> <li>• The emerging heat may demagnetise the magnet.</li> <li>• The magnet will oxidise and disintegrate due to the damaged coating.</li> </ul> <p>Stay away from mechanical treatment of magnets if you do not possess the necessary equipment and experience.</p>

#### 4. Transportation tips

<b>Caution</b> 	<b>Airfreight</b>
	<p>Magnetic fields of improperly packaged magnets could influence airplane navigation devices. In the worst case it could lead to an accident.</p> <ul style="list-style-type: none"> <li>• Airfreight magnets only in packaging with sufficient magnetic shielding.</li> <li>• Please refer to the respective regulations: <a href="http://www.supermagnete.de/eng/faq/airfreight">www.supermagnete.de/eng/faq/airfreight</a></li> </ul>

<b>Caution</b> 	<b>Postage</b>
	<p>Magnetic fields of improperly packaged magnets could cause disturbances in sorting machines and damage fragile goods in other packages.</p> <ul style="list-style-type: none"> <li>• Please refer to our shipping tips: <a href="http://www.supermagnete.de/eng/faq/shipping">www.supermagnete.de/eng/faq/shipping</a></li> <li>• Use a large box and place the magnet in the middle surrounded by lots of padding material.</li> <li>• Arrange magnets in a package in a way that the magnetic fields neutralise each other.</li> <li>• If necessary, use sheet iron to shield the magnetic field.</li> <li>• There are stricter rules for airfreight: Refer to the warning notice "Airfreight".</li> </ul>

#### 5. Disposal tips

Small amounts of used neodymium magnets can be thrown out with the regular trash. Larger amounts of magnets need to be recycled as scrap metal.

#### 6. Statutory provisions

Neodymium magnets are not intended for sale/export to the United States of America, Canada or Japan. You are strictly prohibited from directly or indirectly exporting the neodymium magnets that you received from us or the end products that you produced from those magnets to the countries mentioned above.

**TARIC-Code:** 8505 1100 65 0

**Origin:** China

For more information about magnets please review  
[www.supermagnete.de/faq.php](http://www.supermagnete.de/faq.php).

**Last update:** 15/09/2015

## Appendix B: Technical data of Alpa-Sil Classic



### ALPA-SIL CLASSIC

#### Characterisation

Addition crosslinking 2 component silicone rubber that vulcanises at room temperature

#### Technical Data

	ALPA-SIL CLASSIC A Component A	ALPA-SIL CLASSIC BLAU B Component B		
Aspect	viscous liquid	viscous liquid		
Colour	translucent	blue		
Viscosity	1,050	2,700	mPa·s	Brookfield HBTD <sup>1)</sup>
Density	1.05	1.1	g/cm <sup>3</sup>	DIN 53 479 <sup>1)</sup>
<b>Mixture</b>				
Mixing ratio	100 : 10		acc. to weight	
Viscosity	-		mPa·s	Brookfield HBTD <sup>1)</sup>
Potlife	7		minutes	<sup>1)</sup>
Demouldable after	30		minutes	<sup>1)</sup>
<b>Vulcanizate</b>				
Hardness Shore A	6 - 8			DIN 53 505 <sup>2)</sup>
Tear resistance	1		Mpa	
Elongation at break	245		%	DIN 53 504 S 3 A <sup>2)</sup>
Tear propagation resistance	2.2		N/mm	ASTM D 624 Form B <sup>2)</sup>
Linear shrinkage	-		%	after 7 days
<b>The A component contains the platinum catalyst.</b>				
<sup>1)</sup> = measured under standard climate DIN 50 014-23/50-2				
<sup>2)</sup> = vulcanizate, measured after 14 days of storage under standard climate DIN 50 014-23/50-2				

#### Storability

If stored properly, components A and B can be stored for 12 months. The products have to be stored in closed original containers at temperatures below 30 °C and protected from frost.

The above given values are product describing data. Please consult the 'delivery specification' for binding product specifications. Further data about product properties, toxicological, ecological data as well as data relevant to safety can be found in the safety data sheet.

#### Properties

- Crosslinks at temperatures >23 °C
- Easy mixing of the components
- Easy processing

- 
- Good mechanical properties at low Shore A hardness
  - Quick processing and demoulding time.

---

## Application Technology

### Application Fields

Application for doubling in dental labs and for model making and mould construction.

### Processing

#### 1. Catalysis

ALPA-SIL CLASSIC components A + B are mixed together in a certain ratio (see technical data). The two components are either mechanically mixed (e.g. by hand) or with a stirring unit. To avoid the introduction of air and/or a temperature increase of the mass during the mixing process, please mix at low speed when using a stirring unit. It is also possible and recommended by us to use a dosing machine for 2-component systems. More information is available on request.

After mixing, the mass should be deaerated under vacuum at 30 – 50 mbar for approx. 2 minutes.

#### 2. Vulcanisation

At 23 °C the system vulcanises as indicated under the technical data. At lower temperatures vulcanization is slow down and can be accelerated by heating up.

#### Remarks:

Contact with the following substances can delay vulcanisation or even prevent it:

- chlorine or butyl rubbers containing sulphur
- LSR or RTV types catalysed with metal salts
- stabilizers and softeners
- amine hardeners in epoxy resins
- various organic solvents, e.g. ketones, alcohols, ethers, etc.

Pretrials can be carried out in case of doubt.

### Information for Users

The data given in this technical leaflet result from our experience. They correspond with the best of our knowledge and serve for advising our customers. However, they are not binding. Please observe the trademark rights of third parties.



---

### **Safety**

When handling ALPA-SIL CLASSIC the generally valid working safety regulations must be observed.

### **Delivery Units**

Component A: 0.9 kg or 4.5 kg  
Component B: 0.1 kg or 0.5 kg  
Other sizes on demand

**We reserve the right to modify the product and technical leaflet.**

**Our department for applied technique is always at your service for further information and advice.**

Our technical advice and recommendations given verbally, in writing or by trials are believed to be correct. They are neither binding with regard to possible rights of third parties nor do they exempt you from your task of examining the suitability of our products for the intended use. We cannot accept any responsibility for application and processing methods which are beyond our control.

**Edition: July 2013**

**CHT R. BEITLICH GMBH**

**Works Geretsried, Breslauer Weg 123, 82538 Geretsried, Deutschland**

**Telefon: 08171/3456-0, Fax: 08171/3456-26, Email: [info@cht.com](mailto:info@cht.com), Homepage: [www.cht.com](http://www.cht.com)**

ALPA-SIL CLASSIC total pages 3 page 3

## Appendix C: Technical data of Neukasil RTV 26

### NEUKASIL RTV 26

Silicone Rubber  
addition crosslinking

**altropol**

#### Main features

- low hardness
- very good flowability
- good resistance to initial tearing and tear propagation

#### Applications

- production of products for orthopaedics
- suitable for polyester, epoxides, wax
- casting of electrical component parts
- production of parts, prototypes

#### Properties in the non-crosslinked state (approx. values)

		NEUKASIL RTV 26	NEUKASIL crosslinker A 7
Colour		white	light blue
Mixing ratio	p.b.w.	100	40
Density (20 °C)	g/cm <sup>3</sup>	1.2	0.96
Viscosity (25 °C)	mPa·s	55,000	100

#### Properties of the mixture (approx. values)

Mixed viscosity (25 °C)	mPa·s		7,000
Pot life (RT, 100 g)	minutes		200
Tack-free	hours		24
Hardness	Shore A	DIN 53505	7
Service temperature	° C		160

#### Mechanical values of the cured product (approx. values)

Tensile strength	N/mm <sup>2</sup>	DIN 53504	2
Elongation at break	%	DIN 53455	750
Resistance to tear propagation	N/mm	ASTM D 624 B	5.5
Linear dimensional change	%		0.1
Resistivity	Ω cm	DIN 53482	10 <sup>15</sup>
Dielectric strength	KV/mm	DIN 53481	22
Dielectric constant	ε r	DIN 53483	3
Dissipation factor	tan δ 60 HZ	DIN 53483	0.008

\*RT = room temperature

#### How to process the material

See that as little air as possible gets into the compound while stirring. To obtain a bubble-free vulcanized material, we recommend evacuating the crosslinker-containing formulation before continuing the processing. When the vacuum is created, the mixture may increase in volume by 3 - 4 times of its original volume under formation of bubbles. This process is finished when the bubbles have collapsed and the formulation has reobtained its original volume. Carefully pour the prepared material over the object to be cast.

Whenever working with addition-crosslinking silicone rubbers, take care that the receptacles used are clean and dry. Furthermore, the surface of the object to be cast should be dry and free from dirt.

Certain substances may inhibit or decelerate the vulcanization of additions-crosslinking silicone rubbers. To these substances belong among other things condensation-crosslinking silicones, organic rubbers, plasticizers, amines, heavy-metal compounds and sulphurous substances.



## NEUKASIL RTV 26

Silicone Rubber  
addition crosslinking

# altropol

Under unfavourable circumstances it may happen that also surfaces having been in contact with the mentioned substances lead to vulcanization faults. The same applies to certain modelling materials.

When NEUKASIL RTV 26 is used as mould making material (production of negatives), there is no release agent required for demoulding. Should there still arise any problems, we recommend our NEUKADUR Release Agent N or NEUKADUR Release Spray P 6. For the production of multipart moulds and to avoid an adhesion of NEUKASIL RTV 26 to itself, use the same release agents. Treat the surface of the part already vulcanized with release agent, then cast the second part of the mould.

The vulcanization of NEUKASIL RTV 26 begins after addition of the crosslinker, and there are no cleavage products whatsoever produced during this process. At 20 - 25 °C, the vulcanization is terminated to a large extent after 24 hours. The vulcanization speed is temperature-dependent and can be accelerated considerably by heat supply.

For release agents, please visit our homepage under <http://www.altropol.de/en/produkte/weitere-produkte/trennmittel>

### **Form of delivery**

NEUKASIL RTV 26	1 kg	5 kg	25 kg
NEUKASIL crosslinker A 7 light blue	0.1 kg	0.5 kg	2.5 kg

### **Storage**

We recommend keeping the material in tightly closed original receptacles at temperatures of 20 - 25 °C. When duly stored, the material can be used within the shelf life indicated on the labels (the first 2 digits of the batch number indicate the week, the 3rd digit indicates the year).

### **Measure of precaution**

With the aid of the current safety data sheets, which contain physical, ecological, toxicological and other data relating to safety, the user can inform himself on the safe handling and storage of the products.

---

Our technical service - in words, in writing or by trials - is given according to the current state of our knowledge. It does however not relieve the customer/user from the duty to check by himself if the products supplied by us are suitable for the intended processes and purposes. Application, use and processing of the products take place beyond our control possibilities and lie therefore exclusively in the area of responsibility of the processor. Any existing property rights of third parties are to be considered. We guarantee the perfect quality of our products in accordance with our general terms and conditions of business. When handling our products you have to observe the legal rules and the rules for the industrial hygiene. As for the rest, we refer to the corresponding safety data sheets.

• 2016-12-06.1 / 7 / LW-W •

---

• [www.altropol.de](http://www.altropol.de) •

• Altropol Kunststoff GmbH • Rudolf-Diesel-Straße 9 - 13 • D-23617 Stockelsdorf • Tel. +49 451-499 60-0 •  
• Fax. +49 451-499 60-20 • E - Mail: [info@altropol.de](mailto:info@altropol.de) •

2/2

## Appendix D: Technical data of Xiameter PMX-200 silicone fluid



### XIAMETER<sup>®</sup> PMX-200 Silicone Fluid, 50-1,000 CS

**INCI Name: Dimethicone**  
**Colorless, clear polydimethylsiloxane fluid**

#### FEATURES

- Ease of application and rubout
- Ease of buffing
- Enhances color
- High water repellency
- High compressibility
- High shearability without breakdown
- High spreadability and compatibility
- Low environmental hazard
- Low fire hazard
- Low reactivity and vapor pressure
- Low surface energy
- Good heat stability
- Essentially odorless, tasteless and nontoxic
- Soluble in a wide range of solvents

#### BENEFITS

- For personal care applications
- Skin protection
  - Imparts soft, velvety skin feel
  - Spreads easily on both skin and hair
  - De-soaping (prevents foaming during rubout)
- For industrial applications
- High dielectric strength
  - High damping action
  - Oxidation-, chemical- and weather-resistant

#### COMPOSITION

- Polydimethylsiloxane polymers
- Chemical composition  
(CH<sub>3</sub>)<sub>3</sub>SiO[SiO(CH<sub>3</sub>)<sub>2</sub>]<sub>n</sub>Si(CH<sub>3</sub>)<sub>3</sub>

3

#### APPLICATIONS

- Active ingredient in a variety of automotive, furniture, metal and specialty polishes in paste, emulsion and solvent-based polishes and aerosols
- Various applications including cosmetic ingredient, elastomer and plastics lubricant, electrical insulating fluid, foam preventive or breaker, mechanical fluid, mold release agent, surface active agent, and solvent-based finishing and fat liquoring of leather

#### DESCRIPTION

XIAMETER<sup>®</sup> PMX-200 Silicone Fluid, 50-1,000 CS is a polydimethylsiloxane polymer manufactured to yield essentially linear polymers in a wide range of average kinematic viscosities.

The viscosities generally used in formulating polishes are between 100 and 30,000 cSt. To obtain optimum results, in terms of ease of application and depth of gloss, it is preferable to use a blend of a low-viscosity fluid and a high-viscosity fluid (e.g. 3 parts XIAMETER<sup>®</sup> PMX-200 Silicone Fluid 100 cSt and 1 part XIAMETER<sup>®</sup> PMX-200 Silicone Fluid 12,500 cSt). The low-viscosity silicone fluid acts as a lubricant to make polish application and rubout easier, whereas the high-viscosity silicone fluid produces a greater depth of gloss. Since these polymers are inherently water-repellent, they will cause water to bead up on a treated surface rather than penetrate the polish film.

#### HOW TO USE

XIAMETER<sup>®</sup> PMX-200 Silicone Fluid, 50-1,000 CS is highly soluble in organic solvents such as aliphatic and aromatic hydrocarbons, and the halocarbon propellants used in aerosols. The fluid is easily emulsified in water with standard emulsifiers and

normal emulsification techniques. XIAMETER PMX-200 Silicone Fluid, 50-1,000 CS is insoluble in water and many organic products. Additive quantities as small as 0.1% may suffice where XIAMETER PMX-200 Silicone Fluid, 50-1,000 CS is to be used as a surface agent or for de-soaping creams and lotions. However, 1-10% is needed for applications such as hand creams and lotions to form a more uniform film and effective barrier.

#### PRODUCT SAFETY INFORMATION

XIAMETER PMX-200 Silicone Fluid, 50-1,000 CS may cause temporary eye discomfort.

PRODUCT SAFETY INFORMATION REQUIRED FOR SAFE USE IS NOT INCLUDED IN THIS DOCUMENT. BEFORE HANDLING, READ PRODUCT AND MATERIAL SAFETY DATA SHEETS AND CONTAINER LABELS FOR SAFE USE, PHYSICAL, ENVIRONMENTAL, AND HEALTH HAZARD INFORMATION. THE MATERIAL SAFETY DATA SHEET IS AVAILABLE ON THE XIAMETER WEB SITE AT [WWW.XIAMETER.COM](http://WWW.XIAMETER.COM).

## TYPICAL PROPERTIES

Specification Writers: These values are not intended for use in preparing specifications. Please contact your local XIAMETER® sales representative prior to writing specifications on this product.

Test	Unit	Result		
		50 cSt	100 cSt	200 cSt
Appearance		Crystal clear	Crystal clear	Crystal clear
Specific Gravity at 25°C (77°F)		0.960	0.964	0.967
Refractive Index at 25°C (77°F)		1.4022	1.4030	1.4032
Color, APHA		5	5	5
Flash Point, Open Cup	°C (°F)	318 (605)	>326 (>620)	>326 (>620)
Acid Number, BCP		trace	trace	trace
Melt Point	°C (°F) <sup>1,2</sup>	-41 (-42)	-28 (-18)	-27 (-17)
Pour Point	°C (°F)	-70 (-94)	-65 (-85)	-65 (-85)
Surface Tension at 25°C (77°F)	dynes/cm	20.8	20.9	21.0
Volatile Content, at 150°C (302°F)	percent	0.3	0.02	0.07
Viscosity Temperature Coefficient		0.59	0.60	0.60
Coefficient of Expansion	cc/cc/°C	0.00104	0.00096	0.00096
Thermal Conductivity at 50°C (122°F)	g cal/cm·sec·°C	-	0.00037	-
Solubility Parameter <sup>3</sup>		7.3	7.4	7.4
Solubility in Typical Solvents				
Chlorinated Solvents		High	High	High
Aromatic Solvents		High	High	High
Aliphatic Solvents		High	High	High
Dry Alcohols		Poor	Poor	Poor
Water		Poor	Poor	Poor
Fluorinated Propellants		High	High	High
Dielectric Strength at 25°C (77°F)	volts/mil	400	400	400
Volume Resistivity at 25°C (77°F)	ohm-cm	1.0x10 <sup>15</sup>	1.0x10 <sup>15</sup>	1.0x10 <sup>15</sup>
		<b>350 cSt</b>	<b>500 cSt</b>	<b>1,000 cSt</b>
Appearance		Crystal clear	Crystal clear	Crystal clear
Specific Gravity at 25°C (77°F)		0.969	0.970	0.970
Refractive Index at 25°C (77°F)		1.4034	1.4035	1.4035
Color, APHA		5	5	5
Flash Point, Open Cup	°C (°F)	>326 (>620)	>326 (>620)	>326 (>620)
Acid Number, BCP		trace	trace	Trace
Melt Point	°C (°F) <sup>1,2</sup>	-26 (-15)	-25 (-13)	-25 (-13)
Pour Point	°C (°F)	-50 (-58)	-50 (-58)	-50 (-58)
Surface Tension at 25°C (77°F)	dynes/cm	21.1	21.2	21.2
Volatile Content, at 150°C (302°F)	percent	0.15	0.11	0.11
Viscosity Temperature Coefficient		0.60	0.61	0.61
Coefficient of Expansion	cc/cc/°C	0.00096	0.00096	0.00096
Thermal Conductivity at 50°C (122°F)	g cal/cm·sec·°C	-	0.00038	0.00038
Solubility Parameter <sup>3</sup>		7.4	7.4	7.4
Solubility in Typical Solvents				
Chlorinated Solvents		High	High	High
Aromatic Solvents		High	High	High
Aliphatic Solvents		High	High	High
Dry Alcohols		Poor	Poor	Poor
Water		Poor	Poor	Poor
Fluorinated Propellants		High	High	High
Dielectric Strength at 25°C (77°F)	volts/mil	400	400	400
Volume Resistivity at 25°C (77°F)	ohm-cm	1.0x10 <sup>15</sup>	1.0x10 <sup>15</sup>	1.0x10 <sup>15</sup>

<sup>1</sup>The melt point temperature is a typical value and may vary somewhat due to molecular distribution (especially 50 cSt). If the melting point is critical to your application, then several lots should be thoroughly evaluated.

<sup>2</sup>Due to different rates of cooling, this test method may yield pour points lower than the temperature at which these fluids would melt.

<sup>3</sup>Fedors Method: R.F. Fedors, Polymer Engineering and Science, Feb. 1974.

XIAMETER PMX-200 Silicone Fluid, 50-1,000 CS 2012, October 11  
Form. No. 95-516D-01

XIAMETER is a registered trademark of Dow Corning Corporation.  
Dow Corning is a registered trademark of Dow Corning Corporation.  
© 2009 - 2012 Dow Corning Corporation. All rights reserved.

**USABLE LIFE AND STORAGE**

Product should be stored at or below 60°C (140°F) in the original unopened containers. The most up-to-date shelf life information can be found on the XIAMETER Web site in the Product Detail page under Sales Specification.

**LIMITATIONS**

This product is neither tested nor represented as suitable for medical or pharmaceutical uses. Not intended for human injection. Not intended for food use.

**LIMITED WARRANTY INFORMATION – PLEASE READ CAREFULLY**

The information contained herein is offered in good faith and is believed to be accurate. However, because conditions and methods of use of our products are beyond our control, this information should not be used in substitution for customer's tests to ensure that our products are safe, effective, and fully satisfactory for the intended end use. Suggestions of use shall not be taken as inducements to infringe any patent.

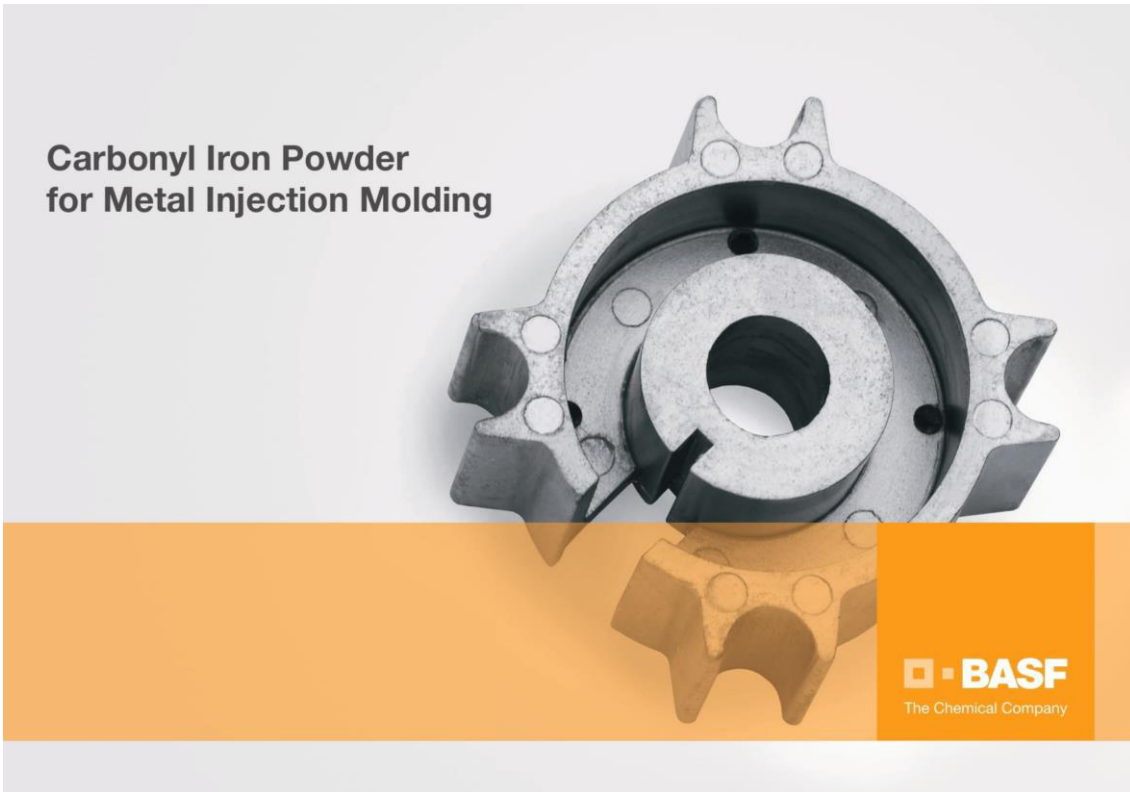
Dow Corning's sole warranty is that our products will meet the sales specifications in effect at the time of shipment.

Your exclusive remedy for breach of such warranty is limited to refund of purchase price or replacement of any product shown to be other than as warranted.

**DOW CORNING SPECIFICALLY DISCLAIMS ANY OTHER EXPRESS OR IMPLIED WARRANTY OF FITNESS FOR A PARTICULAR PURPOSE OR MERCHANTABILITY.**

**DOW CORNING DISCLAIMS LIABILITY FOR ANY INCIDENTAL OR CONSEQUENTIAL DAMAGES.**

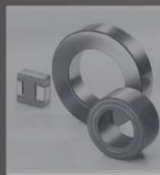
## Appendix E: Technical data of carbonyl iron powder



### Carbonyl Iron Powder for Metal Injection Molding

**BASF**  
The Chemical Company

Inductive Electronic  
Components



Diamond Tools



Metal Injection  
Molding and  
Powder Metallurgy



Microwave and  
Radar Absorption



### ADVANTAGES OF CIP BY BASF BASF'S CIP GRADES

Carbonyl Iron Powder (CIP) is a key raw material for Metal Injection Molding (MIM). The unique fineness of CIP makes it easily compoundable with high load. It provides high density, excellent strength and surface texture quality in the sintered part. CIP's uniform spherical particle shape generates a high flowability and facilitates high accuracy to size in the final part. Using CIP helps to precisely control the carbon-oxygen ratio of the feedstock.

BASF's CIP OS and OM grades are the CIP grades mostly used for MIM applications. They offer excellent sintering properties and outstanding batch-to-batch consistency. CIP OS is additionally silicon-coated to improve the flowability of the feedstock.

CIP CC is a hydrogen-reduced grade with very low carbon and nitrogen content. It is widely applied in combination with OS or OM in order to adjust the carbon-oxygen ratio of the feedstock.

Our specialty H grades are employed when highest demands need to be met. The extraordinary fineness of CIP H-grades provides high density and surface texture quality in micro MIM parts.

### Our CIP grades for high quality MIM parts

With precisely controlled properties, our well-known high-quality CIP grades contribute to superior MIM parts. BASF's excellent batch-to-batch consistency helps our customers to efficiently run their production processes.

Typical Properties							
Grade	Fe min. (%)	C max. (%)	N max. (%)	O max. (%)	d10 (mic.)	d50 (mic.)	d90 (mic.)
CEP OM	97.8	0.75–0.90	0.65–0.90	0.15–0.40	1.7–2.7	3.9–5.2	7.2–9.2
CEP OS	97.5	0.7–0.9	0.5–0.9	0.6–0.9	1.4–2.4	3.4–4.4	6.4–8.4
CEP CC	99.5	0.05	0.01	0.18–0.35	1.7–2.7	3.8–5.3	6.5–10.0
CEP HF	97.7	0.9	0.9	0.5	1.2	2.5	3.5
CEP HQ	97.8	0.6–0.9	0.6–0.9	0.3–0.5	1	2	3
CEP HS	97.5	1	1	0.5		1.8–2.3	



Please contact us to discuss the requirements of your CIP application.

**BASF SE**  
Carbonyl Iron Powder & Metal Systems  
G-CA/MM  
67056 Ludwigshafen  
Germany

**Asia**  
BASF East Asia  
Regional Headquarters Ltd.  
Hong Kong, China  
Phone: +852 2731 3706

**USA**  
BASF Corporation  
Evans City, PA, USA  
Phone: +1 724 538 1300

For information, please send an e-mail to:  
[inorganics@basf.com](mailto:inorganics@basf.com)

Visit our website at:  
[www.carbonylironpowder.com](http://www.carbonylironpowder.com)

CIP MIM G-CAM\_CIP\_0312\_MIM\_e\_03

**BASF**  
The Chemical Company

#### Note

The data contained in this publication are based on our current knowledge and experience. In view of the many factors that may affect processing and application of our product, these data do not relieve processors from carrying out their own investigations and tests; neither do these data imply any guarantee of certain properties, nor the suitability of the product for a specific purpose. Any descriptions, drawings, photographs, data, proportions, weights etc. given herein may change without prior information and do not constitute the agreed contractual quality of the product. It is the responsibility of the recipient of our products to ensure that any proprietary rights and existing laws and legislation are observed. (03/2012)

® = Registered trademark of BASF SE

## Appendix F: Technical data of force sensor



### S2M

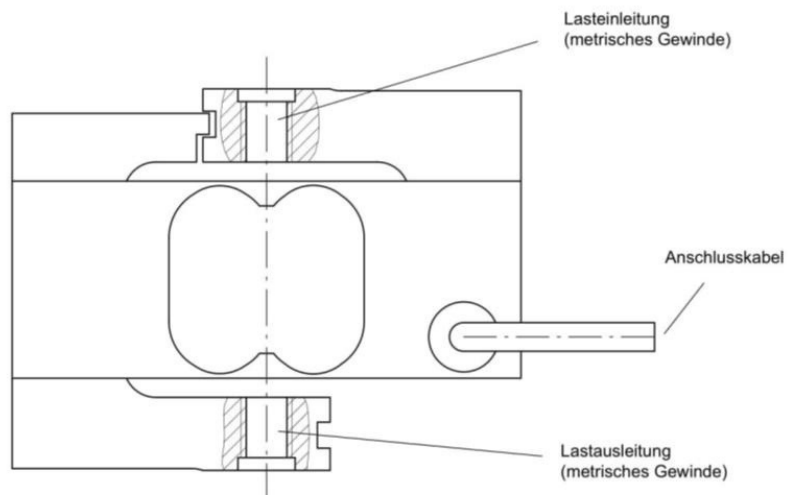
#### Kraftaufnehmer

#### Charakteristische Merkmale

- Zug-/Druckkraftaufnehmer
- Genauigkeitsklasse 0,02
- Nennkräfte: 10 N ... 1000 N
- Hohe Schutzklasse (IP67)
- Hohe Querkraftstabilität
- Sechseleiter-Schaltung

Datenblatt

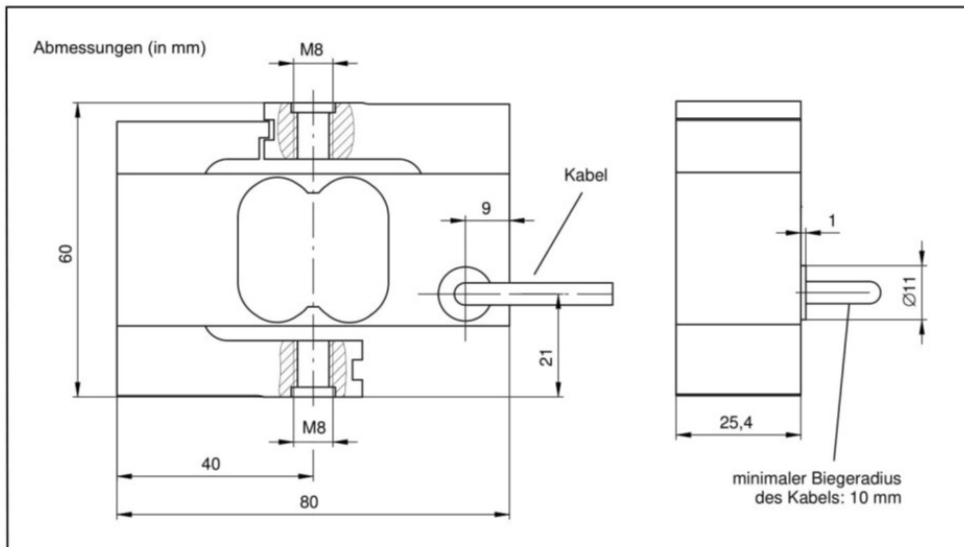
Prinzip Kraftaufnehmer S2M



B3593-1.3 de

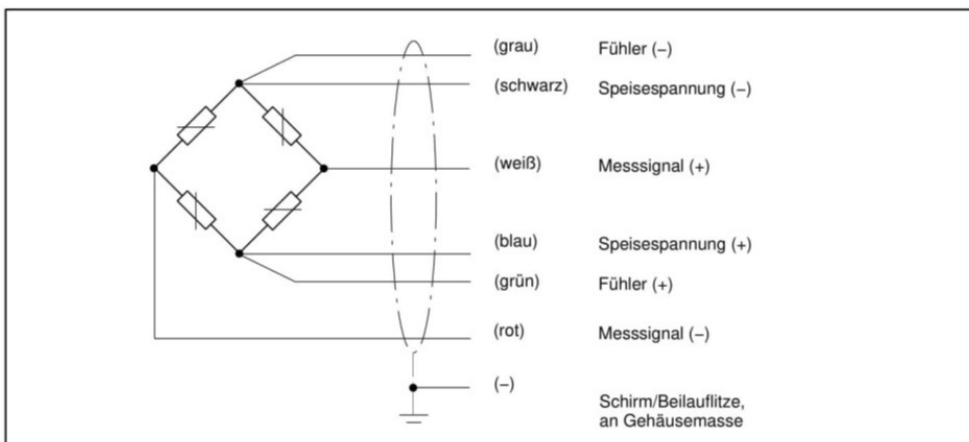


## Abmessungen



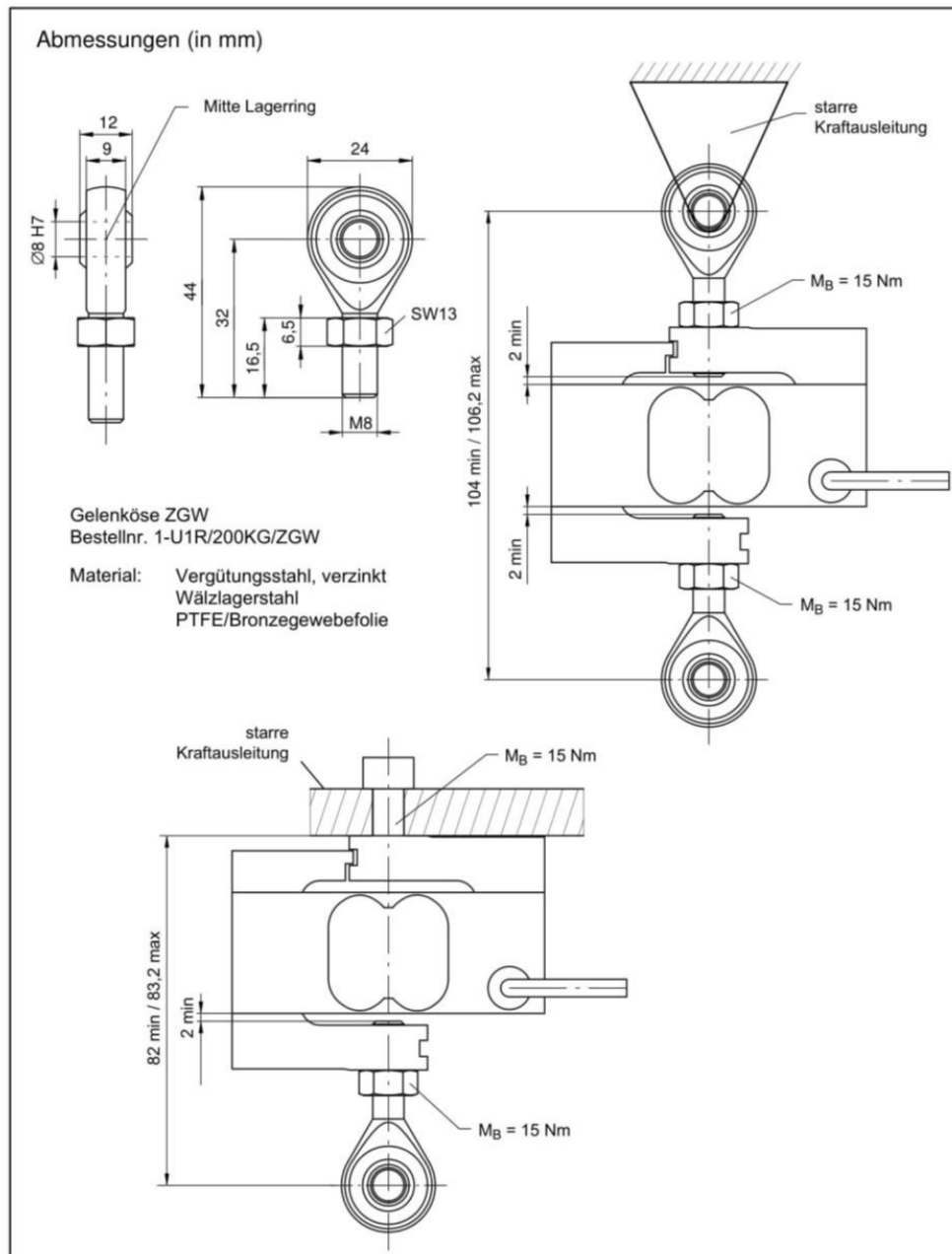
## Kabelbelegung (Sechisleitertechnik)

Bei dieser Kabelbelegung ist bei Belastung des Aufnehmers in Druckrichtung die Ausgangsspannung am Messverstärker positiv.





**Einbaubehör (zusätzlich zu beziehen)**



## Technische Daten (Angaben gemäß VDI/VDE/DKD 2638)

Typ			S2M							
Nennkraft	$F_{nom}$	N	10	20	50	100	200	500	1000	
<b>Genauigkeit</b>										
Genauigkeitsklasse			0,02							
Rel. Spannweite in unveränderter Einbaulage	$b_{rg}$	%	0,02							
Relative Umkehrspanne	$v$		0,02							
Linearitätsabweichung	$d_{lin}$		0,02							
Relatives Kriechen über 30 min.	$d_{cr, F+E}$		0,02							
Biegemomenteinfluss bei 10% $F_{nom} \cdot 10$ mm	$d_{Mb}$		0,02							
Querkrafteinfluss (Querkraft = 10% $F_{nom}$ )	$d_Q$		0,02							
Temperatureinfluss auf den Kennwert	$TK_C$		% / 10 K	0,02						
Temperatureinfluss auf das Nullsignal	$TK_0$			0,02						
<b>Elektrische Kennwerte</b>										
Nennkennwert	$C_{nom}$	mV/V	2							
Relative Abweichung des Nullsignals	$d_{S, 0}$	%	5							
Relative Kennwertabweichung	$d_c$		0,25							
Relativer Kennwertunterschied Zug/Druck	$d_{ZD}$		0,1							
Eingangswiderstand	$R_e$	$\Omega$	> 345							
Ausgangswiderstand	$R_a$		350 ± 50							
Isolationswiderstand	$R_{is}$	G $\Omega$	> 2							
Gebrauchsbereich der Speisespannung	$B_{U, G}$	V	0,5 ... 12							
Referenzspeisespannung	$U_{ref}$		5							
Anschluss			Sechsfach-Schaltung							
<b>Temperatur</b>										
Nenntemperaturbereich	$B_{T, nom}$	°C	-10 ... +45							
Gebrauchstemperaturbereich	$B_{T, G}$		-10 ... +70							
Lagerungstemperaturbereich	$B_{T, S}$		-10 ... +85							
<b>Mechanische Kenngrößen</b>										
Maximale Gebrauchskraft	$F_G$	%	150							
Grenzkraft	$F_L$		1000							
Bruchkraft	$F_B$		1000							
Grenzdrehmoment	$M_G$	Nm	4	8	25	28				
Grenzbiegemoment	$M_{b, zul}$		6	25	34	50	71	95	125	
Statische Grenzquerkraft	$F_Q$	% von $F_{nom}$	100							
Nennmessweg	$s_{nom}$	mm	0,27	0,21	0,18	0,15	0,13	0,12	0,13	
Grundresonanzfrequenz	$f_G$	Hz	94,4	146	243	358	475	582	618	
Relative zulässige Schwingbeanspruchung	$F_{Tb}$	% von $F_{nom}$	140							
<b>Allgemeine Angaben</b>										
Schutzart nach DIN EN 60529			IP 67							
Messkörperwerkstoff			Aluminium							
Vergussmasse			Silikon							
Kabel			Sechsfach-Schaltung, PUR-Isolierung, schleppkettentauglich							
Kabellänge		m	6							
Masse (mit Kabel)	$m$	kg	0,5							

## Ausführungen und Bestellnummern

Code	Messbereich	Bestellnummer Lagerteil	Die grau markierten Bestellnummern sind Vorzugstypen, sie sind kurzfristig lieferbar. Alle Kraftaufnehmer mit 6 m Kabel, offenen Enden und ohne TEDS. Die Bestell-Nr. der Vorzugstypen ist 1-S2M... Die Bestell-Nr. der kundenspezifischen Ausführungen ist K-S2M-MONT...
010N	10 N	1-S2M/10N-1	
020N	20 N	1-S2M/20N-1	
050N	50 N	1-S2M/50N-1	
100N	100 N	1-S2M/100N-1	
200N	200 N	1-S2M/200N-1	
500N	500 N	1-S2M/500N-1	
001K	1000 N	1-S2M/1000N-1	


Kabellänge	Steckerausführung	Aufnehmer- identifikation
<b>01M5</b> 1,5m	<b>Y</b> Freie Enden	<b>S</b> Ohne TEDS
<b>03M0</b> 3m	<b>F</b> Sub-D	<b>T</b> Mit TEDS
<b>06M0</b> 6m	<b>Q</b> Sub-HD	
	<b>N</b> ME3106PEMV	
	<b>P</b> CON P1016	

<b>K-S2M-MONT</b>	<b>010N</b>	<b>03M0</b>	<b>Q</b>	<b>T</b>
-------------------	-------------	-------------	----------	----------

Das Beispiel oben zeigt eine S2M mit 10N Nennkraft, 3 m Kabel, einem montiertem Stecker für das Quantum - System und TEDS.

TEDS sind nur bei der Steckermontage möglich, die Kombination offene Enden und TEDS kann nicht angeboten werden.

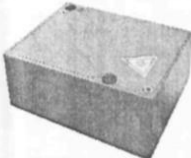
## Appendix G: Technical data of laser sensor



---

# Laser-Wegmesssensor

## AM300



---

- Integrierte Signalaufbereitung All-in-One
- Messbereiche 2 mm ... 1000 mm (bzw. 2000mm)
- Weitere Ausführungen auf Anfrage verfügbar
- Dynamische Messungen mit bis 5.000 Messwerten/s
- Sehr hohe Auflösung ab 0,16 µm
- Sehr gute Linearität ab 1,6 µm
- Versorgungsspannung 4,5 ... 36 VDC
- Hohe Umweltbeständigkeit IP67
- Sonderausführungen, Schutzgehäuse, Zubehör und Optionen
- RS232 / RS485 / CAN-Bus / Ethernet alternativ
- PC-Software für Parametrierung, Visualisierung und Speichern

---

Copyright ALLSENS Messtechnik      Technische Änderungen und Irrtum vorbehalten Ver. 01.2010

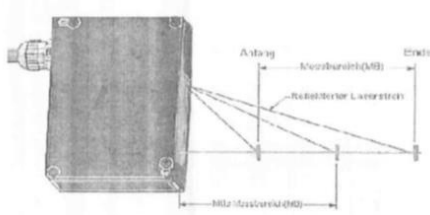
**ALLSENS Messtechnik • Im Bendersgarten 9-11 • D-63303 Dreieich • Germany**  
Telefon +49 – 6074 - 91 43 025 • Fax +49 – 6074 - 91 43 026  
[www.allsens.de](http://www.allsens.de) • [support@allsens.de](mailto:support@allsens.de)



### Messprinzip

Ein ausgesendeter Laserstrahl wird an der Oberfläche des Messobjektes diffus reflektiert und über eine Optik auf einen CMOS-Liniendetektor projiziert. Abhängig von der Entfernung des Messobjektes verändert sich der Reflexionswinkel und damit die Abbildung der Reflexion auf dem CMOS-Zeilendetektor. Hieraus ermittelt der Signalprozessor in Echtzeit den Abstand zwischen Sensor und Messobjekt-Oberfläche.

Der AM300 arbeitet berührungslos mit integrierter Controller-Elektronik mit einem modernen, digitalen CMOS-Detektor mit hoher Empfindlichkeit. Dies ermöglicht eine optimale Anpassung an die Messaufgabe durch schnelle und individuelle Online-Regelung des Laserlichtes mit dem EZR-Verfahren. Der Anwender kann frei wählen, ob er ein festes Zeitraster oder die Optimierung durch die Belichtungsautomatik voll nutzen möchte. Alle Einstellungen sind mit der AM-Mastersoftware oder über die seriellen Schnittstellen parametrierbar und können temporär oder permanent im Sensor abgespeichert werden.



Messbereiche	Weitere Messbereiche und Grundabstände: auf Anfrage möglich					
Messbereich MB in mm	2	5	10	15	25	30
Anfang MB in mm	10	15	60	65	80	95
Mitte MB in mm	11	17,5	65	72,5	92,5	110
Ende MB in mm	12	20	70	80	105	125
Linearität in mm	0,0016	0,004	0,008	0,012	0,020	0,024
Auflösung in $\mu\text{m}$	0,16	0,40	0,80	1,20	2,00	2,40
Messbereich MB in mm	50	100	250	500	750	1000
Anfang MB in mm	105	140	80	125	145	245
Mitte MB in mm	130	190	205	375	520	745
Ende MB in mm	155	240	330	625	895	1245
Linearität in mm	0,04	0,08	0,20	0,40	0,60	0,80
Auflösung in $\mu\text{m}$	4	8	20	40	60	80

Als Referenz-Messobjekt wurde weiße Keramik mit 85% diffuser Reflexion benutzt.